# Modelling Martian Polar Caps

Dissertation

zur Erlangung des Doktorgrades

der Mathematisch-Naturwissenschaftlichen Fakultäten

der Georg-August-Universität zu Göttingen

vorgelegt von

## Rupali Arunkumar Mahajan

aus Beed, Indien

Göttingen  2005

# Contents

# List of Figures

# List of Tables

# Summary

The Martian poles are both covered by ice caps, the seasonal caps and residual polar caps. The seasonal caps are seen only in the respective winter when atmospheric $CO_2$ condenses on to the pole. The smaller residual caps polewards of about $80°N$ and $80°S$ are underlain by massive topographic structures known as polar layered deposits or polar layered terrain. These caps are reffered as north and south polar cap respectively for this study. Due to weak strength of $CO_2$ the composition of $H_2O$ ice with some mixed-in dust is more likely candidate for the polar layered terrains.

The present study models the polar layered terrains using the ice sheet model SICOPOLIS (SImulation COde for POLythermal Ice Sheets). The aim of this study is to model the dynamic and thermodynamic evolution of the polar caps. Mars experiences periodic changes of the orbital parameters known as Milankovitch cycle similar to Earth. These cycles are considered as driving forces for climate changes. The effect of these climate cycles on the extent, thickness and flow of the ice cap are studied. Sensitivity studies of the ice flow for different parameter values of climate inputs and ice dynamics flow parameters are done. Flow laws for the ice are generalised. The dark and white spirals in the polar region suggests the presence of the dust in the polar caps. The dust content is implemented in the model in the form of average volume fraction. The effects of different ice rheologies and dust contents are investigated. Different scenarios are considered that are favourable to reproduce the caps with the present configuration.

It has been found that the extent and volume of the ice cap are mainly governed by the long term *average* climate. This is in contradiction to the studies done before by Greve (2000b) and Greve *et al.*, (2003). Sensitivity studies of the different climate inputs and ice flow parameters suggests that the present north polar cap is not likely to be in a steady state. For both the north and south polar caps basal temperatures are always found below the melting point hence there are rare chances of liquid water present at the ice cap base. Both the polar caps *flow*. The flow velocities are in the range of $0.1$ mm a$^{-1}$ to $1.5$ mm a$^{-1}$ for the north polar cap and $0.01$ mm a$^{-1}$ to $0.16$ mm a$^{-1}$ for the south polar cap. The flow velocities are very small and are about 4-5 orders of magnitude smaller than for the terrestrial ice sheets. These values of flow velocities are found in agreement with average values found by Hvidberg (2003) who uses a finite element model is used to calculate velocities in the regions of white and dark spiralling scarps. For all the experiments carried out, due to extremely small flow velocities the ice dynamics do not influence the evolution of the polar caps.

A large part of this study about the north polar cap has already been published in Greve *et al.*, (2004) and Greve and Mahajan (2005)

Summary

# 1  Introduction

## 1.1  Planet Mars

Mars is the fourth planet from the Sun and is commonly referred to as the Red Planet. The rocks, soil and sky have a red or pink hue. The distinct red colour was observed by stargazers throughout history. It was given its name by the Romans in honor of their "God of war". Other civilisations have had similar names for the Red planet. The ancient Egyptians named the planet "Her Descher" meaning the Red One. Mars has been extensively studied using ground-based observations. But even very large telescopes find it difficult to resolve Mars to great detail owing to its small size. It is still a favourite of science fiction writers as it is the most favourable place in the Solar System (other than Earth!) for human habitation. The first spacecraft to visit Mars was Mariner 4 in 1965. Several others followed including Mars 2, the first spacecraft to land on Mars and the two Viking landers in 1976. Ending a long 20 year hiatus, Mars Pathfinder landed successfully on Mars on 1997 July 4. In 2004 the Mars Expedition Rovers "Spirit" and "Opportunity" landed on Mars sending back geologic data and many pictures; they are still operating after more than a year on Mars. Three Mars orbiters, Mars Global Surveyor, Mars Odyssey, and Mars Express are also currently in operation.

Fig. 1.1 shows global topography of two Martian hemispheres by Mars Global Surveyor (MGS). The most prominent features in this image are the massive Hellas impact basin (upper-left) in the southern hemisphere which is nearly nine kilometers deep and 2,100 kilometers across and the ring of material surrounding the basin that rises about two kilometers above the surroundings and stretches out to 4,000 kilometers from the basin center. The lower-right image shows the Tharsis province that contains Tharsis Montes (Ascraeus, Pavonis, and Arsia), and the Valles Marineris canyon system and related outflow channels.

Mars has many aspects in common with the Earth including their orbital and rotational parameters, atmospheric composition and surface conditions. Mars is a rocky body, roughly half the size of Earth and rotates about its axis with a period approximately 40 minutes longer than the length of day on earth. Surface gravity on Mars is around one third that on Earth. Like the Earth, the circulation of the Martian atmosphere is driven by differential equator-pole heating from the Sun, balanced by infrared cooling from its surface and atmosphere. The obliquity of both the planets is also approximately equal at the present time which implies that their tropics are generally heated more intensively by the Sun than their polar regions. It also implies that there are strong seasonal variations in mid and high latitudes of the two hemispheres. Mars is roughly 50% further away from the Sun than the Earth, so the intensity of solar heating (solar constant) is roughly half
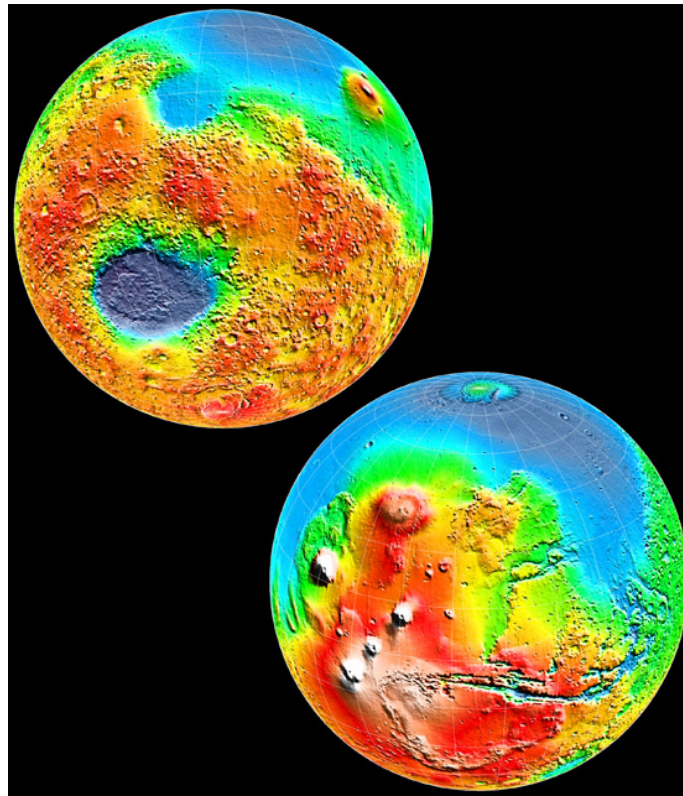
Figure 1.1:  Topography of two Martian hemispheres produced by Mars Global Surveyor, credit: NASA/GSFC

that of Earth. Mars' greater distance from the sun also leads to the Martian year being almost twice as long as that of Earth. Table (1.1) shows a comparison between important parameters for Mars and Earth (Read and Lewis  2004).

## 1.2   Atmospheric properties

Mars has a thin atmosphere composed mainly of $CO_2$ with very small amounts of Nitrogen and Argon. The total surface pressure is about 0.5-1% that of the Earth. Martian atmosphere is dry as compared to that of Earth, with concentrations of water vapour being measured in precipitable microns. Whereas on Earth, water vapour constitutes around 1% of the atmospheric mass. Over much of Mars the temperatures are below freezing point of water and pressure is about 6 hPa so on the phase diagram atmospheric conditions are below the triple point of water. This means that if the temperature somehow reaches the normal freezing point of water, about 273K, ice would directly sublime into water vapour. The resulting environment on Mars is very dry so the typical landscape outside the polar region resembles that of a desert region on Earth. Mars offers a variety of landscapes, ranging from extensive sand-covered desert in the northern tropics and mid-latitudes to arctic ice-fields, especially near the North Pole. Mars also has some examples of mountainous terrain including volcanic mountain Olympus Mons, the largest in the Solar System. It rises about 27 km above the surrounding plains. Each kind of landscape is expected to exhibit their own local weather with different wind patterns, temperature

| Parameter | Earth | Mars |
|---|---|---|
| Mean orbital radius ($10^8$ km) | 1.50 | 2.28 |
| Distance from Sun (AU) | 0.98-1.02 | 1.38-1.67 |
| Orbital eccentricity | 0.017 | 0.093 |
| Planetary obliquity | 23.45° | 25.19° |
| Rotation rate, $\Omega$ ($10^{-5}s^{-1}$) | 7.294 | 7.088 |
| Solar day (s) | 86,400 | 86,775 |
| Year length (Earth days) | 365.24 | 668.98 |
| Equatorial radius (km) | 6378 | 3396 |
| Surface gravity,g ($ms^{-2}$) | 9.81 | 3.72 |
| Surface pressure (hPa) | 1013 | 6 (variable) |
| Atmospheric constituents (molar ratio) | $N_2$ (77%) | $CO_2$ (95%) |
| | $O_2$ (21%) | $N_2$ (2.7%) |
| | $H_2O$ (1%) | Ar (1.6%) |
| | Ar (0.9%) | $O_2$ (0.13%) |
| Mean Solar Constant ($Wm^{-2}$) | 1367 | 589 |
| Bond albedo | 0.306 | 0.25 |
| Equilibrium temperature $T_e$(K) | 256 | 210 |
| Surface temperature (K) | 230-315 | 140-300 |

Table 1.1: Key parameters for Earth and Mars

and sometimes clouds. Water clouds are much rarer on Mars than on Earth, but do occur at times in the form of suspended ice crystals.

The very cold temperatures reached at high latitudes during winter lead to some unusual features of Mars' atmospheric circulation and seasonal cycle. Temperatures at the winter pole are regularly observed as low as 140K, which has significance since this is close to the frost point of $CO_2$ at the typical surface pressure at around 6 hPa. Once this temperature is reached $CO_2$ ice starts condensing on the ground. Since $CO_2$ is the principal constituent of the atmosphere a large amount of it is available for condensation. This leads to the formation of seasonal polar caps. This process ends only when polar night enters the local spring. In the spring the insolation increases allowing temperature to rise and condensed $CO_2$ can be sublimated into the atmosphere. This seasonal $CO_2$ condensation and evaporation cycle entails an annual exchange of approximately one third of the atmospheric mass between the hemispheres.

## 1.3   Polar caps

Mars' polar caps are large enough to be visible from Earth, even with a modest telescope. Polar caps are of particular interest for two reasons; they are major reservoirs of volatiles and secondly, they are the regions of present-day geologic activity. Extensive layered deposits are found surrounding the polar ice and also beneath it. High resolution imaging laser altimetry MOLA (Mars Orbiter Laser Altimeter) on-board MGS has played an important part in enhancing our knowledge about the high latitudes of Mars. Like the

seasonal snow cover of the Earth, Martian polar caps too wax and wane with the seasons. At the present time, southern summers are shorter but warmer than northern ones, and winters are longer and colder. Mars reaches the perihelion during southern summer. This results in an extreme climate in southern high latitudes compared to the north. Because of this the south cap shows a greater variation in size at its maximum, extending as far as 50°S, around 15° closer to the equator than the north polar cap.

Fig. 1.2 shows both the Mars' polar cap in the respective summer. This is a wide angle view of the Martian north polar cap (top) and south polar cap (bottom) as it appeared to the Mars Orbiter Camera (MOC) on-board Mars Global Surveyor (MGS). Fig. 1.3 shows Maps of the global topography of Mars. The projections are Mercator to 70° latitude and stereographic at the poles with the south pole at left and north pole at right. Note the elevation difference between the northern and southern hemispheres. The Tharsis volcano-tectonic province is centered near the equator in the longitude range 220°E to 300°E and contains the vast east-west trending Valles Marineris canyon system and several major volcanic shields including Olympus Mons (18°N, 225°E), Alba Patera (42°N, 252°E), Ascraeus Mons (12°N, 248°E), Pavonis Mons (0°, 247°E), and Arsia Mons (9°S, 239°E). Regions and structures discussed in the text include Solis Planum (25°S, 270°E), Lunae Planum (10°N, 290°E), and Claritas Fossae (30°S, 255°E). Major impact basins include Hellas (45°S, 70°E), Argyre (50°S, 320°E), Isidis (12°N, 88°E), and Utopia (45°N, 110°E). The scale saturates after 8 km.

The deposits associated with the polar regions consists of layered terrain and a residual cap. The residual cap constitutes the perennial ice deposits that are distinguished from the seasonal frosts. MOLA data gives us a clear picture of polar topography. Highest point of the north polar cap is within a few kilometers of rotational pole and has an elevation of -1950 m with respect to average elevation at the equator or reference geoid. The volume of the north polar layered terrain is about 1.2-1.7 $\times 10^6$ km$^3$ and the area is 1.04 $\times 10^6$ km$^2$. The southern ice cap lies at an elevation 6 km higher than the northern cap. The southern cap is visually much smaller than in the north, although south polar layered deposits extend much farther from the ice cap and exhibit a more asymmetric distribution than their northern counterparts. The estimated volume of the south polar layered terrain is about 2-3 $\times 10^6$ km$^3$ and the area is 1.44 $\times 10^6$ km$^2$. The residual ice, which persists throughout the seasonal cycle, is offset from the present rotational pole toward $35° - 40°$ E such that the pole does not fall within the residual ice deposit. The topography is highest in the south polar region within the residual ice deposits (Zuber *et al.*, 1998, Smith, *et al.*, 1999). Both cap consists of two components a seasonal one and permanent one. The seasonal cap consists largely of $CO_2$ which condenses over the residual cap in respective winter and evaporates in respective summer. The seasonal $CO_2$ frost extend down to latitudes $\sim 60°$ and sometimes up to $\sim 50°$ for south polar cap (Cattermole 2001). The northern residual cap is almost certainly water ice whereas southern residual cap is a mixture of water ice and $CO_2$ ice. The amount of dust present in the caps is not known. A characteristic feature of the north polar cap is a system of troughs and scarps organised in a spiralling pattern around the pole. They spiral outwards in counterclockwise direction. For south polar cap the reverse happens. Cutting across this general trend are two very prominent and very large valleys, Chasma Boreale in the north and Chasma Australe in south. Thin alternating dark and light bands probably preserve the record of seasonal and climatic deposition and erosion of ice and dust.
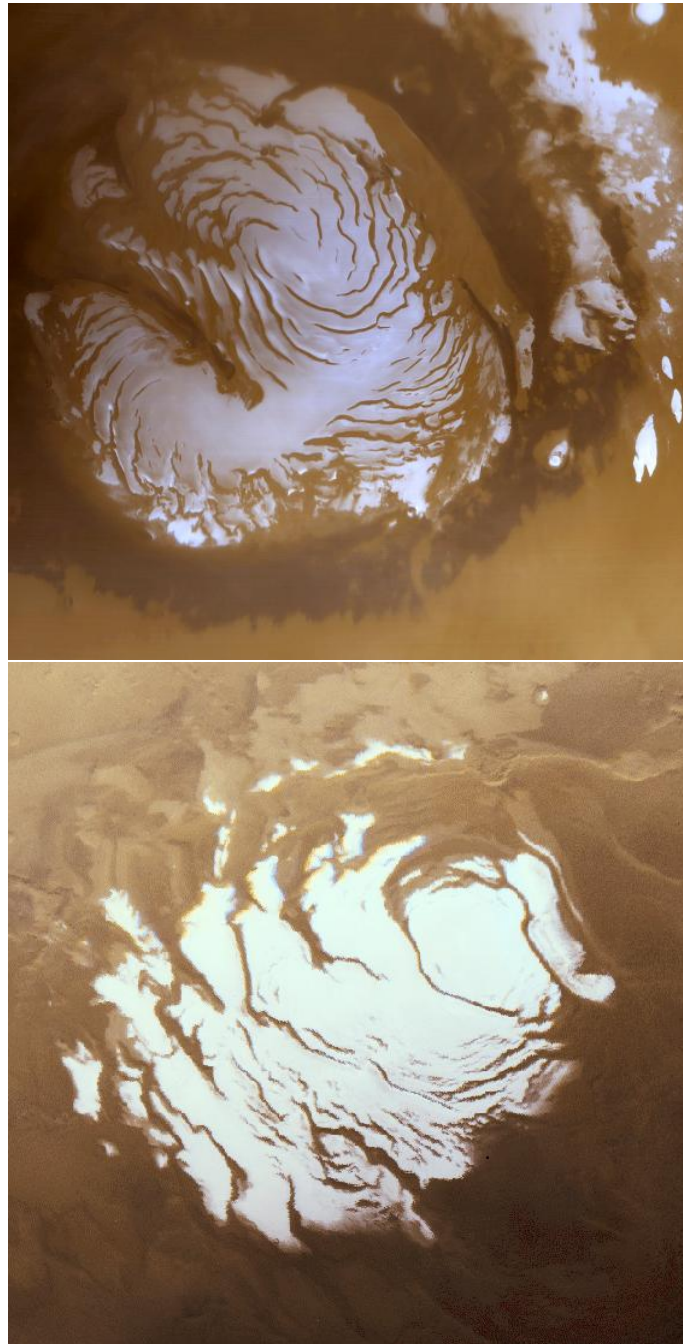
Figure 1.2: Wide angle image of North and South polar cap taken by Mars Orbiter Camera (MOC) of Mars Global Surveyor (MGS). North and South polar caps have approximately   1100 km and ˜400 km diameter respectively . credit: NASA/MGS
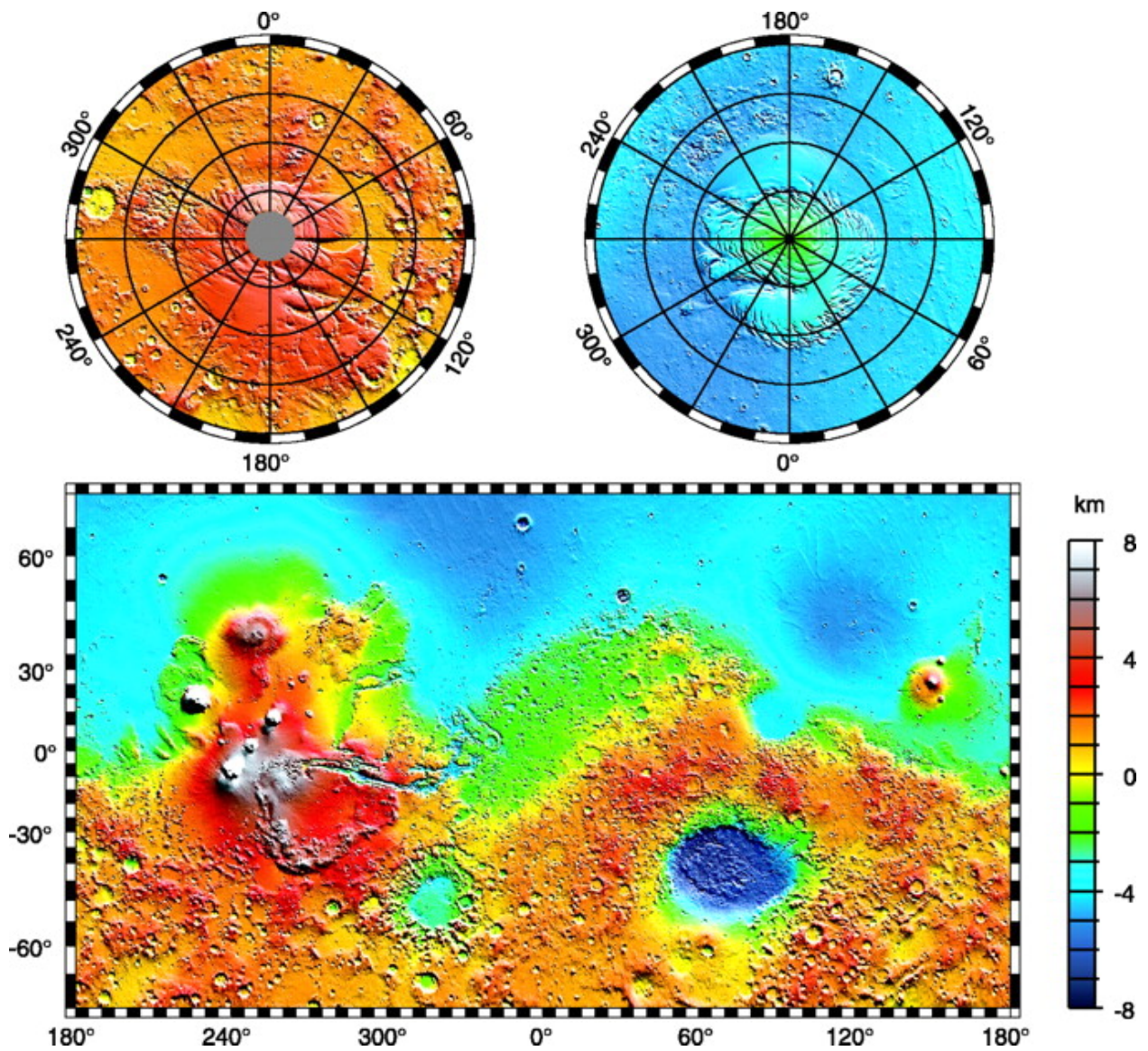
Figure 1.3: MOLA topography for North and South Polar Cap (top) and Global topography (bottom) (Smith, *et al*., 1999) credit: NASA/MGS/MOLA

## 1.4   Past climate

The time scale of around $10^5$ years is an interesting one in the context of the celestial mechanics of Mars. Like Earth, Mars also experiences periodic changes of orbital elements (Milankovitch cycle) like obliquity, eccentricity and longitude of perihelion with respect to the ascending node. Simple theories shows that the eccentricity $e$ varies over the range 0-0.12 as the superposition of two oscillations, one of amplitude 0.05 and period 96 ka and the other of amplitude 0.1 with period $\sim$ 2 Ma. Mars' obliquity $\theta_0$ is found to vary over the range $24.4° \pm 13.6°$ with periods of 125 ka and 1.3 Ma (Ward 1979). Later this turned out to be controversial since more recent calculations using full numerical solutions of the governing equations indicate that obliquity cycle in fact is chaotic and varies between $0° \leq \theta_0 \leq 50°$ (Laskar *et al*., 2002). Variations in the orbital parameters

cause some variations in the distribution of insolation during the year. Among these parameters obliquity is the one which exerts strongest influence on the annually averaged distribution of solar heating. During higher obliquity values polar regions receive more insolation in summer. This is favourable for the volatile release into the atmosphere. This entails warmer climate and thicker dustier atmosphere which may lead to more ice accumulation and dust deposition. During lower obliquity insolation at the poles decrease resulting in colder climate. This has been supported by the light and dark layered deposits of the north and south polar caps indicating a strongly varying dust content and ice due to varying climatic conditions in the past.

A key factor for ice ages on the Earth is climate forcing due to variations in its orbital parameters. Recent Mars exploration has revealed dusty water-ice rich mantling deposits. These deposits are layered, few meters thick and latitude dependent occurring in both the hemispheres from mid latitudes to poles. Head *et al*., (2003) have discussed the possibility that these deposits are formed during the ice age which occurred from about 2.1 to 0.4 Ma BP. This is in response to changing stability in the water ice during the obliquity variation. According to the authors Mars is currently going through interglacial period from the last 300 ka when the obliquity changes are not very high.

## 1.5   Research objective

There have been a few attempts in the past to model the Martian polar layered terrains as dynamic/thermodynamic $H_2O$ ice caps, like the terrestrial Antarctic and Greenland ice sheets. The classical example of such a study is that of Budd *et al*., (1986). These authors used a topography reconstruction of the north polar terrains based on Mariner 9 photometry and surface temperatures derived from Viking thermal mapping as inputs. They computed ice flow and temperature by assuming steady-state conditions of the system. It is argued that the results match at best in orders of magnitude due to many unknown parameters. Also that the resulting water-mass turnover due to ice accumulation and ablation during the Martian year is consistent with independent atmospheric estimates of the seasonal water exchange between the hemispheres. The polar layered terrains have attracted major attention again when MOLA on board MGS provided a better knowledge of Martian topography (Zuber *et al*., 1998, Smith, *et al*., 1999). The entire planet was fully covered in 1999.

Based on this new knowledge, Larson and Dahl-Jensen., (2000) conducted a purely thermodynamic simulations for the north polar terrains forced by periodic variations of the Mars' obliquity. Nye (2000) approximates the north and south polar terrains as axisymmetric profiles and assumes that accumulation and ablation processes at the surface are insignificant so that the profiles slowly spread and thin. Greve (2000b) carried out a dynamic and thermodynamic simulation for the north polar layered terrains. In the model the author describes it as an axi-symmetric, paraboloid like cap with volume, area and maximum thickness which equals the deposits. The effect of periodically varying orbital parameters has been studied. Hvidberg (2003) describes the relationship between topography and flow in the north polar cap on Mars. The ice flow for the scarps and troughs is calculated by a finite-element ice-flow model which includes divergence of the flow, longitudinal stresses and temperature effects.

The main goal of this research is to study the evolution of the polar layered terrains with the help of ice sheet model and to investigate whether the actual topography of the present layered terrains can be reproduced. For this the ice sheet model SICOPOLIS (SImulation COde for POLythermal Ice Sheets) is used. It is a three dimensional dynamic and thermodynamic model which was originally developed for and applied to terrestrial ice sheets like Greenland, Antarctica and glacial northern hemisphere and then to Mars' north polar cap. The model describes the material ice as a density preserving, heat conducting power-law fluid.

To enhance the understanding of the evolution of the polar layered terrains following studies are carried out:

• The boundary conditions of the surface accumulation, ablation and temperature are derived directly from the insolation history by applying newly developed Mars Atmosphere-Ice coupler (MAIC).

• After MAIC another scheme based on a zonal and daily mean energy balance including $CO_2$ condensation and evaporation is developed. With this scheme daily mean surface temperatures can be calculated.

• The effect of different climatic inputs as well as ice dynamic parameters on the extent, thickness and flow of the cap is studied. The steady-state scenario under present climatic conditions and transient scenario over climate cycles is considered to check whether the north polar cap with present state features can be produced.

• In the beginning only Glens flow law which is used in most of the terrestrial ice sheet models was used in the SICOPOLIS. Goldsby and Kohlstedt (1997) and Durham (1998) suggest that ice has a different behaviour under different temperature and stress regimes. Hence the different flow laws for ice are implemented for the different stresses, strain-rate and the different temperature regimes. The effect of different ice rheologies is investigated.

• Satellite imagery shows that parts of the polar caps appear dark, indicating the ice in the polar layered terrain may include a substantial amount of dust. The dust is taken as volume fraction of the ice cap. The strength of the ice cap is considered to have an exponential dependence on this dust volume fraction. As the dust content changes the density and heat conductivity of the material affecting the temperatures. The dust content is implemented in terms of density and heat conductivity. The effect of different dust contents is investigated.

• The model SICOPOLIS was adapted for the south polar cap. The effect of different ice rheologies and dust contents is studied.

## 1.6   Thesis outline

This first chapter is an introduction to the planet Mars, its atmospheric properties and polar caps. The research goals are also discussed in this chapter. The second chapter presents a brief discussion on ice flow, ice models and the model SICOPOLIS which is used in this research to investigate the evolution of polar layered terrains. The third chapter outlines the different climate forcing the model SICOPOLIS uses. It also discusses the different schemes developed and implemented for climate forcing during the research. Fourth and fifth chapters give an insight into the simulation set-up and different boundary conditions used to carry out this work. All the results obtained during the research are summarized and discussed in the sixth chapter. The important conclusions and outlook are presented in the last chapter.

# 2   Ice Model

## 2.1   Ice

### 2.1.1   Ice structure

Water ice can exists in a great variety of different phases. Most of these phases form under high pressure, which results in a denser packing of the water molecules compared to the "ordinary" ice, which in glaciology is termed as ice Ih. Ordinary ice consists of two inter penetrating lattices with a hexagonal close packed stacking arrangement. The stacking arrangement is that of hexagonal close packing, but the molecules themselves are not close packed. The stability range of the later is for pressures P $\leq$200 MPa, which is equivalent to the hydrostatic pressure of an ice layer (density $\rho$ = 910 kgm$^{-3}$) of approximately 22 km on Earth (gravity acceleration g = 9.81 ms$^{-2}$), 60 km on Mars (g = 3.72 ms$^{-2}$).This thickness is much higher than any ice sheet found either on Mars or Earth

Ice Ih forms hexagonal crystals, that is, the water molecules are arranged in layers of hexagonal rings (Paterson  1994). The plane of such a layer is called the basal plane, which actually consists of two planes shifted slightly (by 0.0923 nm) against each other. The direction perpendicular to the basal planes is the optic axis or c-axis, and the distance between two subsequent basal planes is 0.276 nm. This leads to the very low packing factor of 34% which is responsible for the density anomaly of ice Ih (smaller density than liquid water). Further, the basal planes can glide on each other when a shear stress is applied, comparable to the deformation of a deck of cards. This effect is strongly enhanced by the existence and generation of dislocations (structural defects) in real crystals, and the mechanism is consequently called *dislocation creep*.

On the macro-scale, ice aggregates on planetary bodies (grounded ice sheet/cap/glacier, ground ice, floating ice shell etc.) are composed of a vast number of individual crystals. For instance, for terrestrial ice sheets and glaciers, the typical grain size is of the order of millimeters to centimeters. Such a compound is called *polycrystalline ice*.

### 2.1.2   Ice rheology

Several forms of a non-linear viscous rheology for the flow of polycrystalline ice for different stress, strain rate and temperature regimes have been proposed. They have in common to relate the strain rate tensor $D = \text{sym} \nabla v$ to the Cauchy stress deviator $t^D$, and can be subsumed as

$$D = EA(T,P)\frac{\sigma^{n-1}}{d^p}t^D \tag{2.1}$$

where $\sigma = [tr(t^D)^2/2]^{1/2}$ is the effective stress, $n$ is the stress exponent, $d$ is the grain size and $p$ is the grain size exponent (e.g Paterson 1994, Durham *et al.* 1997, Goldsby and Kohlstedt 1997, van der Veen 1999). The flow rate factor $A(T,P)$ depends via the Arrhenius law (2.2) on the absolute temperature $T$ and the pressure $P$.

$$A(T,P) = A_0 e^{-(Q+PV)/RT} \tag{2.2}$$

In the above equation $A_0$ is the preexponential constant, $Q$ is the activation energy, $V$ is the activation volume and $R = 8.314$ $\mathrm{Jmol^{-1}K^{-1}}$ is the universal gas constant. The flow enhancement factor $E$ is equal to unity for pure ice and can deviate from unity due to the softening or hardening effect of impurities in the ice. Since appropriate values for the activation volume $V$ are poorly constrained and the pressure effect is very small for typical thickness of ice sheets and caps, we account for it in an appropriate way by setting $V = 0$ and measuring the temperature relative to the pressure melting point $T_m = T_0 - \beta P$ instead. $T_0 = 273.15 K$ is the melting point at zero pressure and $\beta$ is the Clausius-Clapeyron constant for air-saturated glacier ice. This gives us the simplified flow rate factor

$$A(T') = A_0 e^{-Q/RT'} \tag{2.3}$$

This law depends exclusively on the homologous temperature $T' = T - T_m = T + \beta P$ (Rigsby 1958, Paterson 1994, van der Veen 1999). By introducing the effective strain rate $\sigma = (trD^2/2)^{1/2}$, in (2.1) we can get

$$\delta = EA(T')\frac{\sigma^n}{d^p} \tag{2.4}$$

when it is solved for $\sigma$

$$\sigma = [EA(T')]^{-1/n}d^{p/n}\delta^{1/n} \tag{2.5}$$

Using this in the (2.1) and solving for $t^D$

$$\begin{aligned} t^D &= [EA(T')]^{-1}d^p \left([EA(T')]^{-1/n}d^{p/n}\delta^{1/n}\right)^{1-n} D \\ &= [EA(T')]^{-1/n}\frac{d^{p/n}}{\delta^{1-1/n}}D \end{aligned} \tag{2.6}$$

Hence the inverse from the general power law (2.1) with the flow rate factor (2.3) is obtained as

$$t^D = E_s B(T')\frac{d^{p/n}}{\delta^{1-1/n}}D \tag{2.7}$$

(van der Veen 1999). Here $E_s = E^{-1/n}$ denotes the stress enhancement factor, and $B(T') = [A(T')]^{-1/n}$ is the associated rate factor. For terrestrial ice the well established Glen's flow law uses the stress exponent $n = 3$, the grain size exponent $p = 0$ and for the temperature range $T' \leq 263 K$ the preexponential constant $A_o = 3.985 \times 10^{-13}$ $\mathrm{s^{-1}Pa^{-3}}$ and the activation energy Q = 60 $\mathrm{kJmol^{-1}}$ (Paterson 1994). The rheology defined by these parameters describes the grain size independent flow mechanism of dislocation creep, which prevails in terrestrial glaciers and ice sheets. The flow enhancement factor for ice formed during glacial period is often set to $E = 3$, interpreted as softening influence of very small amounts of dust, approximately 1 mg $\mathrm{kg^{-1}}$ with particle sizes of 0.1 to 2 $\mu$m (Hammer *et al.* 1985). This softening is attributed to thin films of liquid water which forms around the

dust particles and lubricate ice deformation. However, at the low temperatures expected in the Martian polar caps this effect will not be present and in fact the presence of dust particles will make direct hardening influential. This is discussed in the next section about the dust content.

Durham *et al.* (1997) have proposed an alternative flow law for grain-size independent dislocation creep, based on laboratory creep tests at a confining pressure of 50 MPa. For the temperature regime T = 195-240 K, which corresponds approximately to $T' = 200 - 245K$, they report the parameters $n = 4, p = 0, A_0 = 1.259 \times 10^{-19} \mathrm{s}^{-1} \mathrm{Pa}^{-4}$ and $Q = 61 \mathrm{kJmol}^{-1}$. However it is not clear whether dislocation creep is the predominant creep mechanism for the low temperatures and low strain rates in the Martian caps. There is evidence that other, grain-size dependent flow mechanisms like grain-boundary sliding become favoured instead. (Goldby and Kohlstedt 1997). These can be described by the parameters $n = 1.8, p = 1.4, A_0 = 6.20 \times 10^{-14} \mathrm{s}^{-1} \mathrm{Pa}^{-1.8} \mathrm{m}^{1.4}$ and $Q = 49 \mathrm{kJmol}^{-1}$ (Nye 2000).

For this flow law an upper limit for the grain size $d$ can be obtained by assuming that it is a result of normal grain growth only. From a variety of data from terrestrial polar ice masses and theoretical considerations, the growth rate was derived as

$$\frac{d}{dt}\left(d^2\right) = k \tag{2.8}$$

where $t$ is time and $d/dt$ is the material time derivative which follows the motion of the ice particles. The growth-rate parameter $k$ depends on the absolute temperature via the Arrhenius law

$$k(T) = k_0 e^{-Q_k/RT} \tag{2.9}$$

with the activation energy $Q_k = 42.5 \, \mathrm{kJmol}^{-1}$ and the constant $k_0 = 9.5 \, \mathrm{m}^2 \mathrm{a}^{-1}$ (Thorsteinsson 1996). As an example, for T = 173 K this yields a growth rate of 1.40 mm$^2$Ma$^{-1}$. By assuming a typical age of millions of years for the ice at depth (cf. Greve *et al.* 2004), a reasonable range for the grain size is d = 1...10 mm.

The relative contributions of the several flow laws can be estimated as follows. For simple shear in the $x - z$ plane and E = 1, Eq. (2.1) reduces to

$$\dot{\gamma} = 2A(T')\frac{\tau^n}{d^p} \tag{2.10}$$

where $\tau = t_{xx}^D$ is the shear stress and $\dot{\gamma} = \partial v_x/\partial z = 2D_{xx}$ is the shear rate. Contribution of different flow laws is shown together in Fig. 2.1 shows the shear rates resulting from Eq. (2.10) for $T' = 200K$, which is typical near basal ice for north polar cap and the stress range from 10 kPa to 100 MPa. For Goldby and Kohlstedt (G&K), the grain size $d = 1$ mm and 10 mm have been assumed (Greve and Mahajan 2005) (With our simulations it has been shown that the basal temperatures of south polar cap are colder by $\sim 20°C$ than that of north polar cap. This temperature variation will be discussed under section results). This show clearly that the relative contributions of the different flow laws vary strongly. For very low stresses, grain-size dependent flow with a low stress exponent dominates, whereas for higher stress dislocation creep with a higher stress exponent becomes more important. With the ice density $\rho_i = 910 \mathrm{kgm}^{-3}$ and acceleration due to gravity on Mars, $g_0 = 3.72 \mathrm{ms}^{-2}$, the thickness of north polar cap $H \sim 3$ km, radius of the cap $R = 550$

13

km, the mean slope $\alpha = H/R$ a shear stress will follow $\tau^* = \rho_i g_0 H \alpha \approx 55.4$kPa.  For south polar cap with thickness $H \sim 4$km and the radius $R = 650$ km, the shear stress will be $\tau^* = \rho_i g_0 H \alpha \approx 83.3$kPa.  For this shear stress, the shear rate decreases by roughly an order of magnitude between subsequent values in the order Goldby and Kohlstedt (grain size, d = 1 mm) > Glen > Goldby and Kohlstedt (grain size, d = 10 mm) > Durham
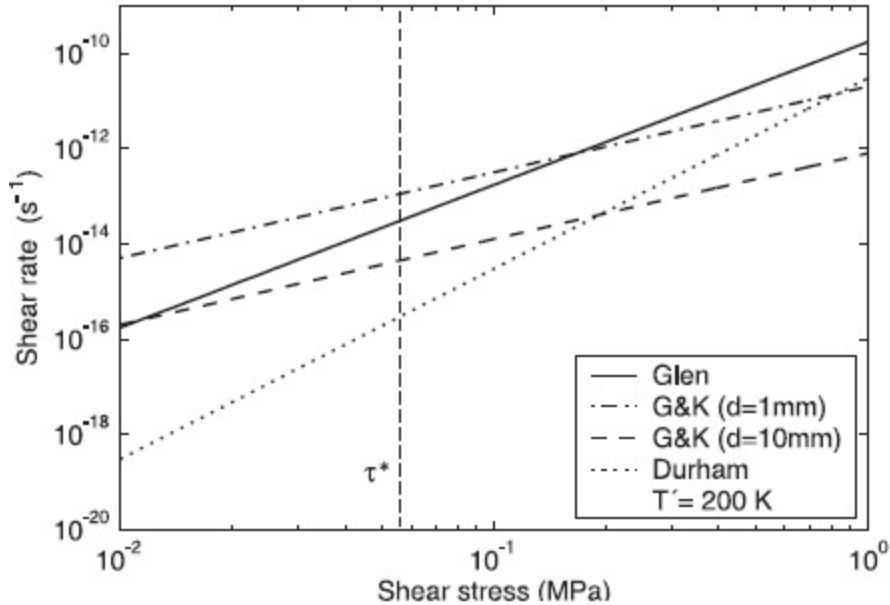


**Figure 2.1:** Variation of shear rate $\dot{\gamma}$ with shear stress $\tau$ calculated by Eq (2.10) at $T' = 200$K. Flow laws: Glen (n = 3), Durham (n = 4), G&K (n = 1.8, p = 1.4, d = 1 mm), G&K (n = 1.8, p = 1.4, d = 10 mm).

### 2.1.3   Ice models

Ice appearing in glaciers and ice sheets exists basically in two different states. Cold ice is characterised by a temperature below the pressure melting point and can be described as an incompressible, viscous and heat-conducting fluid whereas temperate ice is exactly at the pressure melting point so it may contain small quantities of water in addition. Temperate ice must be regarded as two component fluid. In ice sheets, regions of temperate ice may exist in a thin near-basal layer, with significant consequences for the flow behaviour. Glaciers and ice sheets that are made up of cold as well as temperate regions are referred as polythermal (Paterson  1994). In case of Mars the temperatures for the polar layered terrain are found as low as 140K which is well below melting point of ice. This rules out the possibility of having regions of temperate ice in the Martian polar caps.

In the past, several models for the numerical simulation of ice sheets have been developed. It became possible only due to modern high performance computers. The first, a still vertically integrated model is by Mahaffy  (1976) which has been applied to the Barnes Ice Cap in the Canadian Arctic. The first genuinely 3D model was developed by Jenssen  (1977) and is used to model Greenland Ice Sheet. It was a coarse grid model due to the limited computing power at that time. Numerous more and more sophisticated

models followed, with applications to different problems such as the Greenland Ice Sheet, the Antarctic Ice Sheet, the glacial Laurentide Ice Sheet, the hypothetical classical Tibetan Ice Sheet and others (Budd and Smith 1982, Oerlemans 1982, Calov 1994, Huybrechts 1994, Fabré *et al.*, 1995, Calov and Hutter 1996). Especially remarkable are the simulations of the Antarctic Ice Sheet carried out with the Huybrechts model (e.g. Huybrechts (1992, 1993)), in which the coupled ice sheet/ice shelf/lithosphere problem is modelled with high spatial resolution.

 A study has been done to present a continuum-mechanical formulation for the polythermal ice sheet (Greve 1997a). It is in large parts similar to previous formulations (Fowler and Larson 1978, Hutter 1982, Blatter 1991); however this new formulation contains some crucial features, like

1. consideration of the contribution of the diffusive water flux to the total heat flux in temperate ice,

2. a new formulation of the boundary conditions for a temperate ice base, where especially the different behaviour of temperate ice with and without diffusion is incorporated,

3. a new formulation of the transition conditions at the cold-temperate-transition surface (CTS), with the inclusion of water surface production at the CTS,

4. three-dimensional derivation of the shallow-ice approximation (SIA) for the polythermal ice.

### 2.1.4   The polythermal ice-sheet model

A polythermal ice sheet consists of cold-ice regions as well as temperate-ice regions, in the later, besides the ice, water may also be present. Below the ice sheet there is the lithosphere, which is represented as a solid rock layer of approximately 80-120 km thickness that floats on the viscous asthenosphere. However only the first few kilometers of the lithosphere influence the thermal response of the ice sheet. Typical geometry is sketched in Fig. (2.2). In this figure also a Cartesian co-ordinate system ($x$,$y$,$z$) is introduced, $x$ and $y$ indicating the horizontal plane and $z$ is vertical and anti-parallel to the direction of the gravity acceleration. The following field equations, boundary and transition conditions extend the previous formulations of Fowler and Larson (1978), Hutter (1982), Blatter (1991) and Hutter (1993).

## 2.2   Field equations

Cold ice is the ice with a temperature below the pressure melting point. If additional traces of salt, sediment, debris or air are neglected, it can be regarded as a viscous, heat-conducting and incompressible one-component fluid.

$$\nabla \cdot v = trD = 0 \qquad (2.11)$$

15
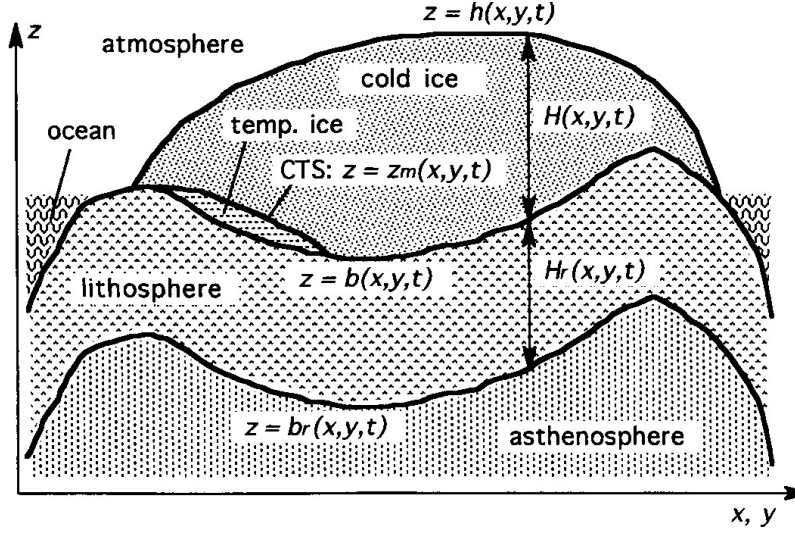
**Figure 2.2:** Sketch of a polythermal ice sheet, heavily exaggerated in the vertical. Definition of the Cartesian coordinate system used in this study: *x* and *y* span the horizontal plane, *z* is the vertical coordinate. Adopted from Greve (1997a)

where *v* is the ice particle velocity, and *D* is the strain rate tensor. The stress tensor *T* is split into an isotropic pressure tensor and a deviatoric (frictional) stress tensor.

$$t = -p\delta_{ij} + t^D \tag{2.12}$$

The *momentum balance* equation is

$$\rho\dot{v} = \nabla T + \rho g \tag{2.13}$$

using (2.12) we can write

$$\rho\dot{v} = -\nabla P + \nabla T^R + \rho g \tag{2.14}$$

where *g* is the acceleration due to gravity. A superposed dot indicates the mathematical time derivative. The scaling analysis (cf Greve 1997a) shows that the acceleration term $\rho\dot{v}$ is negligible hence pure Stokes flow prevails.

Three constitutive relations are needed, a stress strain rate relation, a second for the internal energy $\varepsilon$ and another for the heat flux $q$ (which is equal to sensible heat flux $q_s$, sensible heat is the heat absorbed or transmitted by a substance during a change of temperature which is not accompanied by a change of state). The first constitutive relation is the stress strain rate relation given below:

$$D = EA(T')f(\sigma)T^R \quad with \quad \sigma = \sqrt{\tfrac{1}{2}tr(T^R)^2} \tag{2.15}$$

This equation gives the ice fluidity which factories into (i) a function $A(T')$ called 'rate factor', which is a function of the homologous temperature $T'$. The homologous temperature $T'$ is defined as $T' = T - T_M$, where $T_M$ is the pressure melting point, (ii) a function $f(\sigma)$ called as 'creep response function' of the effective shear stress $\sigma$. The effective shear stress is given by the square root of the second invariant of the stress deviator

$II_T^R = \frac{1}{2}tr(T^R)^2$ (Hutter 1983), The rate factor and creep response function are not specified here, and (iii) the additional factor E ('enhancement factor') which can be set greater than unity to account, for instance, for the increased softness of glacial dust-containing ice compared with ordinary interglacial ice (Paterson 1994).

The second constitutive relation is

$$\dot{\varepsilon} = c(T)\dot{T} \tag{2.16}$$

This equation gives the rate of change of internal energy to that of temperature. Here $c$ is the specific heat.

The third constitutive relation is

$$q = q_s = -\kappa(T)\nabla T \tag{2.17}$$

This equation gives the heat loss (which is equal to sensible heat flux) in terms of temperature gradient. Negative sign indicates the heat flow from higher temperature towards the lower. $\kappa$ is the heat conductivity. This equation is Fourier's law for heat conduction. Heat loss per unit volume can be given by

$$\nabla \cdot q = q_s = -\nabla(\kappa(T)\nabla T) \tag{2.18}$$

Using the above constitutive equations (2.15) to (2.18) and neglecting heat supply due to radiation, the *energy balance* takes the form

$$\rho c\dot{T} = -\nabla q + tr(T^R D) \tag{2.19}$$

resulting into

$$\rho c\dot{T} = \nabla(\kappa\nabla T) + 2EA(T')f(\sigma)\sigma^2 \tag{2.20}$$

This equation gives the balance between local temperature changes and advection which is included in the material time derivative, heat conduction and dissipative strain heating.

## 2.2.1  Lithosphere

Since the objective of this work is ice sheet modelling, the lithospheric processes relevant to the ice sheet are considered. These processes include the conduction of heat in the lithosphere and the resulting thermal inertia effect on the ice sheet. Another process taken into account is the isostatic adjustment as a consequence of the varying ice load.

Analogous to the procedure for cold ice, the temperature equation in the lithosphere becomes

$$\rho_r c_r \dot{T} = \kappa_r \nabla^2 T \tag{2.21}$$

The subscript $r$ refers to the lithosphere (rock bed). So $\rho_r$, $c_r$, $\kappa_r$ are its density, specific heat and heat conductivity respectively. In contrast to the cold ice $c_r$ and $\kappa_r$ are assumed to be constant and strain heating is neglected. Let the sinking depth of the lithosphere

into the asthenosphere below it $\Delta b(x, y, z, t)$. If $h$ and $b$ are the $z$ coordinates of the free ice surface and base respectively then the ice thickness can be given by $H = h - b$. If we consider a vertical column of transect area $dA$, a local force balance between the buoyancy and the ice load for the vertical column can be given by,

$$\rho_a g \Delta b dA = \rho g H dA \qquad (2.22)$$

where $\rho_a$ is the density of the asthenosphere. In this affirmation vertically moving lithosphere column do not interact with each other and they do not have horizontal velocity. When there is no ice load on the lithosphere, the lithosphere comes to a relaxed steady state say $z = b_0(x, y, t)$. The general steady state position $b_{ss}$ of the lithosphere can be given by $b_{ss} = b_0 - \Delta b$, from the above equation the sinking depth $\Delta b$ is given by $\frac{\rho}{\rho_a}H$ so the general steady state position is now given by

$$b_{ss} = b_0 - \frac{\rho}{\rho_a}H \qquad (2.23)$$

Since asthenosphere has some viscosity, there is time lag $\tau_v$ taken by lithosphere to reach this equilibrium state. The evolution equation for the position of the lithosphere surface at $z = b_0(x, y, t)$ is (Herterich,1990):

$$\frac{db}{dt} \equiv \frac{\partial b}{\partial t} = -\frac{1}{\tau_v}(b - b_{ss}) = \frac{1}{\tau_v}[b - (b_0 - \frac{\rho}{\rho_a}H)] \qquad (2.24)$$

For a fixed ice thickness $H$ this corresponds to an exponential approach of $b$ towards the equilibrium state $b_{ss}$.

Under the additional assumption that each vertical column of the lithosphere is rigid, the velocity field in the lithosphere is

$$v = \frac{\partial b}{\partial t}(x, y, t)e_z \qquad (2.25)$$

where $e_z$ is the unit vector pointing in the $z$ direction.

## 2.3 Boundary and transition conditions

### 2.3.1 Boundary condition at the free surface

Free surface here means the ice atmosphere interface. For this free surface *kinematic conditions* can be obtained. The free surface is given implicitly by equation $F_s(x, t) = 0$, (fig 2.3). The positive side is considered adjacent to atmosphere, the normal unit vector $n = \nabla F_s / \|\nabla F_s\|$ points into the atmosphere. Therefore, the time derivative of $F_s$ following the motion of the free surface with velocity $w$ must vanish,

$$\frac{d^w F_s}{dt} = \frac{\partial F_s}{\partial t} + w \cdot \nabla F_s = 0 \qquad (2.26)$$

Then, introducing the ice volume flux through the free surface, $a_s^{\perp} = (w - v^-) \cdot n$

$$\frac{\partial F_s}{\partial t} + v^- \cdot \nabla F_s = -\|\nabla F_s\| \cdot a_s^{\perp} \qquad (2.27)$$
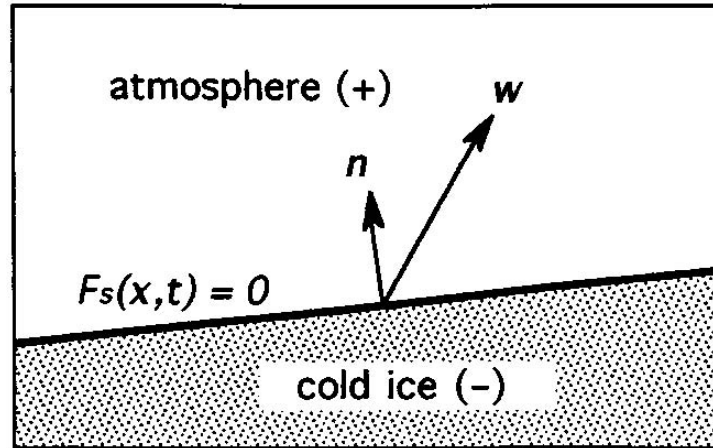
Figure 2.3: Geometry of the free surface. Adopted from Greve (1997a)

In Cartesian coordinates the free surface can be represented $z=(x,y,t)$ and $F_s(x,t) = z - h(x,y,t)$, so

$$\frac{\partial h}{\partial t} + v_x^- \frac{\partial h}{\partial x} + v_y^- \frac{\partial h}{\partial y} - v_z^- = \left(1 + \left(\frac{\partial h}{\partial x}\right)^2 + \left(\frac{\partial h}{\partial y}\right)^2\right)^{1/2} a_s^\perp \qquad (2.28)$$

The ice volume flux, $a_s^\perp$ through the free surface is nothing but the difference between snowfall rate $S_s$ (accumulation) and surface melting rate $M_s$ (ablation). It is an input quantity determined by the climate given by accumulation minus ablation.

## 2.3.2   Transition conditions at the cold ice base
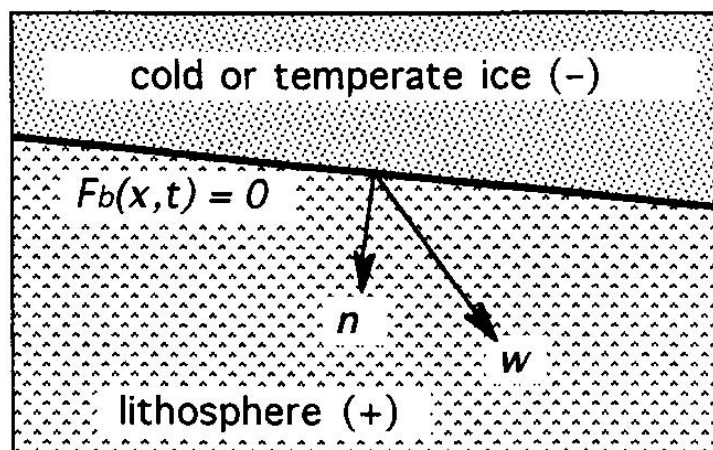


Figure 2.4: Geometry of the ice base. Adopted from Greve (1997a)

Cold and temperate ice have different properties so the transition conditions between ice and lithosphere have to be dealt with separately. The first case is that of cold ice base

(ice base below pressure melting point ) and lithosphere. Second case is of temperate ice base (ice base at pressure melting point) and lithosphere. Here the case of cold ice base is considered as temperate ice region is not relevant to Mars due to temperatures lower than pressure melting point of ice

The bedrock below the ice sheet is assumed to be impermeable, meaning the possible mass exchange between the cold ice base and the lithosphere is ignored. The ice sheet base showed (Fig. 2.4) is given by the equation $z = b(x,y,t)$. The positive side is with lithosphere and negative side is with ice. Setting $F_b(x,t) = b(x,y,t)$, gives us the normal vector $n = \nabla F_b / \|\nabla F_b\|$ pointing into the lithosphere. These definitions hold true for both cold and temperate ice base.

The *sliding law* is considered which relates the basal sliding velocity to basal shear stress through the sliding function $C$. Generally in the case of cold ice base this sliding function $C = 0$, meaning adhesion of the basal ice at the bedrock is assumed in ice-sheet and glacier models.

### 2.3.3  Boundary conditions at the lithosphere base
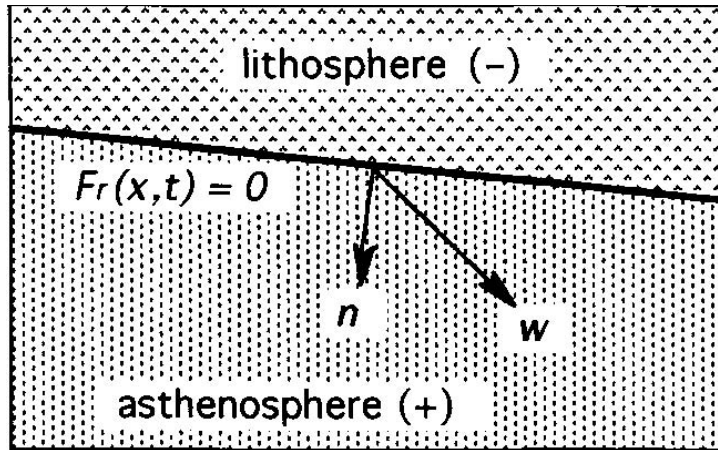


Figure 2.5: Geometry of the lithosphere base. Adopted from Greve (1997a)

The base of the modelled lithosphere is situated at $z = b_r(x,y,t)$, or $F_r(x,t) = b_r(x,y,t)$, Fig 2.5. The positive side is identified with the asthenosphere and the negative side with the lithosphere giving us normal vector $n = \nabla F_r / \|\nabla F_r\|$ pointing into the asthenosphere.

Within the framework of the simple lithosphere model applied here, it is merely required to prescribe a thermal boundary condition at the lithosphere base. To achieve this, the geothermal heat flux is given by $Q^{\perp}_{\text{geoth}} = -\overrightarrow{q}^{-} \cdot n$ in the lithosphere, then the Fourier heat conduction law is specified.

$$\kappa_r(\nabla T^{-} \cdot n) = Q^{\perp}_{geoth} \tag{2.29}$$

which is a Neumann condition for the temperature.

## 2.4   Ice-sheet model SICOPOLIS

In the above few sections it has been discussed continuum mechanical and continuum thermodynamical formulation of the polythermal ice sheet. In the case of SICOPOLIS all the model equations are subjected to shallowness assumption. In this assumption the ratio of typical ice thickness to typical horizontal ice extent is very small, meaning ice sheet is *shallow*. This leads to simplified model equations known as *shallow ice approximation* (SIA). In SIA lateral shear stresses and also normal shear stress deviators are neglected, the pressure is considered hydrostatic and the shear parallel to bed. The complete set of SIA equation is listed in Greve  (1997a).

Now in order to solve these equations, a model SICOPOLIS (SImulation COde for POLythermal Ice Sheet) based on shallow ice approximation has been developed. This model was first developed successfully for ice sheet Greenland. After that it has been successfully adopted for another terrestrial ice sheets like Antarctica, Scandinavia and finally to the Martian polar caps. Model equations are solved numerically with a finite difference integration method.

SICOPOLIS is a dynamic thermodynamic three dimensional model. The flow chart for SICOPOLIS is shown in Fig. 2.6. The sketch is with climate forcing Mars Atmosphere-Ice Coupler (MAIC). The oval boxes corresponds to input to the model from outside the system and rectangular boxes indicate prognostic model components. The sea level has to be considered for terrestrial applications only and not in the case of Mars.

SICOPOLIS computes the temporal evolution of the ice extent, thickness, three-dimensional velocity, temperature, water content and age in response to external forcing given by

1. The mean annual air temperature at the ice surface.

2. Surface mass balance. Mass balance is given by accumulation (in the form like snowfall, condensation) minus ablation (melting, sublimation, erosion)

3. The global sea level (this is relevant only for terrestrial application and not for Martian).

4. Geothermal heat flux heating the ice from below.

All the computations are carried out in a stereographic plane with standard parallel 71°N, spanned by the Cartesian coordinates $x$ and $y$. The vertical coordinate $z$ is taken positive upwards, and the zero level is reference geoid. The distortions due to the stereographic projection are taken care by appropriate metric coefficients.

## 2.5   Bedrock Topography

The present topography of the Mars is now known very precisely from Mars Orbiter Laser Altimeter (MOLA) measurements of the Mars Global Surveyor (MGS) spacecraft (Zuber *et al.*, 1998). These data shows that earlier stereogrammetric reconstructions based on Mariner 9 images (Dzurisin and Blasius  1975) overestimated the extent and thickness of the polar ice caps distinctly. The isostatic depression and the rebound of the lithosphere
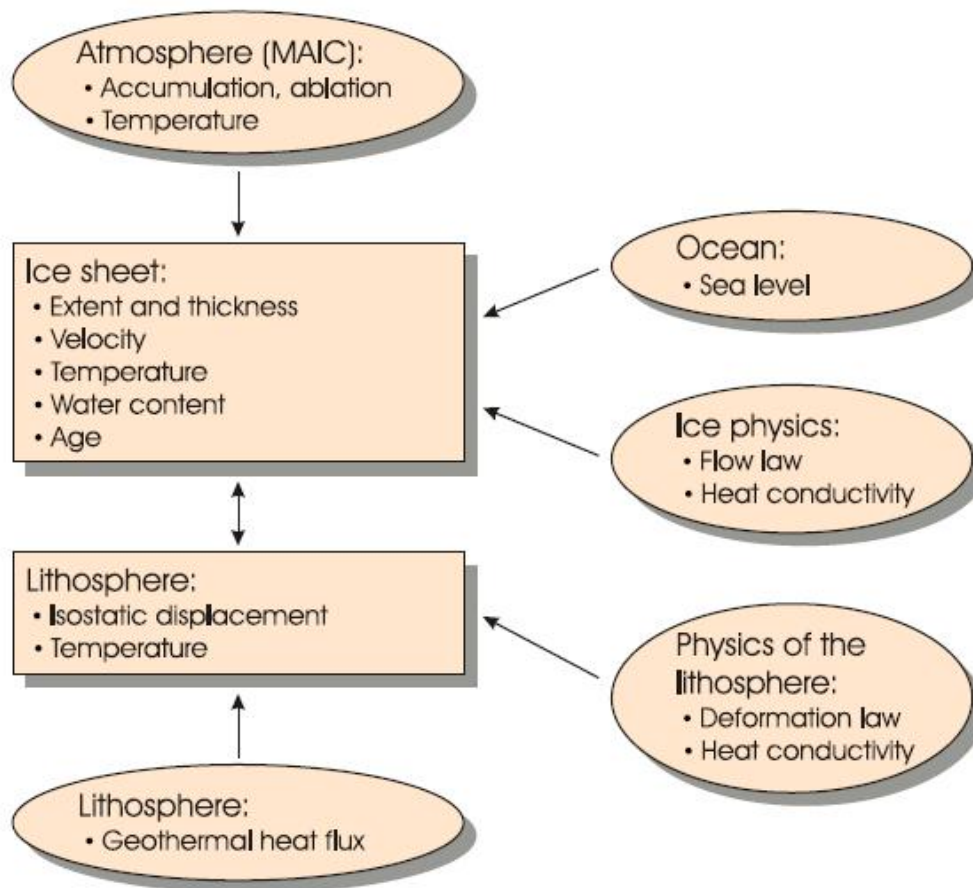
Figure 2.6: Sketch of the polythermal ice sheet model SICOPOLIS with the Mars Atmosphere-Ice Coupler (MAIC) (Figure by R. Greve, personal communication)

due to changing ice load is described by a local-lithosphere-relaxing-asthenosphere model with an isostatic time lag $\tau_{iso}$ (Le Meur and Huybrechts 1996, Greve 2001). Owing to the non-local response of the elastic lithosphere plate, local isostatic compensation of the ice load is not likely. This is considered by introducing the fraction of isostatic compensation, $f_{iso}$, steady-state downward displacement of the lithosphere $w_{ss}$ is given by

$$w_{ss} = f_{iso} H \frac{\rho}{\rho_a} \tag{2.30}$$

Here $H$ is the thickness, $\rho$ is the ice density and $\rho_a$ is the density of the asthenosphere (upper mantle) (Greve *et. el.*, 2003). The actual displacement $w$ as a function of time $t$ is then given by

$$\frac{\partial w}{\partial t} = -\frac{1}{\tau_{iso}}(w - w_{ss}) \tag{2.31}$$

To compute the actual ground (Martian surface without ice) topography $z = b(x,y,t)$, the position of the equilibrated ground for ice-free conditions, $z = b_0(x,y)$ is required as a reference. $b(x,y,t) = b_0(x,y) - w(x,y,t)$ It is constructed by a smooth extrapolation of the ice-free ground surrounding the polar cap.

The actual displacement $w$ as a function of time $t$ is then given by ,

$$\begin{aligned} \nabla^2 b_0(x,y) &= 0 && \text{under the polar cap} \\ b_0(x,y) &= b(x,y,t=0) && \text{outside the polar cap} \end{aligned} \tag{2.32}$$

The result is shown in Fig.(2.7) with the MOLA surface topography which defines the present ground topography $b(x,y,t) = 0$ outside the polar cap.
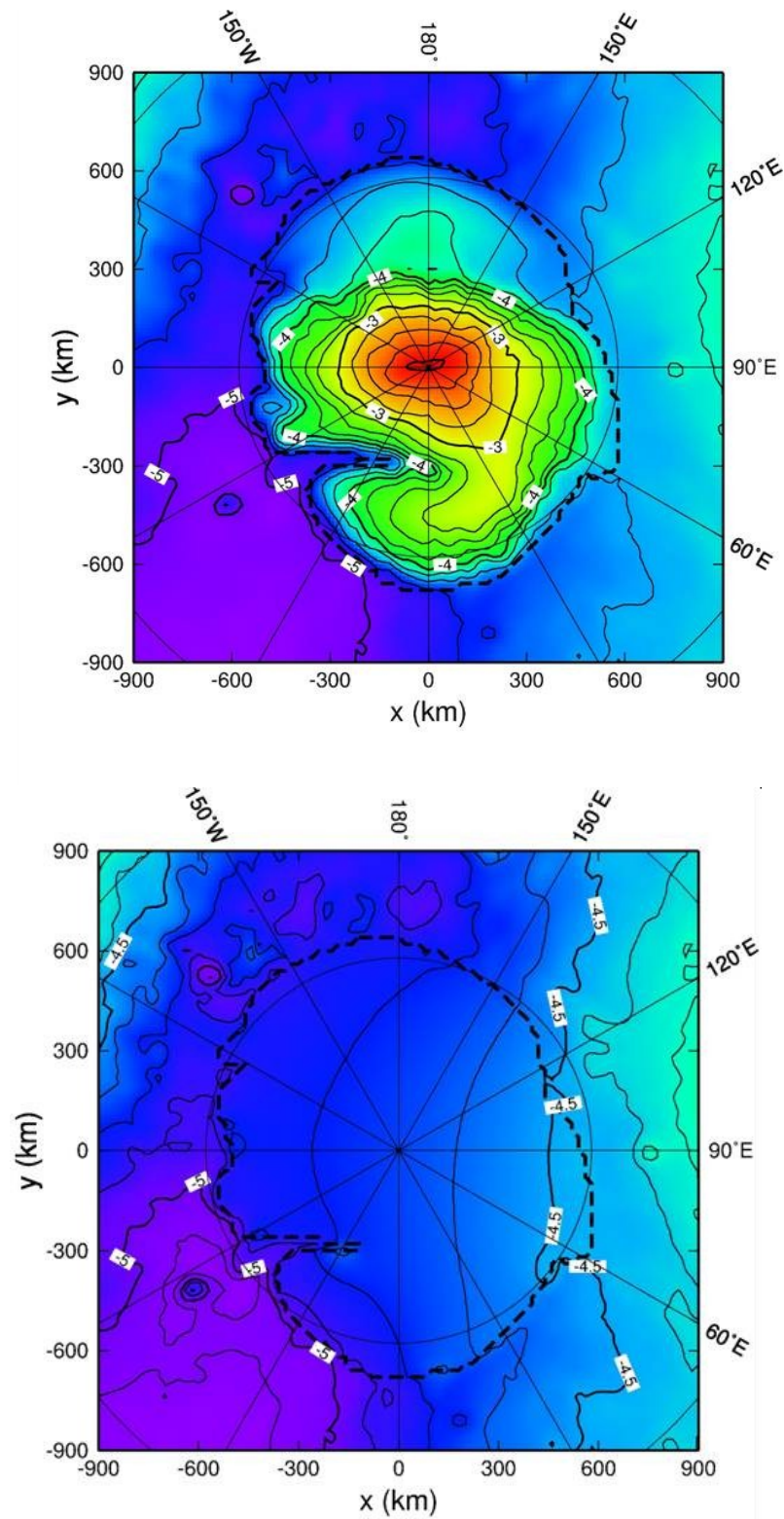
Figure 2.7: Present MOLA topography and equilibrated bedrock topography for the north polar cap

# 3   Climate forcing

## 3.1   Introduction

The last chapter **Ice Model** discusses the basic equations for polythermal ice sheets on which the model SICOPOLIS is based. The model uses the external forcing given by mean annual temperature at the ice surface, surface mass balance and the geothermal heat flux from below which is implemented as a spatially and temporally constant quantity. Since its development the model has been under constant development. Mainly the different climate forcing and other vital upgrading of the model which are done during this research period are discussed. The dust content implemented is also discussed here being important for the ice flow. The ice rheology was already discussed in the previous chapter.

All these climate forcing discussed here along with ice rheology and dust content in the cap have been implemented over the study period. After successful results for north polar cap the model has been also adapted to the south polar cap successfully. Now its possible to study the dynamical and thermodynamical evolution of both the Martian caps with SICOPOLIS.

## 3.2   Climate forcing with the coupler MAIC

For climate forcing the module Mars Atmosphere-Ice Coupler MAIC has been developed. MAIC parameterises the boundary conditions of surface accumulation, ablation and temperature based on the history of solar insolation. Insolation is derived directly by Milankovich (orbital) parameters obliquity and eccentricity. These Milankovich parameters have been computed by Laskar *et al.*, (2002, 2004) for the last 20 million years and future 10 million years with a celestial-mechanical model for the whole solar system. The parameterisations are assembled into the module MAIC to drive SICOPOLIS.

### 3.2.1   Surface temperature

First the approach based on simplified two-cycle obliquity is discussed and then an approach based on "real" obliquity and eccentricity. The obliquity is approximated $\theta$ for the last 4 million years, during which the average was close to the present value $\theta_0 = 25.5°$, by a simplified two-cycle obliquity. Now the main cycle is defined as

$$\theta_t = \theta_0 + \hat{\theta}_t sin \frac{2\pi t}{t_{\text{obl}}^{main}} \tag{3.1}$$

with the period $t_{\text{obl}}^{main} = 125$ ka. The second oscillation which modulates the amplitude of first one is defined as,

$$\hat{\theta}_t = \frac{\hat{\theta}_{\text{max}} + \hat{\theta}_{\text{min}}}{2} - \left( \frac{\hat{\theta}_{\text{max}} - \hat{\theta}_{\text{min}}}{2} \right) cos \frac{\pi t}{t_{\text{obl}}^{main}} \tag{3.2}$$

with the maximum amplitude $\hat{\theta}_{\text{max}} = 10°$, the minimum amplitude $\hat{\theta}_{\text{min}} = 2.5°$ and the period $t_{\text{obl}}^{main} = 1.3$ Ma (cf. Ward (1992), Touma and Wisdom (1993), Laskar *et al.*, (2002)). The resultant obliquity is shown in the Fig. 3.1. The mean insolation for the north pole, $I_{\text{np}}^{in}(t)$, follows from the obliquity $\theta$ and the eccentricity $e$ as

$$I_{\text{np}}^{in}(t) = \frac{I_s}{\pi} sin\theta (1 - e^2)^{-1/2} \tag{3.3}$$

(Kieffer and Zent, 1992) where $I_s = 590$ Wm$^{-2}$ is the solar flux at the average Martian distance from the sun. Since for the regarded period, $0 < e < 0.12$ (Laskar *et al.*, 2002), it is clear that the influence of the obliquity in Eq. (3.3) over weighs by far that of eccentricity, so that $e = 0$ is set for simplicity. By assuming near-steady-state conditions, $I_{\text{np}}^{in}$ can be balanced with the outgoing mean annual long wave radiation, $I_{\text{np}}^{out}$, via

$$I_{\text{np}}^{in}(1 - A) = I_{\text{np}}^{out} \tag{3.4}$$

where $A$ is the albedo. Stefan-Boltzmann law tells us about the energy flux density or total energy radiated per unit surface area of a black body in unit time. The outgoing radiation which is given by Eq. (3.4) can be compared with the temperature as

$$I_{\text{np}}^{out} = \varepsilon \sigma T_{\text{np}}^4 \tag{3.5}$$

where $\sigma = 5.67 \times 10^{-8}$ Wm$^{-2}$K$^{-4}$ is the Stefan-Boltzmann constant, $\varepsilon$ is the emissivity and $T_{\text{np}}$ is the mean annual surface temperature at the north pole. Inserting (3.5) in (3.4) and solving for $T_{\text{np}}$ yields

$$T_{\text{np}}(t) = \left( \frac{I_{\text{np}}^{in}(t)(1 - A)}{\varepsilon \sigma} \right)^{\frac{1}{4}} \tag{3.6}$$

With the albedo A=0.43 (Thomas *et al.* 1992), the emissivity $\varepsilon$ taken as unity and the present insolation $I_{\text{np}}^{in}(0) = 79.96$ Wm$^2$, the present temperature is obtained $T_{\text{np}}(0) = 168.4$ K. The whole temperature history, which varies by ca. 30 K within the considered range of obliquities, is depicted in Fig. 3.1(right ordinate axis). The above albedo and emissivity values are interpreted as long-term averages for the north polar cap, therefore the temporal changes are not accounted for. If an uncertainty of $\Delta A = 0.05$ for albedo and $\Delta \varepsilon = 0.1$ for the emissivity is assumed, the terms $(1 - A)$ and $1/\varepsilon$ in Eq. (3.6) are both affected with relative error of approximately 2.5% for $T_{\text{np}}$. In absolute terms this is approximately $\pm 4$K due to the albedo uncertainty and $+4$K due to the emissivity uncertainty. Here the first approach taken to calculate the mean annual surface temperature $T_s$ was based on the dependency on elevation by an atmospheric temperature lapse rate. So
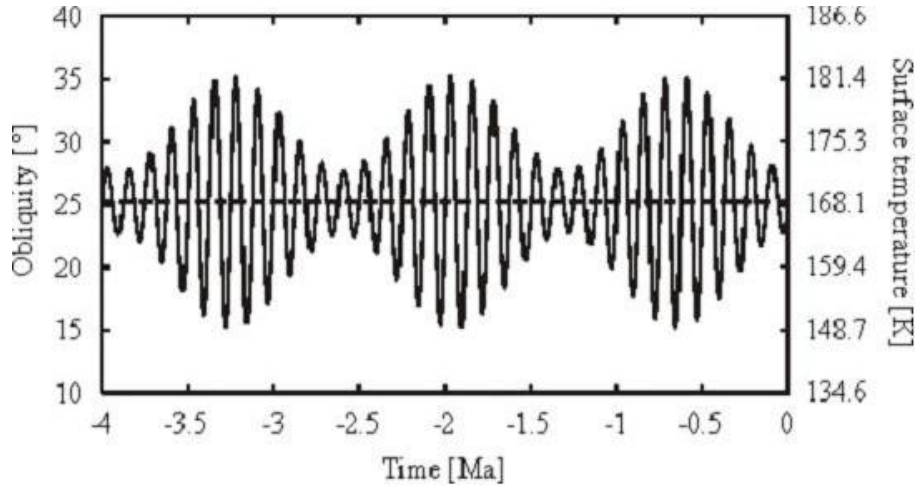
Figure 3.1: Simplified two-cycle obliquity cycle (left ordinate) and resulting mean-annual surface temperature at the north pole (right ordinate) for the last 4 million years

$T_s$ for an arbitrary position $x$, $y$ on the polar cap, $T_s$, is now prescribed similarly to (Greve 2000b) and (Greve *et al.*, 2003).

$$T_s(x,y,t) = T_{np,s}(t) + \gamma_s[h(x,y,t) - h_{np}(x,y,t)(0)] + c_s\tilde{\phi}(x,y) \tag{3.7}$$

where $h$ is the surface topography with respect to the reference geoid, $h_{np}$ is the surface elevation of the north pole, $\tilde{\phi}$ is the co-latitude, and the constants are $\gamma_s = -2.5$ Kkm$^{-1}$ (mean lapse rate) and $c_s = 1.5$ K($^\circ$colat)$^{-1}$. If Eq. (3.7) is decomposed to

$$\begin{aligned} T_s(x,y,t) &= T_{np}(0) + \gamma_s[h(x,y,t) - h_{np}(x,y,t)(0)] + c_s\tilde{\phi}(x,y) \\ &\quad + T_{np}(t) - T_{np}(0) - \gamma_s[h(x,y,t) - h_{np}(t)(0)] \end{aligned} \tag{3.8}$$

the first line is the temperature parameterisation for present conditions, and the second line is the temperature deviation from it.

$$\Delta T_s(t) = T_{np}(t) - T_{np}(0) - \gamma_s[h(x,y,t) - h_{np}(t)(0)] \tag{3.9}$$

In contrast to above approach the second approach is where explicit dependency on elevation by an atmospheric temperature lapse rate is refrained. The reason is that the computation of the north-polar surface temperature according to Eq. (3.6) is based on the idea of a radiation-dominated environment due to the tenuous Martian atmosphere. Because of this, it is consequent to attribute the surface warming off the north pole to the increasing insolation with increasing distance from the north pole (colatitude) and not to the decreasing surface elevation. Therefore the warming is parameterised by the colatitude coefficient only. So now $T_s$ is given as

$$T_s(x,y,t) = T_{np}(t) + c_s\tilde{\phi}(x,y) \tag{3.10}$$

and hence temperature anomaly is given by

$$\Delta T_s(t) = T_{np}(t) - T_{np}(0) \tag{3.11}$$

A suitable value for colatitude coefficient $c_s = 2.25$ K($^\circ$colat)$^{-1}$ is chosen. The surface temperature parameterisation described by Eqs. (3.6) and (3.10) is not influenced directly by the atmospheric pressure variations.

## 3.2.2   Approach based on "real" obliquity and eccentricity

Laskar *et al.*, (2002, 2004) have published a history of Martian obliquity $\theta$ and eccentricity *e* over the last 20 million years and also for the future 10 million years as shown in Fig. 3.2 and 3.3. The authors have computed it with a celestial-mechanics model for the whole solar system. Corresponding to the discussion in the previous section these data sets are used to derive the mean annual insolation and the mean annual surface temperatures in the model domain.
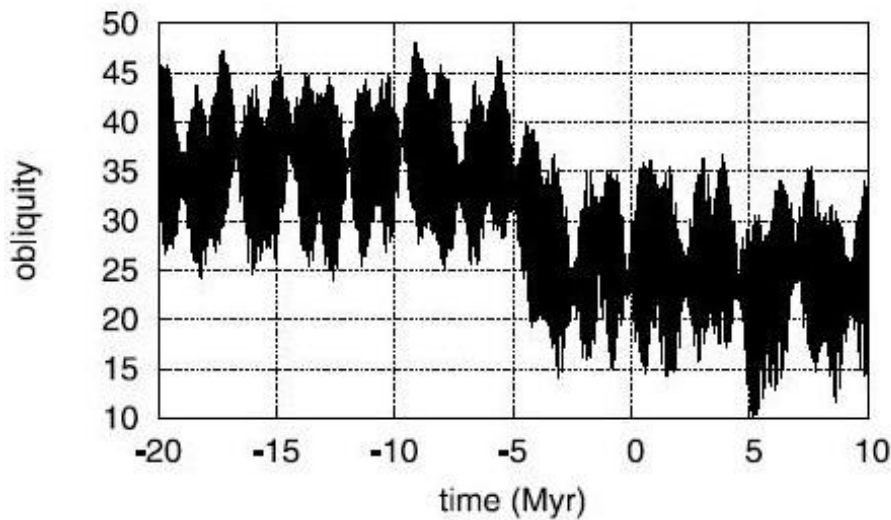


Figure 3.2:  Obliquity in degrees from -20 Ma to +10 Ma (Laskar *et al.* 2004)
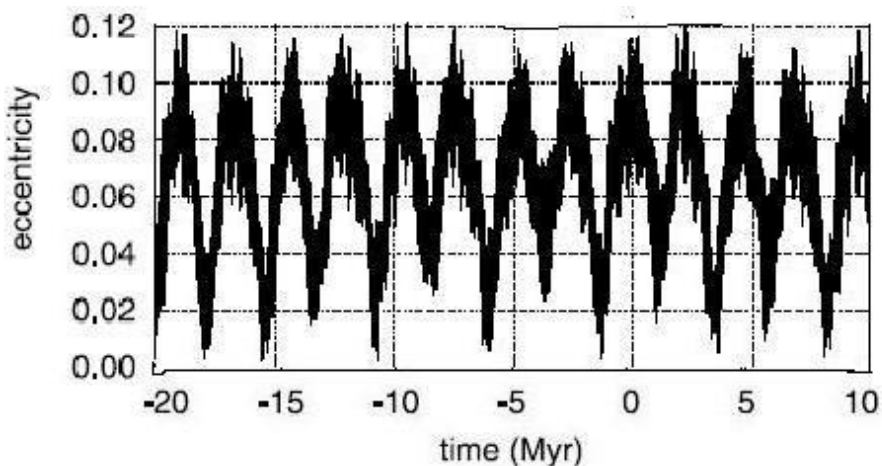


Figure 3.3:  Eccentricity from -20 Ma to +10 Ma (Laskar *et al.* 2004)

## 3.3   Parameterisation based on local insolation

This parameterisation is based on radiative balance. The basic idea behind this is to use the local daily mean insolation. As discussed in the previous section, at near equilibrium, the short wave radiation received by the planet should be in balance with outgoing long wave radiation. The day time mean temperatures can be found out the same way as that of equations (3.4) and (3.5). Instead of annual mean values here daily mean values for the insolation are taken into account. This scheme enables us to find the daily mean surface temperatures globally if the daily mean insolation is known. However it fails to obtain polar night time temperatures due to lack of insolation. In this scheme the insolation $I$ is considered a function of orbital parameters and vernal equinox anomaly. At polar night when the temperature drops down the atmospheric $CO_2$ condenses over the surface. It is assumed that condensation of the atmospheric $CO_2$ keeps the surface temperature at $CO_2$ condensation temperature. The temperatures can reach below $CO_2$ condensation only when all the $CO_2$ in the atmosphere has condensed out, which is unlikely. When the polar night ends condensed $CO_2$ starts evaporating. After the complete $CO_2$ evaporation surface temperature attains radiative equilibrium temperature value. Here the thermal inertia of the surface is neglected. The energy released by $CO_2$ condensation balances the energy radiated away from the surface. The energy balance is given by Stefan-Boltzmann law as,

$$W_{cond} = \int_{t_{\text{dusk}}}^{t_{\text{dawn}}} \varepsilon \sigma T_{\text{cond}}^4 \, dt \tag{3.12}$$

The subscripts *dusk* and *dawn* refers to polar night dusk and polar night dawn. $CO_2$ itself freezes to form dry ice at a temperature around 146 K at the pressures found on Mars. After the polar dawn polar cap starts receiving insolation. The polar cap will be at the $CO_2$ condensation temperature till all the condensed $CO_2$ evaporates. The time span from polar dawn to the time $t$ when all $CO_2$ is evaporated is considered. The first term on the R. H. S. of Eq. (3.13) is the energy received by insolation and the second term is the energy radiated away. The difference in the energy available for the evaporation. When the $CO_2$ has evaporated completely, the energy used up for the evaporation equals the energy previously released by condensation.

$$W_{\text{evap}} = \int_{t_{\text{dawn}}}^{t} (1-A) I \, dt - \int_{t_{\text{dawn}}}^{t} \varepsilon \sigma T_{\text{cond}}^4 \, dt \tag{3.13}$$

Here $I$ is the insolation. When $CO_2$ is completely evaporated after time t then

$$W_{\text{evap}} = W_{\text{cond}} \tag{3.14}$$

The time $t$ at which $CO_2$ evaporates can be obtained by solving the above equation numerically.

## 3.4   Accumulation-ablation rate

The accumulation rate $a_{\text{sat}}^+$ (saturation accumulation) over the north polar cap is assumed to be proportional to the water vapour saturation pressure in the atmosphere $p_{\text{sat}}$, which is

given by the Clausius-Clapeyron relation (Müller 2001),

$$a_{\text{sat}}^{+} \propto p_{\text{sat}}(t) \propto exp\left(-\frac{\lambda}{R_m T_{\text{ref}}(t)}\right) \tag{3.15}$$

with the latent heat $\lambda = \lambda_{sol \to liq} + \lambda_{liq \to vap} = (335 + 2525) \text{ kJkg}^{-1} = 2860 \text{ kJkg}^{-1}$ and the gas constant $R_m = R/M_{\text{H}_2\text{O}} = 8.314 \text{ Jmol}^{-1}\text{K}^{-1} / 18.015 \text{ kgkmol}^{-1} = 461.5 \text{ Jkg}^{-1}\text{K}^{-1}$. The Clausius-Clapeyron relation describes the relationship between the water vapour pressure and the absolute temperature. The vapour pressure increases as the temperature increases so does the water content in the atmosphere. Accumulation rates are related to water vapour pressure since it gives the amount of precipitable water content available in the atmosphere for accumulation. In case of Mars accumulation is in the form of condensation or deposition due to low temperatures but the form of the accumulation is not important for the modelling purpose in this study. The atmospheric reference temperature for the north polar region $T_{\text{ref}}$ is prescribed as

$$T_{\text{ref}}(t) = T_{\text{ref}}^{0}(t) + \Delta T_{\text{s}}(t) \tag{3.16}$$

with the present value $T_{\text{ref}}^{0} = 173\text{K}$. The surface temperature anomaly is given by Eq. (3.11). Note that the term with an atmospheric temperature lapse rate is not present, as elevation dependency is not taken into account as discussed above.

With the present accumulation rate $a_{\text{sat},0}^{+}$ Eqs (3.15) and (3.16) yields

$$a_{\text{sat}}^{+}(t) = a_{\text{sat},0}^{+}(t)exp\left(\frac{\lambda}{R_m T_{\text{ref}}^{0}(t)} - \frac{\lambda}{R_m T_{\text{ref}}(t)}\right) \tag{3.17}$$

which is depicted in Fig. 3.4. Based on different methods (amount of water vapour in the atmosphere, shortage of craters, mass-balance modelling) $a_{\text{sat},0}^{+}$ has been estimated to be of the order of 0.1 mm w.e. a$^{-1}$, here *w.e.* denotes water equivalent, with an uncertainty of a factor 10 in either direction (Kieffer and Zent 1992). Further, it is not clear whether water-ice accumulation takes place mainly as snowfall, or mainly as direct condensation at the surface. However, the form of accumulation is of no importance for this study.
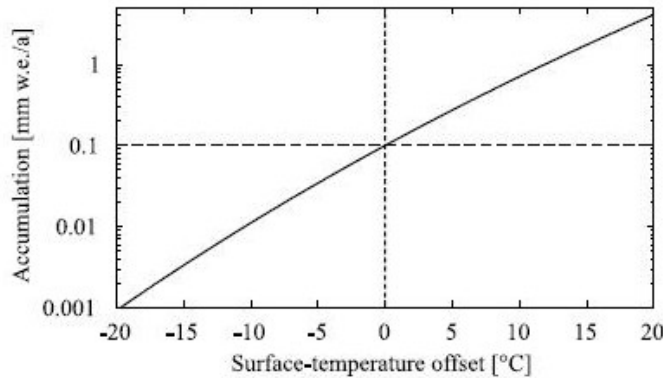


Figure 3.4: Accumulation rate $a_{\text{sat}}^{+}$ as a function of surface temperature anomaly $\Delta T_{\text{s}}$

For the net mass balance, that is, the accumulation-ablation rate $a_{\text{net}} = a_{\text{sat},0}^{+} - a^{-}$ ($a^{-}$ is the ablation rate), two different parameterisations are employed. The first approach

is an equilibrium-line concept dependent on the horizontal distance from the north pole, $d$. This is a widely used approach for terrestrial ice-sheet and glacier problems, and it is employed in the variant of the ice-sheet-modelling inter comparison study by Payne *et al.*(2000). It is given by

$$a_{\mathrm{net}}(x,y,t) = min[a_{\mathrm{sat}}^+(t), g(t) \times (d_{\mathrm{el}}(t) - d(x,y))] \tag{3.18}$$

where $g$ is the accumulation-ablation-rate gradient and $d_{\mathrm{el}}$ the distance of the equilibrium line from the north pole (see Fig. 3.5).
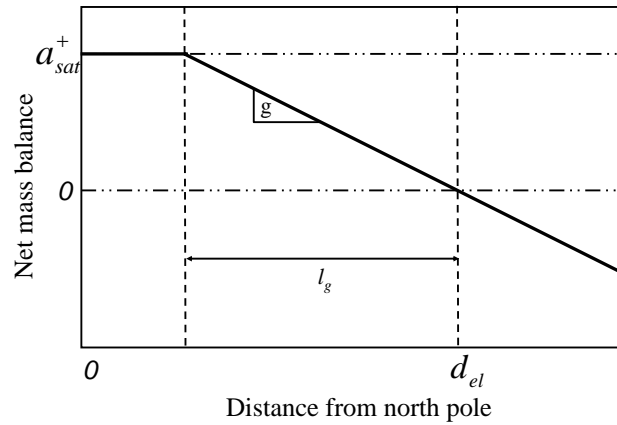


Figure 3.5: Distance dependent parameterisation of the net mass balance (accumulation-ablation rate)

For present conditions, the values of the two parameters $d_{\mathrm{el}}^0$ and $g_0$ should be chosen such that the equilibrium line is close to the ice margin. The interior of the north-polar cap must lie in the accumulation area where $a_{\mathrm{net}} = a_{\mathrm{net},0}^+$. This can be achieved by choosing $d_{\mathrm{el}}^0 = 550$ km and $g_0 = 2.5 \times 10^{-4}$ mm w.e. a$^{-1}$km$^{-1}$. Thus, for $a_{\mathrm{sat},0}^+ = 0.1$ mm w.e. a$^{-1}$ the accumulation area where $a_{\mathrm{net}} = a_{\mathrm{net},0}^+$ lies within $d \leq 150$ km, and the distance from the accumulation area to the equilibrium line is $l_g^0 = 400$ km (Fig. 3.5). For other times, for simplicity and lack of better knowledge it is assumed that $d_{\mathrm{el}}$ is unchanged, so that

$$d_{\mathrm{el}}(t) = d_{\mathrm{el}}^0 \tag{3.19}$$

The gradient $g$ is taken proportional to the accumulation rate,

$$g(t) = g_0 \frac{a_{\mathrm{sat},0}^+(t)}{a_{\mathrm{sat},0}^+} \tag{3.20}$$

so that the size of the accumulation area remains constant, and therefore $l_g(t) = l_g^0 = 400$ km.

## 3.5 Dust Content

Satellite imagery shows that parts of the polar caps appear dark, which indicates that they consist of ice with some amount of mixed-in dust. However, for the average volume

fraction $\varphi$ of dust in the ice no quantitative information is available. For modelling studies of the polar caps this is a serious problem because the dust content can affect the ice flow via direct hardening, an increasing density and a decreasing heat conductivity which leads to basal warming. Hammer *et al.*, (1985) suggests that very small amounts of dust, approximately 1 mg kg$^{-1}$ with particle sizes of 0.1 to 2 $\mu$m can make the ice soft. This softening is attributed to thin films of liquid water which forms around the dust particles and lubricate ice deformation which is true in case of terrestrial ice sheets. However, at the low temperatures expected in the Martian polar caps this effect will not be present and the presence of dust particles will make direct hardening influential. Therefore, the density, $\rho$ and heat conductivity, $\kappa$ of the ice-dust mixture is computed as volume-fraction-weighed averages of the values for pure ice and crustal material,

$$\rho = (1 - \varphi)\rho_i + \varphi\rho_c \tag{3.21}$$

$$\kappa = (1 - \varphi)\kappa_i + \varphi\kappa_c \tag{3.22}$$

where $\rho_i = 910$ kg m$^{-3}$ is the ice density, $\rho_c = 2900$ kg m$^{-3}$ is the density of the crustal material. $\kappa_i = 9.828\,e^{-0.0057T}$ W m$^{-1}$ K$^{-1}$ is the heat conductivity of ice which is a function of temperature T measured in Kelvin. $\kappa_c = 2.5$ W m$^{-1}$ K$^{-1}$ is the heat conductivity of the crustal material (Greve *et al.* 2003). Direct hardening is described by a stress enhancement factor $E_s < 1$ based on laboratory measurements of the deformation of ice-dust compounds.

$$E_s = e^{b\varphi} \tag{3.23}$$

where $b = 2$ (hardening parameter) and $\varphi \leq 0.56$ (Durham *et al.* 1997). This is equivalent to a flow enhancement factor

$$E = E_s = e^{-nb\varphi} \tag{3.24}$$

Hence, for given stress, temperature and grain-size condition and stress exponent $n = 3$ a dust content of 10% ($\varphi = 0.1$) leads to an almost twice as hard material as that of pure ice ($E = 0.55$).

# 4    Steady state simulations

## 4.1    Introduction

The meaning of *steady state* in the title is that this study is carried out keeping the climate conditions steady or constant. As the first phase of the research, the steady state simulations have been carried out. Simulations are done for the present climatic conditions. In this case the obliquity is kept constant over time at its present value $\theta_0 = 25.5°$.

The main purpose to carry out this study is to assess the influence of several different parameters separately on the dynamics of polar caps. Keeping the obliquity constant through out the simulation period is not a realistic scenario, but it serves the purpose of testing the influence of different parameters on the dynamics of the polar cap independently. In this chapter only the set-up for the simulations needed to carry out this study is discussed. The results are discussed separately in the chapter 6.

## 4.2    Simulation set-up

For the simulations carried out the model domain consists of $1800 \times 1800$ square km for the north polar cap and $2400 \times 2400$ square km for the south polar cap. The horizontal resolution can be chosen as 40 km or 20 km in the stereographic plane with the standard parallel 71° N/S and the vertical resolution is 21 grid points in the cold ice column and 11 grid points in the lithosphere column. 11 grid points are chosen for the temperate ice column if it exists.

In the first stage of the research the ice mechanics or the ice flow is described by the standard values used for the terrestrial Greenland ice sheet simulation. Hence the power law exponent in the Eq. (2.1) is $n = 3$ and flow enhancement factor $E = 3$. At later stage of the research different flow laws are implemented for the different stress, strain-rate and the different temperate regimes.

At this stage the composition of the ice is only water with no dust inside. The terrestrial values for power law exponent and flow enhancement factor includes the influence of small amount of dust $\sim 0.1 - 0.2\,\mu$m. This was measured in the Wisconsin-ice-age part of the ice core Dye 3 in south Greenland (Hammer *et al.*, 1985). Ice with $E = 3$ is more deformable than that of $E = 1$ (Paterson 1991) .

For this study, the simulations are started at ice free conditions. The ground is isostatically equilibrated. At the ice-bedrock interface, no-slip conditions are adopted independent of the basal temperature. Due to large obliquities in the past (Laskar *et al.*, 2002, Jakosky *et al.*, 1993) there may have been strongly increased sublimation rates between 10 and 5 Ma BP. It is highly likely that the north polar cap did not survive this period.

This is the reason to choose the ice free condition for the study. The value of geothermal heat flux $q_{\text{geo}} = 35$ mW m$^{-2}$ is taken as standard value. (Budd *et al.*, 1986, Schubert *et al.*, 1992). This value is about the 2/3 of the terrestrial geothermal heat flux. The standard value for the fraction of isostatic compensation is taken as $f_{\text{iso}} = 0.65$. This value is approximately 2/3 of full local compensation. This value is found out to be likely estimate in a separate study (Greve *et al.*, 2003) which uses more sophisticated viscoelastic multi-layer ground model.

## 4.3   Influence of different parameters

The simulation carried out as reference simulation is called the standard set and the parameters used for this set are shown in Table 4.1. To assess the influence of different parameters additional simulations are run. The parameters which influences is assessed are the geothermal heat flux, the flow enhancement factor in the flow law, the fraction of isostatic compensation and the accumulation rate. The varied values of these parameters are shown in Table 4.2.

The constant value of the obliquity (current value $\theta_0 = 25.5°$) gives the surface temperature at the north pole $T_{\text{np}} \approx 168.4$ K $= -105°$C with climate forcing MAIC (Sec. 3.2). The temperature anomaly $\Delta T_s(t) \equiv 0$ (Eq. 3.11). For temperature parameterisation in Eq. (3.7) the value of colatitude factor $c_s$ is taken as 2.25 K($°$colat)$^{-1}$ and $\gamma_s = 0$. This enables for the temperature to be dependent only on the colatitude factor $c_s$. The standard set showed in Table 4.1 uses the first approach discussed in section (3.4) for parameterising the accumulation and ablation. The set of parameters used are $a_{\text{sat}}^+ = 0.1$ mm w.e. a$^{-1}$, $d_{\text{el}}$ = 550 km for the north polar cap and 650 km for the south polar cap. The mass balance gradient $g = 2.5 \times 10^{-4}$ mm w.e. a$^{-1}$km$^{-1}$.

Gradually a polar cap is built which resembles the present maximum surface elevation. The present topography for both the north and the south polar cap is obtained from MOLA. The simulations are carried out for 500 million years (Ma) with time step of 10 ka. The 500 Ma long time span enables the polar cap to reach the dynamic and thermodynamic equilibrium. The ice temperature, velocity and bottom topography are allowed to grow freely until the steady state is reached.

## 4.4   Different flow laws and dust content

In the second phase of research the effect of the different ice rheologies and the different amount of dust content is investigated. Detailed discussion of this can be found out in the sections (2.1.2) and (3.5). For the steady state, the simulations are done for the Glen's law ($n = 3$) since it is the generalised flow law for for terrestrial ice sheet (Paterson 1994). In section (3.5) a dust content of 20% or $\varphi = 0.2$ is chosen for both the south and the north polar caps (Hvidberg 2003). The detailed transient simulations about all the flow laws and range of dust content are carried out for which are discussed separately.

For testing the flow laws, both the parameterisation schemes discussed for ice-atmosphere coupling, MAIC in the section (3.2) and scheme based on local insolation in section (3.3) are used. Table 4.3 shows the standard physical parameter set used for the scheme MAIC.

| Quantity | Value |
|---|---|
| Acceleration due to gravity, $g$ | $3.72 \text{ ms}^{-2}$ |
| Density of ice, $\rho$ | $910 \text{ kgm}^{-3}$ |
| Power law exponent, $n$ | 3 |
| Flow enhancement factor, $E$ | 3 |
| Heat conductivity of ice, $\kappa$ | $9.828 e^{-0.0057 T[K]} \text{ Wm}^{-1}\text{K}^{-1}$ |
| Specific heat of ice, $c$ | $(146.3 + 7.253 \text{ T[K]}) \text{ Jkg}^{-1}\text{K}^{-1}$ |
| Latent heat of ice, $L$ | $335 \text{ kJkg}^{-1}$ |
| Clausius-Clapeyron gradient, $\beta$ | $3.3 \times 10^{-4} \text{ Km}^{-1}$ |
| Geothermal heat flux, $q_{\text{geo}}$ | $35 \text{ mWm}^{-2}$ |
| Fraction of isostatic compensation, $f_{\text{iso}}$ | 0.65 |
| Isostatic time lag, $\tau_{\text{iso}}$ | 3000 years |
| Asthenosphere density, $\rho_a$ | $3300 \text{ kgm}^{-3}$ |
| Density $\times$ specific heat of the lithosphere, $\rho_r c_r$ | $2000 \text{ kJm}^{-3}\text{K}^{-1}$ |
| Heat conductivity of the lithosphere, $\kappa_r$ | $3 \text{ Wm}^{-1}\text{K}^{-1}$ |

Table 4.1: Standard parameters

Unlike the north polar cap where the simulations begin at the ice free condition, for the south polar cap it starts at the present MOLA topography. The surface of the south polar cap appears rugged and is much older ($7 - 15 \times 10^6$ yr) than the north polar cap ($\sim 100 \times 10^3$) (Fishbaugh and Head, 2001). The rugged and cratered surface of the south cap gives the hint that the cap is less dynamic on longer time scales of the climate cycles. This goes in favour of choosing the current topography as initial conditions for the south cap at all the time.

When the scheme based on local insolation is used (Sec. 3.3) for temperature parameterisation, the results are matched quite well with that of the Martian Climate Database (Lewis *et al.*, 1999). Both Martian Climate Database and scheme based on local insolation fail in producing the $CO_2$ cover observed on the residual south polar cap through out the year. Therefore the south polar cap's mean annual temperature is corrected so that it is equal to the $CO_2$ sublimation temperature, $-128°C = 145$ K within $85°$S. For the insolation, $I$, the daily mean values are used. The south polar cap is treated as a water ice and dust. Possible presence of some amounts of $CO_2$ ice and $CO_2$ clathrate hydrate is not considered. Due to its low strength $CO_2$ ice can not be the main constituent of the south polar cap and can occur only in small amount. Hence neglected for modelling purpose (Nye *et al.*, 2000).

| Simulation | Parameter variation |
|---|---|
| # 1 | Standard set |
| # 2 | $a_{\mathrm{sat}}^+ = 1$ mm w.e. a$^{-1}$, $g = 2.5 \times 10^{-3}$ mm w.e. a$^{-1}$ km$^{-1}$ |
| # 3 | $a_{\mathrm{sat}}^+ = 0.01$ mm w.e. a$^{-1}$, $g = 2.5 \times 10^{-5}$ mm w.e. a$^{-1}$ km$^{-1}$ |
| # 4 | $q_{\mathrm{geo}} = 20$ mW m$^{-2}$ |
| # 5 | $q_{\mathrm{geo}} = 50$ mW m$^{-2}$ |
| # 6 | E $= 0.3$ |
| # 7 | E $= 30$ |
| # 8 | $f_{\mathrm{iso}} = 0$ |
| # 9 | $f_{\mathrm{iso}} = 1$ |

Table 4.2:  Steady state simulation set up

| Quantity | Value |
|---|---|
| Solar flux at average distance Sun-Mars, $I_s$ | 590 Wm$^{-2}$ |
| Albedo, $A$ | 0.43 |
| Emissivity, $\varepsilon$ | 1 |
| Stefan Boltzmann constant, $\sigma$ | $5.67 \times 10^{-8}$ Wm$^{-2}$K$^{-4}$ |
| Colatitude temperature coefficient $c_s$ | 2.25 K($^\circ$colat)$^{-1}$ |
| Latent heat of sublimation of water , $\lambda$ | 2860 kJkg$^{-1}$ |
| Material gas constant for water, $R_m$ | 461.5 Jkg$^{-1}$K$^{-1}$ |
| Present atmospheric reference temperature, $T_{\mathrm{ref}}^0$ | 173 K |
| Equilibrium line distance (north polar cap), $d_{\mathrm{el}}$ | 550 km |
| Equilibrium line distance (south polar cap), $d_{\mathrm{el}}$ | 650 km |
| mass-balance-gradient parameter, $l_g$ | 400 km |

Table 4.3: Standard physical parameters of the atmosphere-ice coupler MAIC

# 5 Transient simulations

## 5.1 Introduction

Transient simulations are carried out over climate cycles which are more realistic than assuming a steady state climate. Like steady state simulations for the first phase of research, influence of different parameters on the dynamics of the north polar cap are assessed. The model domain, grid points and simulation set up for the transient simulations are same as those for steady state simulations (Sec. 4.2). The main difference between these two types of simulations is they are carried out with and without a climate cycle. In this chapter only the set-up for the simulations needed to carry out this study is discussed. The results are discussed separately in chapter 6.

## 5.2 Influence of different parameters

The simulation carried out as reference simulation is called the standard set and the parameters used for this set are shown in Table 4.1. This part of the experiment is done only for the north polar cap. Like in steady state simulations, the standard set for temperature parameterisation in Eq. (3.7) the value of colatitude factor $c_s$ is taken as $2.25\,\mathrm{K}(^\mathrm{o}\mathrm{colat})^{-1}$ and $\gamma_s = 0$. The set of parameters used for accumulation-ablation are $a_{\mathrm{sat}}^+ = 0.01$ mm w.e. $\mathrm{a}^{-1}$ and $d_{\mathrm{el}} = 550$ km for the north polar cap. The mass balance gradient is $g = 2.5 \times 10^{-4}$ mm w.e. $\mathrm{a}^{-1}\mathrm{km}^{-1}$. For other parameters describing time dependence, the equilibrium line distance $d_{\mathrm{el}}$ is kept at present value. With $d_{\mathrm{el}}$ fixed the accumulation-ablation-rate slope $g$ varies with the saturation accumulation $a_{\mathrm{sat}}^+$. The transient simulations start from ice free initial condition too. The temperatures are derived from the parameterisation MAIC with the simplified two cycle obliquity (Sec. 3.2). An additional simulation is conducted with present MOLA topography as initial condition. The simulations are carried out for 100 Ma with the time step of 10 ka. The reason behind choosing MOLA topography as initial condition is to study the future behaviour of present north polar cap with varying climate.

## 5.3 Different flow laws and dust content

### 5.3.1 Approach based on "real" obliquity cycle

First two paragraphs of this section are addressed to the north polar cap and the last one to the south polar cap. The influence of the applied flow laws and the average dust content

on the dynamics of the ice cap is studied. Due to large obliquities in the past (Laskar *et al*., 2002, Jakosky *et al*., 1993) there may have been strongly increased sublimation rates between 10 and 5 Ma BP. It is highly likely that the north polar cap did not survive this period. The present cap most likely started to build up its present form from ice free initial conditions at 5 Ma BP. This scenario has been used to carry out the simulation. It starts with ice free initial condition at 5 Ma BP and then it is runs until present. The present accumulation rate $a^+_{\text{sat},0}$ (Eq. 3.17) is adjusted such that the simulated north polar cap reaches the present maximum surface elevation (MOLA value) in 5 Ma. To find out the exact value of $a^+_{\text{sat},0}$ a number of simulations are run with different values of $a^+_{\text{sat},0}$ till the value fits the the requirement. For different flow laws and varying dust content two series of simulations are carried out. The temperatures are derived from the parameterisation MAIC (Sec. 3.2). For the obliquity the approach based on the "real" obliquity (Sec. 3.2.2) is used. The reference run is done with Glen's flow law with the power law exponent in the Eq. (2.1) $n = 3$ and without any dust content or $\varphi = 0.0$ in section (3.5).

In the first series different flow laws are tested. Glen's flow law is replaced by Durham's flow law ($n = 4$). The Goldsby and Kohlstedt flow law ($n = 1.8, p = 1.4$) is tested for two different grain sizes $d = 1$ mm and $d =10$ mm (Eq. 2.1). In the second series dust content is increased initially from zero to $10\%, 20\%, 30\%, 40\%$ and $50\%$. For all the simulations the present accumulation rate $a^+_{\text{sat},0}$ is adjusted such that the north polar cap reaches its present maximum surface elevation in 5 Ma. The accumulation rate is in ice equivalent for the zero dust content runs. The runs with non-zero dust content have the accumulation rate in ice and dust equivalent.

As stated earlier the present south polar cap is much older than the north polar cap. Hence the present MOLA topography is taken as initial condition for its simulation. The standard set for temperature parameterisation in Eq. (3.7) the value of colatitude factor $c_s$ is taken as $1.0 \text{ K} (^{\text{o}}\text{colat})^{-1}$ and $\gamma_s = 0$. The set of parameters used for accumulation-ablation are $a^+_{\text{sat}} = 0.01$ mm w.e. $\text{a}^{-1}$, $d_{\text{el}} = 650$ km. The mass balance gradient for the south polar cap is taken as $g = 2.0 \times 10^{-4}$ mm w.e. $\text{a}^{-1}\text{km}^{-1}$. The Glen's flow law is tested with $20\%$ dust content. This study is done for the temperatures derived by the schemes MAIC (Sec. 3.2) and daily mean local insolation cycle (Sec. 3.3). In both these cases the "real" obliquity approach is used. The scheme based on daily local insolation is unable to produce the $CO_2$ cover observed on the residual south polar cap. Therefore the south polar cap mean annual temperature is corrected so that it is equal to $CO_2$ sublimation temperature $-128°$ C = 145 K within 85°S. The present accumulation rate is $a^+_{\text{sat}} = 0.1$ mm w.e. $\text{a}^{-1}$ (Budd *et al*., 1986, Kieffer 1990) to study how the south polar cap reacts to the climate cycles in the past 10 Ma BP. For the south polar cap the simulations are carried out for the last 10 Ma. The simulations start at initial time -10 Ma BP and are run till the time reaches $t = 0$, indicating present time. This time setup gives the chance to check the influence of climate cycle on the dynamics of the south polar cap.

## 5.3.2 Approach based on simplified two cycle obliquity

The evolution of the north polar cap is studied for the temperatures derived by the scheme MAIC (Sec. 3.2) with a simplified two cycle obliquity approach. The set of parameters used is shown in Table 4.3 For different flow laws and varying dust content two series of simulations are carried out. In the first series different flow laws are tested. Glen's

flow law is replaced by Durham's flow law ($n = 4$). The Goldsby and Kohlstedt flow law ($n = 1.8, p = 1.4$) is tested for two different grain sizes $d = 1$ mm and $d = 10$ mm (Eq. 2.1). In the second series zero dust content is increased to $10\%, 20\%, 30\%, 40\%$ and $50\%$. Simulations are started with initial ice free conditions and carried out for 100 Ma with 10 ka time step.

For the evolution of north polar cap another series of simulations is carried out with temperatures derived from the scheme based on daily local insolation (Sec. 3.3). Here too an approach based on the simplified two cycle obliquity is used. It is not necessary to correct the mean annual temperatures for this case since $CO_2$ cover is not observed through out the year. The flow law used here is the Glen's flow law and and 20% dust content is used (Hvidberg 2003). Simulations are started with initial ice free conditions and carried out for 100 Ma with 10 ka time step.

# 6 Results and discussion

## 6.1 Introduction

The results for the simulation runs with the set-up discussed in the previous two chapters are summarised here. The two small subsections below give a brief idea about the types of forcing used, varied parameters, different approaches used for obliquity for the simulations carried out. The whole study has been done for the two type of simulations,

    i. Steady state simulations: The time varying climate is not taken into the account.

    ii. Transient simulations: Climate cycle varying with time is considered.

### 6.1.1 Steady state simulations

The steady state simulations are carried out as the first phase of the research work for the north polar cap. The main purpose to carry out steady state simulations is to asses the sensitivity of several parameters separately on the dynamics of the polar cap. The parameters under consideration for this experiment are (i) geothermal heat flux $q_{\text{geo}}$, (ii) flow enhancement factor $E$ in the flow law given in Eq. (2.1), (iii) fraction of isostatic compensation $f_{\text{iso}}$ and (iv) accumulation rates $a_{\text{sat}}^{+}$. All the steady state simulations also aim at checking when the north polar cap reaches equilibrium or steady state. All the runs are started with an initial ice free condition and are continued till the newly built cap reaches its equilibrium.

### 6.1.2 Transient simulations

Transient simulations gives the more realistic scenario since climate cycles are taken care of. These simulations are carried out for both the polar caps south and north. Two approaches are used for the obliquity cycle for both the north and south polar cap: (i) An approach based on a simplified two cycle obliquity (Sec. 3.2.1). This approach enables to run the simulations on longer time scales to study the effect of long term average climate. (ii) An approach based on reconstructed "real" obliquity (Sec. 3.2.2). The realistic obliquity data is available for the last 10 Ma by Laskar *et al.*, (2004) calculated using a celestial model. With this data available, it is possible to get insight into the response of the polar caps to the recent past climate.

Two approaches for temperature parameterisation schemes are used: (i) The approach based on mean annual insolation using radiative balance (Sec. 3.2), (ii) The approach based on local daily mean insolation (Sec. 3.3). This approach enables to calculate the surface temperatures globally if the local mean insolation is known.

The generalised flow laws are used (see Sec. 2.1.2). In the beginning only Glens flow law, which is used in most terrestrial ice sheet models, was used in the model.

Goldsbdy and Kohlstedt (1997) and Durham (1998) suggest that ice has a different behaviour under different temperature and stress regimes. Hence the simulations are done with different flow laws implemented for the different stresses, strain-rate and the different temperature regimes. First Glen's flow law is tested ($n = 3$). Secondly Glen's flow law is replaced by Durham's flow law ($n = 4$). Goldsby and Kohlstedt flow law ($n = 1.8, p = 1.4$) is tested for two different grain sizes $d = 1$ mm and $d = 10$ mm (Eq. 2.1).

Satellite imagery shows that parts of the polar caps appear dark, which indicates that they consist of ice with some amount of mixed-in dust. However, for the average volume fraction $\varphi$ of dust in the ice no quantitative information is available for modelling studies of the polar caps. The dust content is prescribed in terms of density and heat conductivity. For the simulations dust content is increased from initially zero to $10\%, 20\%, 30\%, 40\%$ and $50\%$. This makes it possible to study the behaviour of polar caps consisting water ice and dust.

## 6.2   Steady state simulations

### 6.2.1   Reference simulation: North Polar Cap

For the steady state the simulation, the set-up is stated in the chapter 4. In this section the influence of the different parameters on the dynamics of the north polar cap is discussed. Due to large obliquities in the past (Laskar *et al.*, 2002, Jakosky *et al.*, 1993) there may have been strongly increased sublimation rates between 10 and 5 Ma BP. It is highly likely that the north polar cap did not survive this period. This is the reason to choose the ice free condition for the experiment.

The evolution of the total ice volume and the ice covered basal area are shown in Fig. 6.1 for the standard steady state run. The ice volume increases linearly for the first 100 Ma. It reaches its steady state value of $5.62 \times 10^6$ km$^3$ after 250 Ma. The ice covered basal area shows a different behaviour than the total volume. Over the first 50 Ma it remains essentially constant at $1.00 \times 10^6$ km$^2$. This coincides with the area with a positive mass balance. Positive mass balance means the accumulation is more than the ablation, making their difference positive. After 50 Ma the area of the ice cap starts increasing. Due to increase in the ice flow the cap starts spreading into the ablation zone making its area grow. Finally at about 250 Ma its steady state value of $2.19 \times 10^6$ km$^2$ is reached. At this steady state stage it is clearly evident that both the total volume and ice covered basal area of the north polar cap have much higher values than the current values. The present values of the volume and area are estimated as $1.2 - 1.7 \times 10^6$ km$^3$ and $10^6$ km$^2$ respectively from the MOLA topography (Zuber *et al.*, 1998, Smith, *et al.*, 1999).
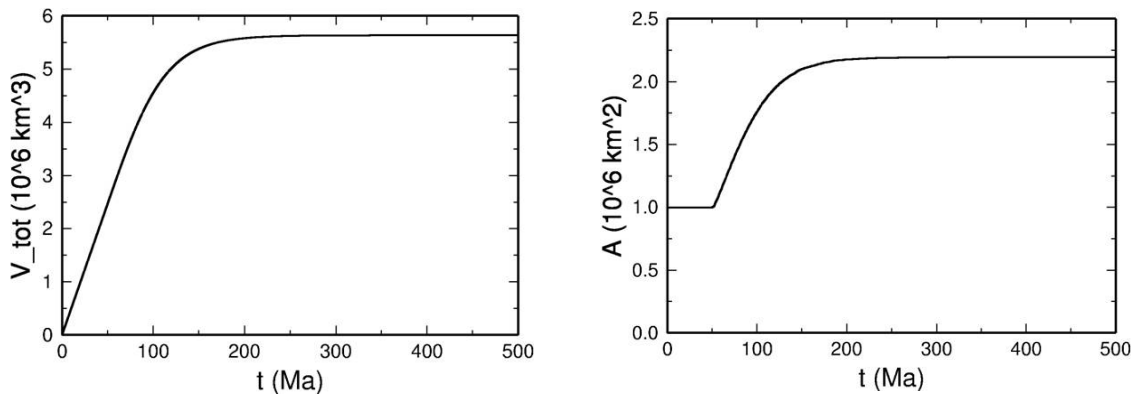
Figure 6.1: Steady state simulation, standard set. Total ice volume $V_{tot}$ (km$^3$) and ice covered basal area $A_{i,b}$ (km$^2$) as functions of time $t$.

The obliquity cycles have time scales of 125 ka and 1.3 Ma (Ward 1992). Hence the real Martian climate would not have been constant for a period as long as 250 Ma. The time taken for the cap to reach its steady state is many times higher than the orbital parameter cycle so the steady state obtained is unrealistic. Hence it is clear that the north polar cap can not be in a steady state condition. The simulations are started with a initial ice free condition. The build-up time $t_{build}$ is defined as follows for the present cap. The build up time is the time taken by the north polar cap to reach the MOLA value for present maximum surface elevation, $h_{max}$. The MOLA value of $h_{max}$ is 1.95 km. For the standard steady state run the build-up time is $t_{build} = 29.66$ Ma. Simulated surface topography, surface velocity and the basal temperature relative to pressure melting for the build-up time $t_{build} = 29.66$ Ma are shown in Figs. 6.2, 6.3 and 6.4 respectively. The over all shape and extent of the cap agree well with that of the MOLA topography. The valley like structure Chasma Borealis, and structures like the canyon cutting through the western part of the cap or the spiralling scarps and troughs are not reproduced. This is due to the climate forcing which is applied axi-symmetric with respect to the north polar cap. The only possible source for non axisymmetric structure is the applied bedrock topography.

The ice flow velocity reaches a maximum value of 1.162 mm a$^{-1}$. This is four to five orders of magnitude less than the terrestrial ice sheet values. The ice flow velocity is slightly larger in the western hemisphere than in the eastern hemisphere. This is due to the fact that in the west the bedrock elevations are lower so the ice thickness is higher. Basal temperatures relative to pressure melting are always below $-65°$C or 208 K which is well below the melting point of the ice. Therefore the temperate ice and liquid water can not occur anywhere in the ice cap. The north polar cap is assumed to be in a steady state for time $t \geq 250$ Ma. Its topography at this stage shows a much larger cap than the present one.
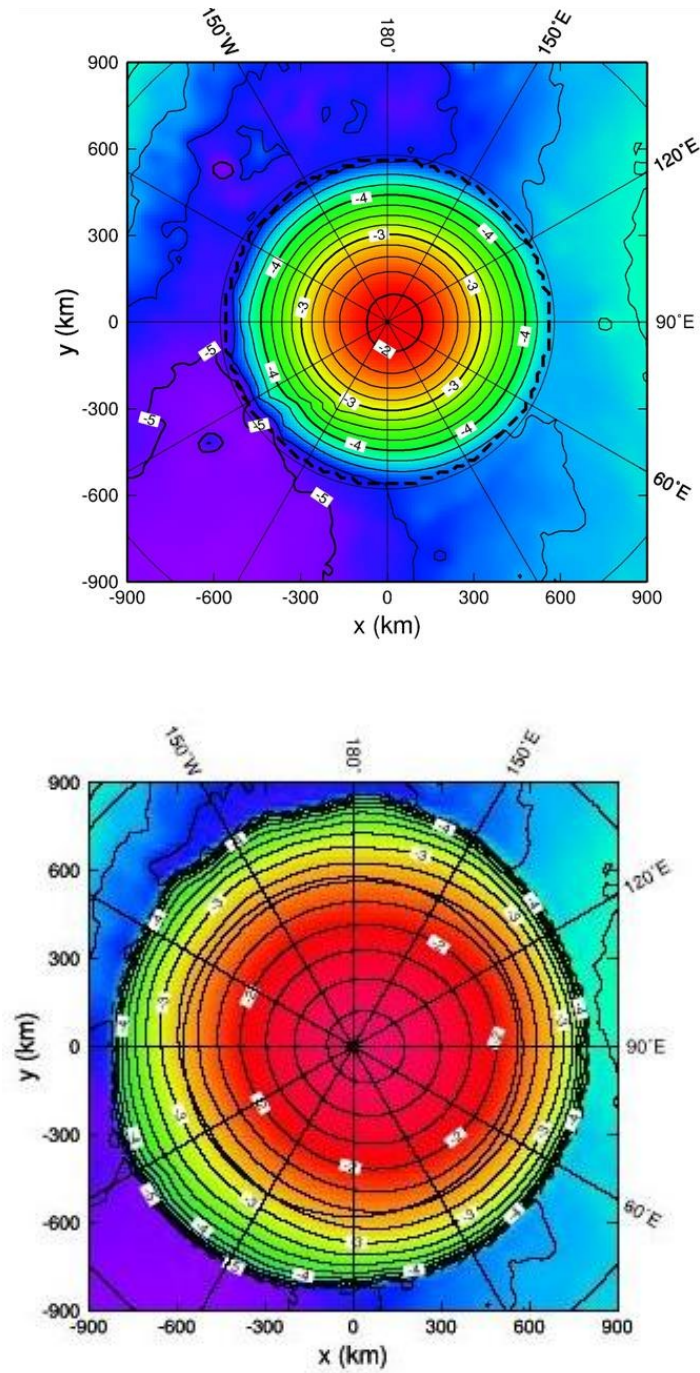
Figure 6.2: Surface topography (km) for the steady state simulation for the time $t_{\text{build}} = 29.66$ Ma (top) and for 500 Ma (Topography is with respect to reference geoid).
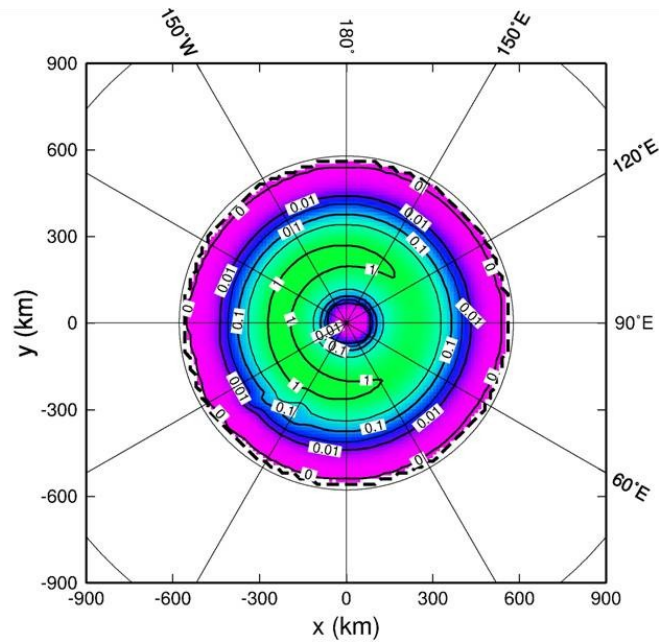
Figure 6.3: Surface velocities (mm/a) for the steady state simulation for the time $t_{build}$ = 29.66 Ma.
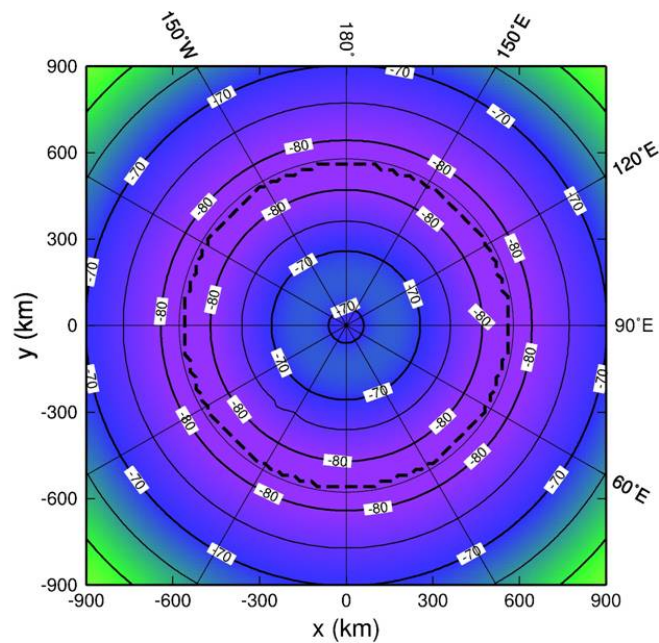


Figure 6.4: Basal temperature relative to pressure melting point (°C) for the steady state simulation for the time $t_{build}$ = 29.66 Ma.

## 6.2.2 Influence of different parameters: North Polar Cap

The results of the parameter studies (Table 4.2) are summarized in Figs. 6.5 and 6.6.

The build-up time $t_{build}$ is most sensitive to the saturation accumulation $a_{sat}^+$. Saturation accumulation is directly responsible for the ice cap growth. The ice flow, which is extremely slow, does not influence the build-up times significantly so the static relation $t_{build} \propto 1/a_{sat}^+$ holds approximately. This finding is supported by the fact that even strong variations in the geothermal heat flux $q_{geo}$ and the flow enhancement factor $E$ in the flow law given in Eq. (2.1) have little influence on the build-up time (see Fig. 6.5). Whereas the geothermal heat flux $q_{geo}$ and the flow enhancement factor $E$ have a strong influence on the ice flow (see Fig. 6.6). More important is the effect of the fraction of isostatic compensation $f_{iso}$ on the build-up time. Its value is varied over the full possible range between no compensation to full compensation i.e. 0% to 100%. The increased isostatic compensation is responsible for bedrock lithosphere to be more depressed in to the asthenosphere underneath. With increased isostatic compensation the north polar cap need to build more thickness to reach the target MOLA surface elevation $h_{max}$ = -1.95 km. Since the more ice thickness is required to build the ice cap this results into more build-up time. In contrast to build-up times the maximum surface velocities $v_{s,max}$ (see Fig. 6.6) are more sensitive to the variations of the investigated parameters. However in all the cases surface velocities fall in the interval between 0.25 mm a$^{-1}$ and 5 mm a$^{-1}$. These values are very small in absolute terms and as compared to the terrestrial ice sheet values.
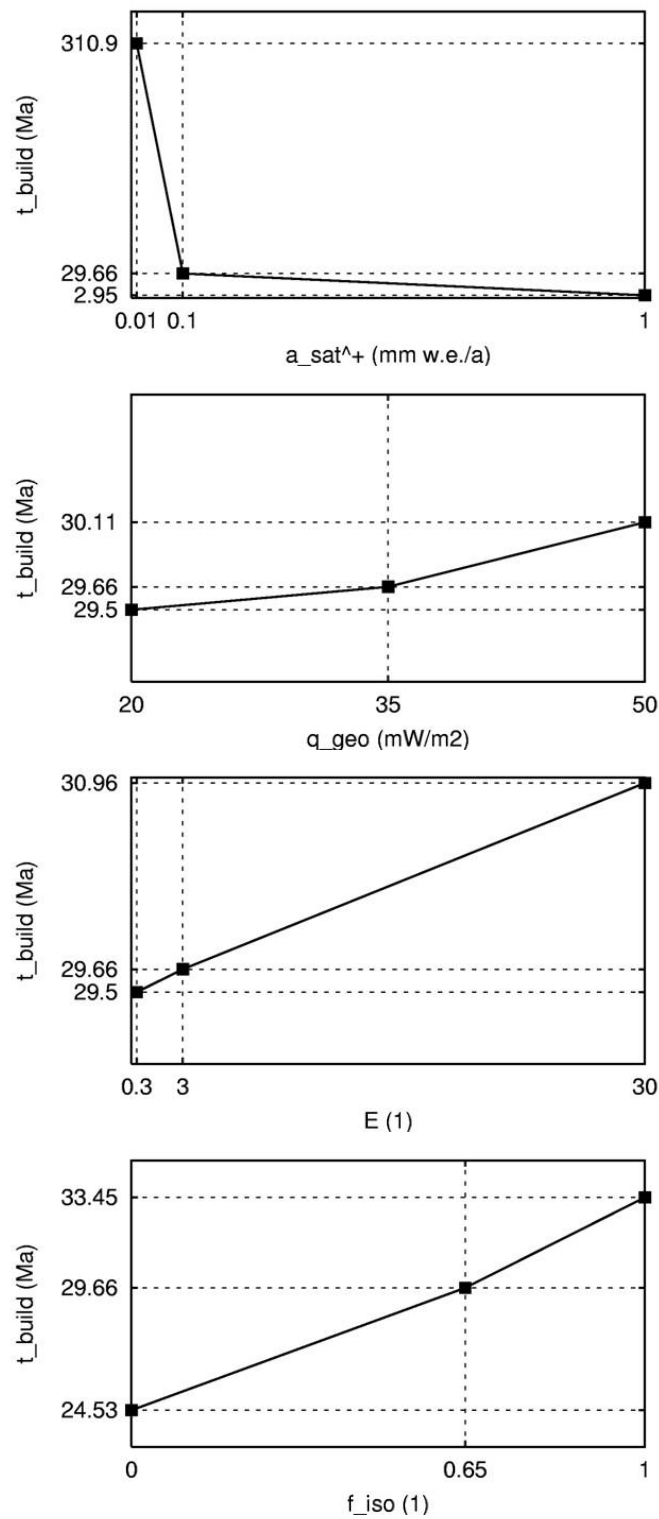
Figure 6.5: Steady state simulation: Build-up time $t_{\text{build}}$ (Ma) as a function of saturation accumulation $a_{\text{sat}}^+$, geothermal heat flux $q_{\text{geo}}$, flow enhancement factor $E$ and the isostatic compensation $f_{\text{iso}}$ .
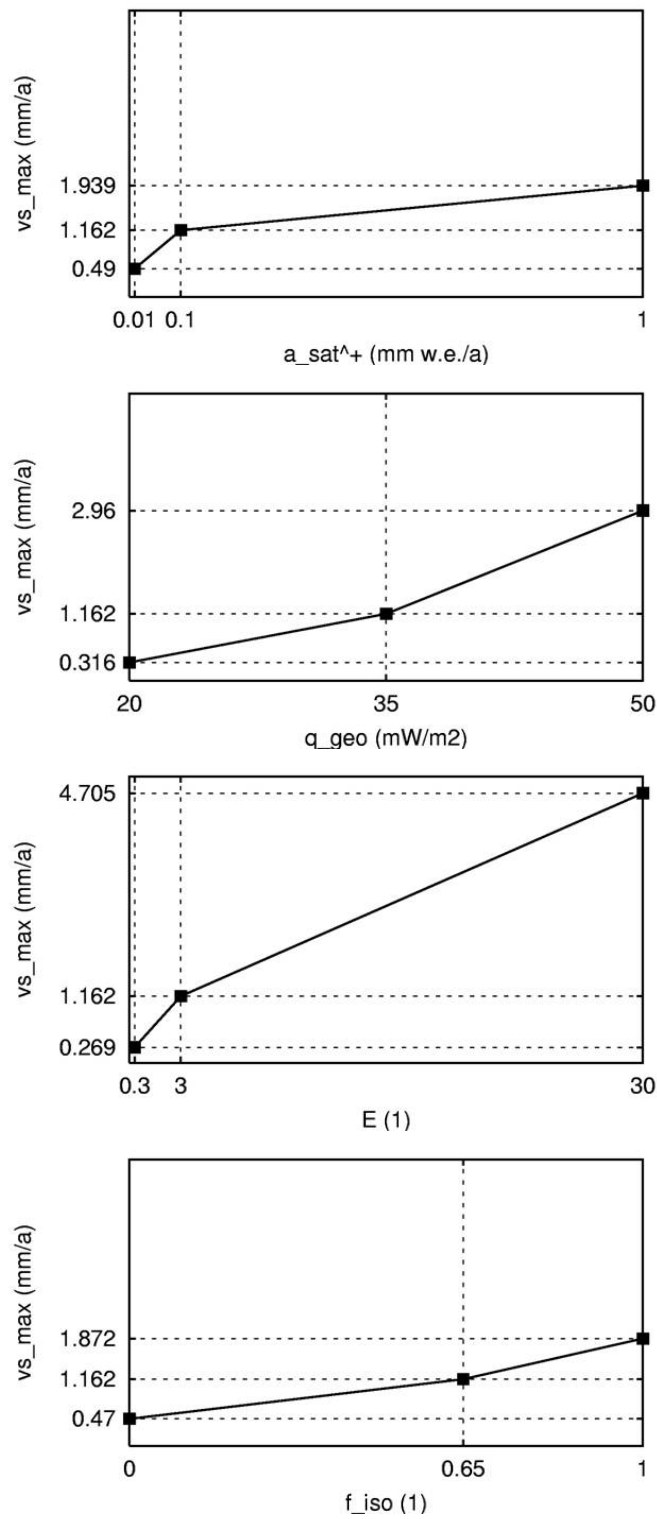
Figure 6.6: Steady-state simulation: Maximum surface velocity $v_{s,max}$ (mm/a) as a function of saturation accumulation $a_{sat}^+$, geothermal heat flux $q_{geo}$, flow enhancement factor $E$ and the isostatic compensation $f_{iso}$ .

# 6.3   Transient simulations

## 6.3.1   Approach based on simplified two cycle obliquity: North Polar Cap

### 6.3.1.1   Ice free initial condition:

First the transient simulation runs with the initial ice free conditions are discussed. The evolution of the total ice volume and the ice covered basal area are shown in the Fig. 6.8 for the standard transient simulation run. Both the curves are very much similar to those of steady state run. The ice covered area of the cap remains constant with value $10^6$ km$^2$ for the first 30 Ma. It increases linearly and becomes steady after 80 Ma. The constant value of the area coincides with the area of positive mass balance. For the first 30 Ma of the simulation run there is not enough ice volume to produce ice flow. Once the ice volume is sufficient to produce the ice flow, the ice cap starts spreading in to the ablation zone, growing in area. When the area becomes steady its value is $2.25 \times 10^6$ km$^2$ and that of volume reaches almost $6 \times 10^6$ km$^3$. These values are much higher than the present estimated values of area and volume.

The obliquity cycles can hardly be seen in area and volume plot (Fig. 6.8) because of their extremely low amplitude. This means that the imposed climate cycles with 125 ka and 1.3 Ma periods are not reflected in the evolution of the area and the volume. Hence the ice cap area and total volume are mainly governed by a long term *average* climate (see also Greve *et al.*, (2004)). The reason for this is as follows. The accumulation rate is proportional to the saturation pressure of water vapour in the atmosphere, which is strongly obliquity dependent through temperature (see Eq. 3.15). The ablation variations are proportional to accumulation variations as expressed in Eq. (3.19) for the mass balance gradient $g$. At high obliquities polar region gets higher insolation increasing the polar temperature. This will lead to higher ablation rates. These variations due to obliquity changes are not reflected in the topography because obliquity cycles are too short to produce remarkable changes. If sublimation rates of 0.05-0.5 mm/a (Hvidberg 2005) are considered at high obliquity then rough estimates shows that the polar cap will lose its thickness only by few meters which is very small to reflect in topography evolution. This is contradiction to the study done previously by Greve (2000b) and Greve *et al.*, (2003). In the previous studies it was assumed that climate cycles cause major variations of the ice cap topography. The build-up time for the present cap is $t_{\text{build}} = 13.78$ Ma now. This is much less than the 29.66 Ma in the case of standard steady state run. This happens because saturation accumulation has much larger value than its present value. In the steady state case where the climate cycle is switched off, only present values of climate forcing are used through out the simulation. This makes the temperature anomaly (temperature deviation from its present value) in Eq. (3.11) $\Delta T_{\text{s}} = 0$. The mass balance is non-linearly temperature dependent (see Fig. 3.4, please note the logarithmic scale). The zero temperature anomaly restricts the accumulation rate to its present values and can not reach any higher values. Whereas in case of transient simulations, the climate cycles play an important role. The surface temperatures varying according to climate cycles also change the mass balance. The accumulation saturation value which is quite higher than the present value can be achieved at higher temperatures. Hence with higher values for saturation

accumulation ice cap is built faster than in the steady state simulations. With the activated climate cycle in the transient simulations based on simplified two cycle obliquity it is not possible to build the present polar cap within the last five million years with the current accumulation rate. It takes 13.78 Ma to build the cap. The large obliquities prior to 5 Ma BP might have left the north polar region completely devoid of ice (Laskar *et al.*, 2002). If this is true then the north polar cap is very recent and is built is last 5 Ma. Hence either this notion is not reasonable or the present accumulation rate must be 2.5 times larger than the value assumed in the simulation. So the value of present accumulation has to be, $a_{\text{sat},0}^{+} \geq 0.25$ mm w.e. a$^{-1}$ km$^{-1}$.

Simulated surface topography, surface velocity and basal temperatures relative to pressure melting for the build-up time are shown in Figs. 6.7 and 6.9 respectively. The surface topography after 100 Ma run is also shown in Fig. 6.7. Both the surface topographies are similar to their counterpart for steady state run at the end of the simulation. The topography of the transient simulation for the final time (100 Ma) show larger elevation due to larger accumulation rate. At the build-up time $t_{\text{build}} = 13.78$ flow velocities are 50% higher they have been 30 ka before. The maximum value attained by surface velocity is 1.596 mma$^{-1}$. The basal temperatures relative to pressure melting are higher up to 10°C than the steady state run values. Still the basal temperatures relative to pressure melting are well below pressure melting point. These higher values of surface velocities and basal temperatures relative to pressure melting are due to the fact that at the time $t_{\text{build}}$, the surface temperature anomaly is $\Delta T_s = 12.41$°C. This value is by chance closer to the highest temperature throughout the climate cycle. 30,000 years earlier at time t = 13.75 Ma the temperature is the same as that of today making temperature anomaly $\Delta T_s = 0$°C. The maximum surface velocity that this time reaches attains the value of 0.588 mma$^{-1}$ which is almost three times smaller.

### 6.3.1.2   MOLA topography as initial condition:

For the second type of experiment transient simulations are run with the present MOLA surface topography as initial conditions. This enables us to study the behaviour of the present cap with varying climate cycles. Here the temperatures are derived from the scheme MAIC (see Sec. 3.2). This approach is based on simplified two-cycle obliquity. To have a closer look the ice cap evolution over the first 1.3 Ma cycle is shown in Fig. 6.10. The figure shows the influence of climate variation on the total ice volume and the ice covered basal area. It also shows the temperature anomaly from the present temperature. Surface velocity variation as a function of time is shown. The cap shows larger area and volume changes when the surface temperatures are higher where as the cap is stagnant at the time of low temperatures. The absolute values of area and volume changes are small compared to long term trends. In this first 1.3 Ma time the basal ice covered area is seen decreasing slightly. The reason behind this is the simulation is started with present MOLA topography as initial condition so some part of the cap is spread in the negative mass balance zone or ablation area. This part of the cap starts to sublimate in the beginning. The volume is seen increasing in this first 1.3 Ma time even though the area is decreasing. The central part of the cap always falls under positive mass balance depositing the ice through out the simulation time. On contrary to small changes in area and volume the surface velocities vary by a factor of 10 between 0.5 mma$^{-1}$ to 5 mma$^{-1}$. Surface veloci-
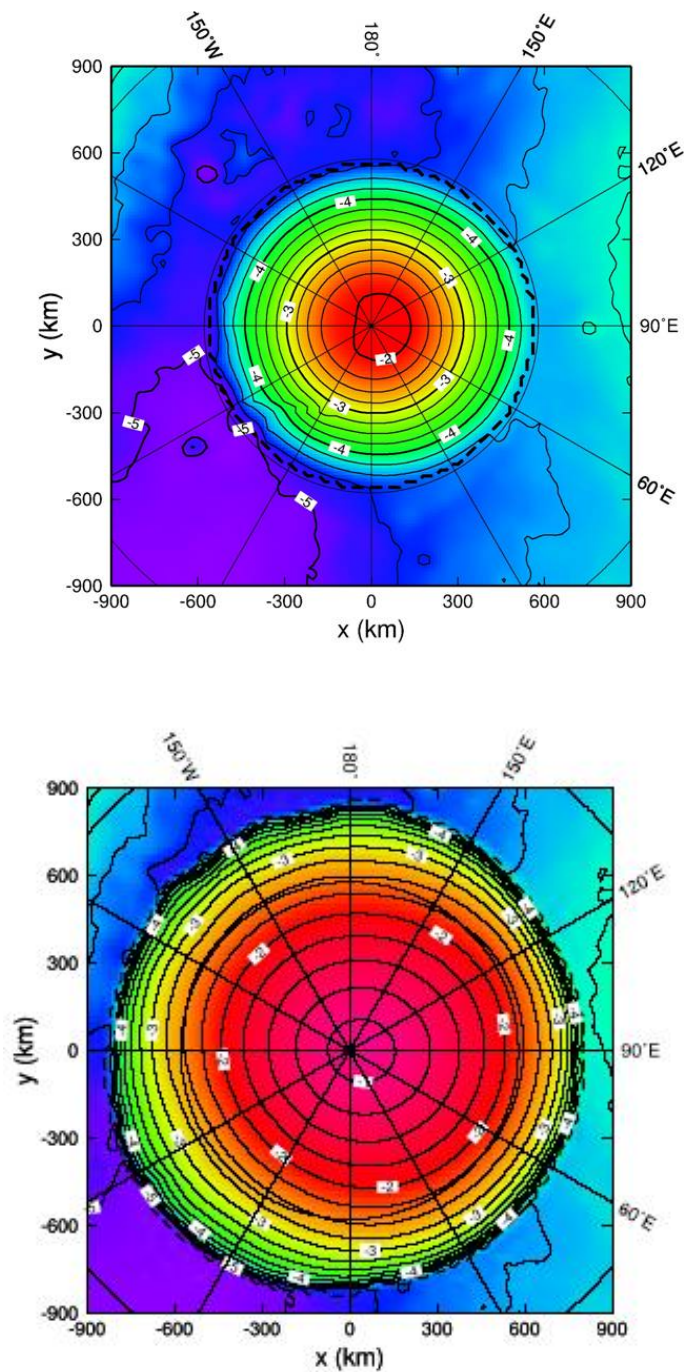
Figure 6.7: Surface topography (km) for the transient simulation for the time $t_{\mathrm{build}}$ = 13.78 Ma (top) and for 100 Ma (Topography is with respect to reference geoid).

ties follow closely the temperature cycle with maximum values during maximum surface temperatures. The velocity maxima is seen lagging behind the temperature anomaly maxima by infinitesimal amount of time. The ice cap take some time to react on increased temperatures due to its heat conductivity so the flow velocity increases after certain time.

A sequence of topography evolution is given in Fig. 6.11. The simulated growth in the volume and then area is clearly seen. The axi-symmetric forcing influences the small and
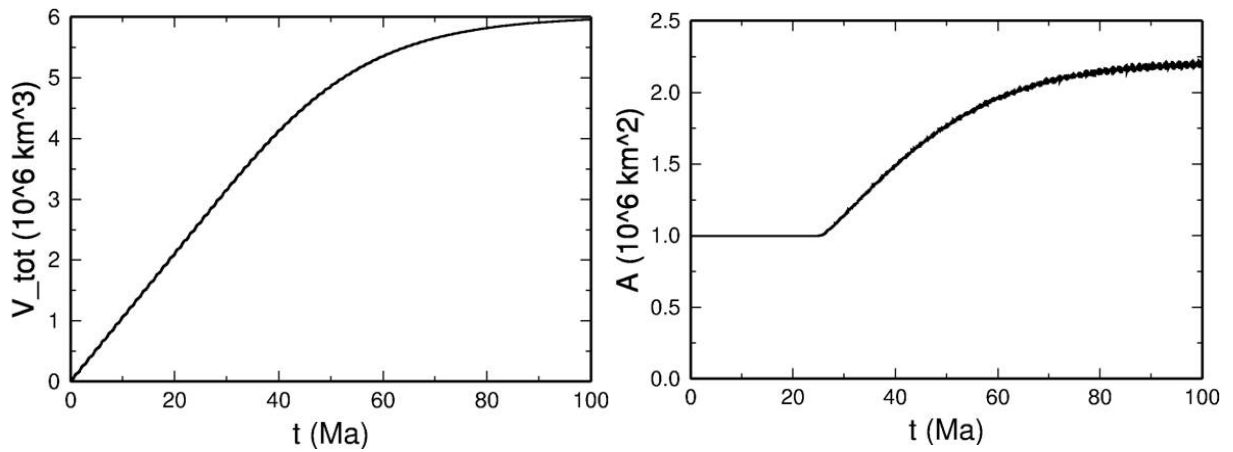
Figure 6.8: Transient simulation, standard set. Total ice volume $V_{\text{tot}}$ (km$^3$) and ice covered basal area $A_{\text{i,b}}$ (km$^2$) as functions of time $t$.

medium scale surface structures by smoothing them. After 10 Ma only a small remnant of Chasma Borealis is visible. After 20 Ma all the structure vanishes completely. Finally at 100 Ma, the topography looks the same as in case of steady state simulation as shown in Fig. 6.2. The system has completely lost the memory of its initial condition at that time. The total volume and maximum surface elevation increases monotonically in time. The main 125 ka obliquity cycle dominating $\Delta T_s$ is seen only smaller step like structure. This supports the finding by Greve *et al.*, (2004) that the north polar cap responds to the long term average climate.
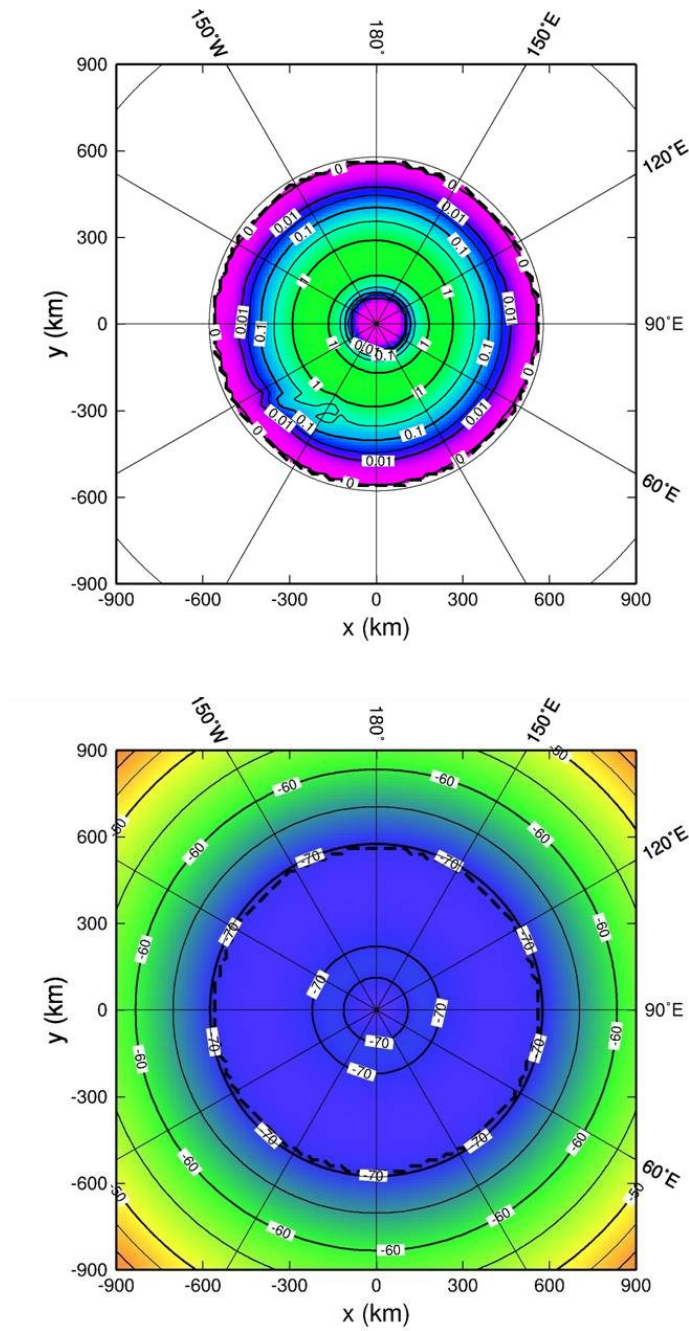
Figure 6.9: Surface velocity (mm/a) and basal temperature relative to pressure melting point (°C) for the transient simulation for the time $t_{\text{build}}$ = 13.78 Ma.
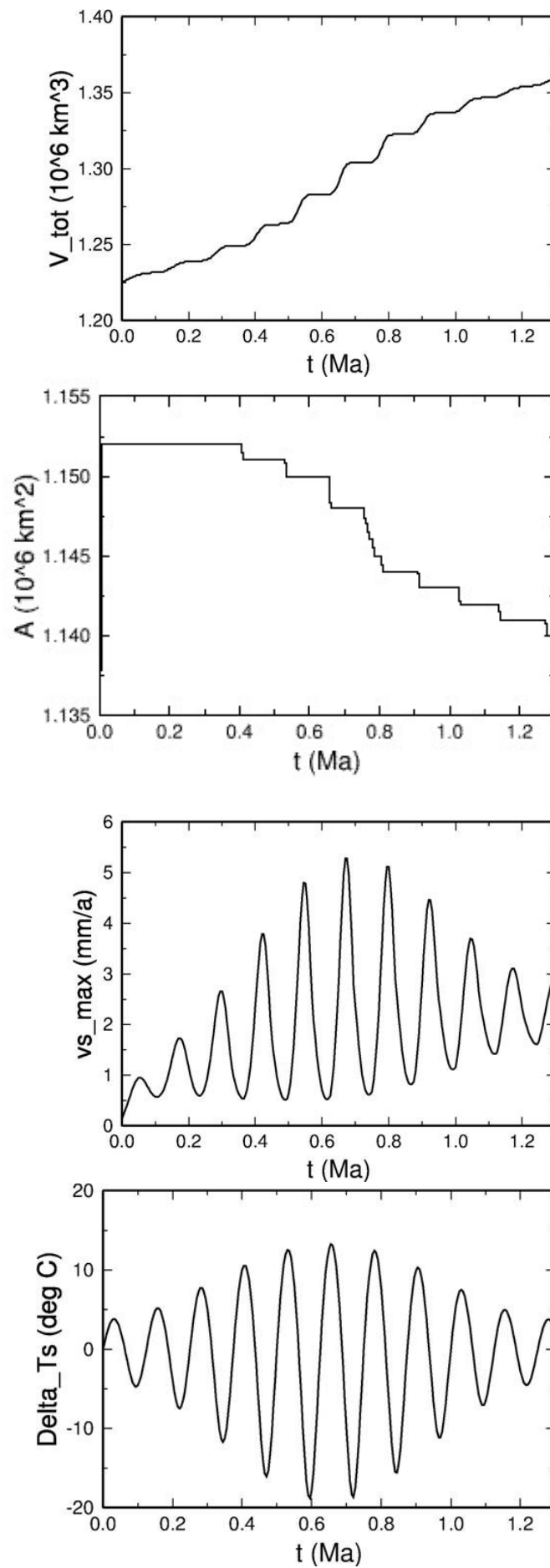
Figure 6.10: Simulations based on simplified two cycle obliquity starting from present MOLA topography: Total ice volume $V_{\text{tot}}$, ice covered basal area $A_{\text{i,b}}$, surface velocity $v_{\text{s,max}}$, Temperature anomaly $\Delta T_s$ as function of time $t$ for first 1.3 Ma.
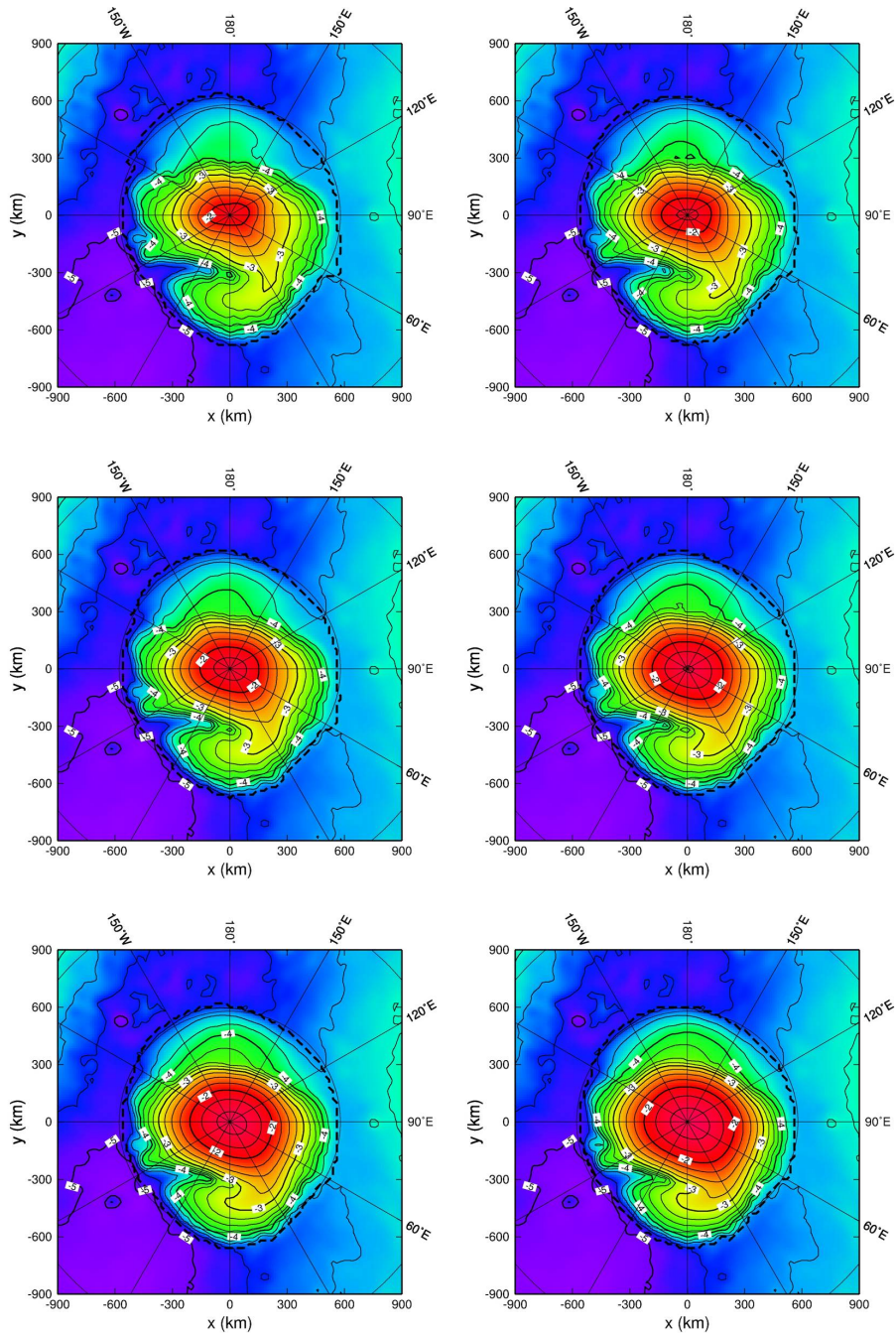
Figure 6.11: Simulations started with present MOLA topography. Surface topography (km) for the time $t = 1, 2, 3, 4, 5, 6$ Ma. Surface topography is with respect to reference geoid. The figure is continued on the next page.
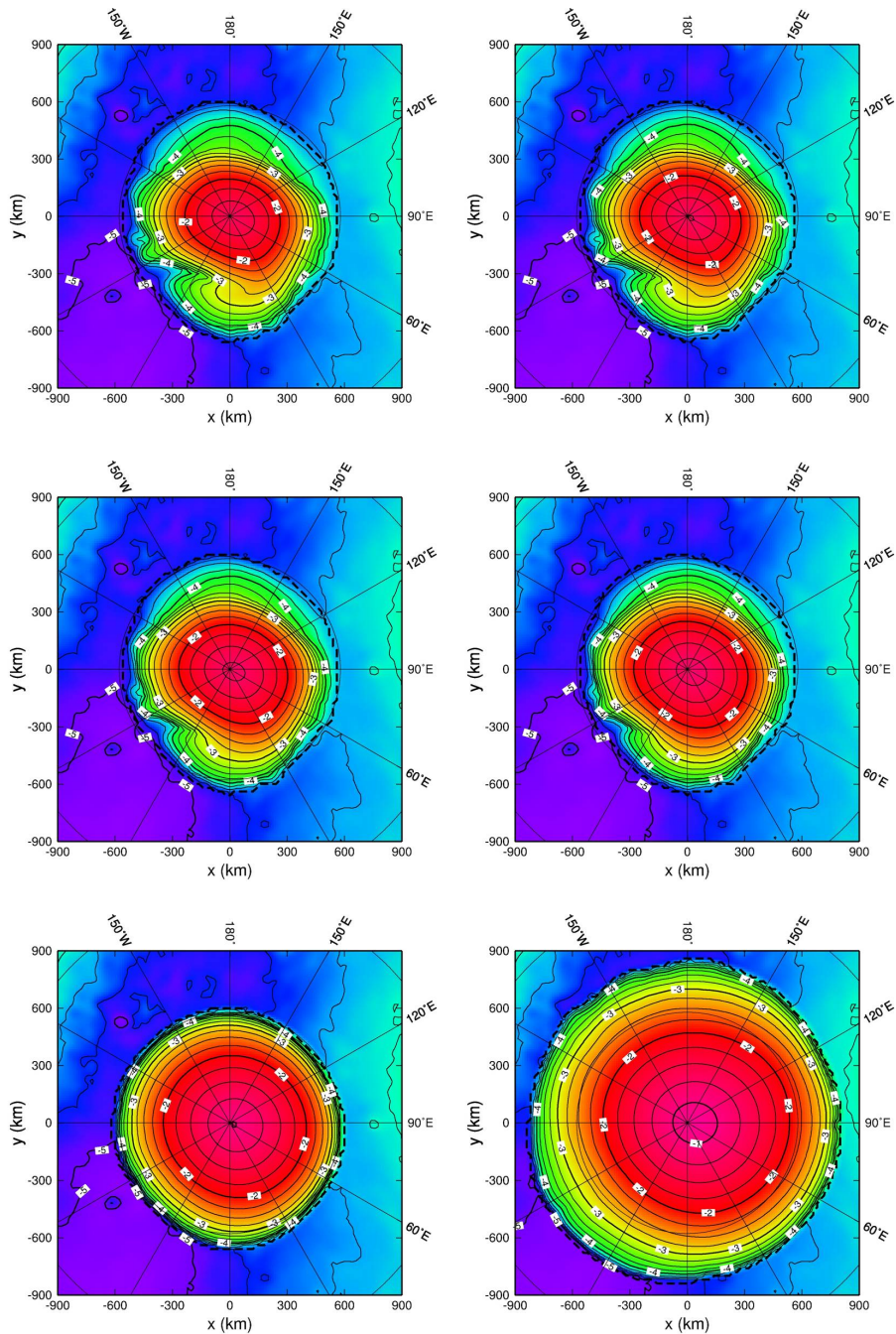
Figure 6.11: Continued Fig. 6.11 Simulations started with present MOLA topography. Surface topography (km) for the time $t = 7, 8, 9, 10, 20, 100$ Ma. Surface topography is with respect to reference geoid.

# 6.4  Effect of different flow laws and dust content

## 6.4.1  Approach based on the "real" obliquity cycle: North Polar Cap

### 6.4.1.1  Reference simulation:

With the obliquity data available for the 10 Ma in past (Laskar *et al.*, 2004), it is possible to use it for the simulations. This discussion in this section refers to results obtained by simulation set up in section 5.3.1. Laskar *et al.*, (2002) suggests that due to high obliquity 5 Ma BP the north pole might have been complete devoid of ice. Considering this to be true, an attempt has been made to build the north polar cap in the last 5 Ma BP. To achieve this the accumulation rates are tuned in such a way that the north polar cap can be built within 5 Ma. To find out the exact value of $a_{\mathrm{sat},0}^{+}$, the simulations are repeatedly run with different values of $a_{\mathrm{sat},0}^{+}$ till the cap is built within the required time span. This results in the present accumulation rate $a_{\mathrm{sat},0}^{+} = 0.1575$ mm i.e.a$^{-1}$ (mm ice equivalent per year). From variety of estimates based on different methods it is agreed that the value of present accumulation rate is in the range of 0.01 to 1 mm/a (Budd *et al.*, 1986, Kieffer 1990). Hence the estimated $a_{\mathrm{sat},0}^{+} = 0.1575$ mm i.e. a$^{-1}$ can be considered to be realistic.

The time variation of total volume $V_{\mathrm{tot}}$, ice covered basal area $A$, maximum surface velocity $v_{\mathrm{s,max}}$, maximum surface elevation $h_{\mathrm{max}}$, temperature anomaly $\Delta T_s$ and maximum basal temperature $T'_{\mathrm{b,max}}$ with respect to pressure melting is shown in Figs. 6.12 and 6.13. Temperature and accumulation are related nonlinearly (see Eq. 3.17) so the volume increase depends not only on the average $\Delta T_s$ but also on its amplitude. When time $t = -2.5$ Ma and 0, the $\Delta T_s$ has very small amplitude resulting in almost constant ice volume. The total ice covered area of the cap remains constant through out the simulation. The ice flow velocities are so small that the ice cap does not enter into the ablation or negative mass balance zone and remains in accumulation zone or positive mass balance for all the simulated time. Hence the area remains the same through out the simulation. Like steady state simulations the quantities maximum surface velocity and the maximum basal temperature reflect the main 125 ka obliquity cycle. The topographic quantities total volume, maximum surface elevation and the ice covered area do not reflect this 125 ka cycle. The ice flow starts significantly almost 2 Ma BP when the ice cap has already reached two third of its present volume. The ice flow is governed by the power law which produces extremely low strain rates at low stresses. Therefore ice flow starts significantly only when there is enough volume to produce high stresses. The ice flow varies from 0.1 to 1.5 mm/a which is orders of magnitude smaller than that for the terrestrial ice sheets. Still these values for flow velocities are not negligible. These smaller values explain why ice topography evolution is not affected by the internal ice dynamics.

The maximum basal temperatures relative to pressure melting follow the trend of the surface temperature while the ice cap is thin during the first half of the simulation time. As the cap becomes thicker and thicker the basal temperatures tends to grow. This is because of the thermal insulation of the growing cap against the cold surface. The warmest temperature attained by the ice cap during the total simulated time is $-65°$C. This temperature is obviously far below the melting conditions. Sequential surface topography maps at 1 Ma intervals are shown in Fig. 6.14. It can be clearly seen that the cap grows monotonically. The area which remains constant through out the simulation time can also

be seen. Like in steady state simulations here also the large scale features (extent, surface elevation, shape) are represented quite well. The comparison with the MOLA topography reveals this. On the contrary small and medium scale features like spiralling scarps and troughs, Chasma Borealis and detailed margin contour are not produced. This happens due to the axi-symmetric climate forcing. This forcing does not account the local details and this can not be expected from the large scale modelling approach like in SICOPOLIS. This may be refined by prescribing different ablation rates for the white areas and the dark scarps. (Fisher *et al.*, 2002, Hvidberg 2003, Hvidberg and Zwally 2003). Still this does not answer the open question which mechanism forms these structures in the first place.
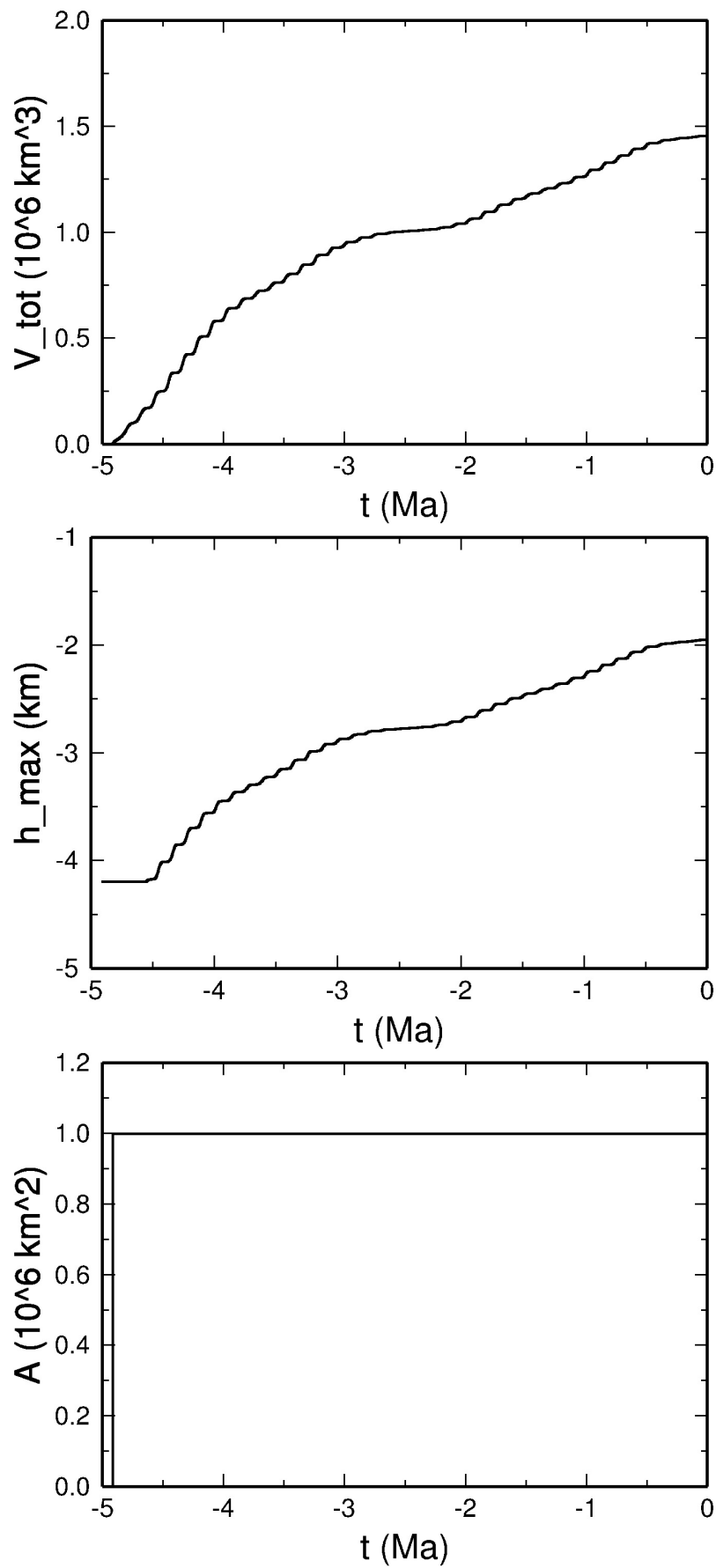
Figure 6.12: Total ice volume $10^6$ km$^3$, maximum surface elevation (km) and ice covered area $10^6$ km$^2$ as function of time. 0 indicates present time and minus sign indicates time BP. The simulations are carried out for north polar cap with approach based on "real" obliquity.
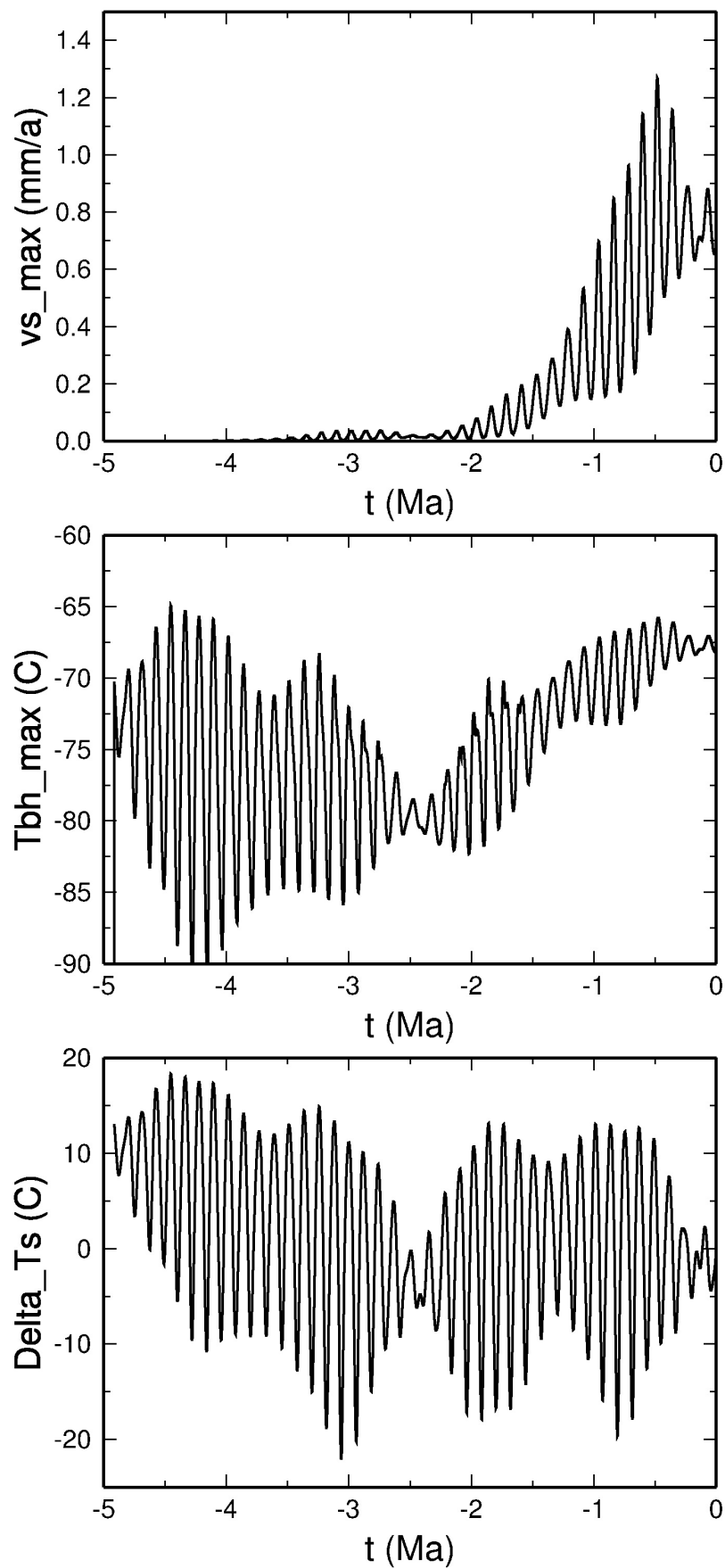
Figure 6.13: Maximum surface velocities mm a$^{-1}$, maximum basal temperature (°C) and temperature anomaly from the present surface temperature(°C) as function of time. 0 indicates present time and minus sign indicates time BP. The simulations are carried out for north polar cap with approach based on "real" obliquity
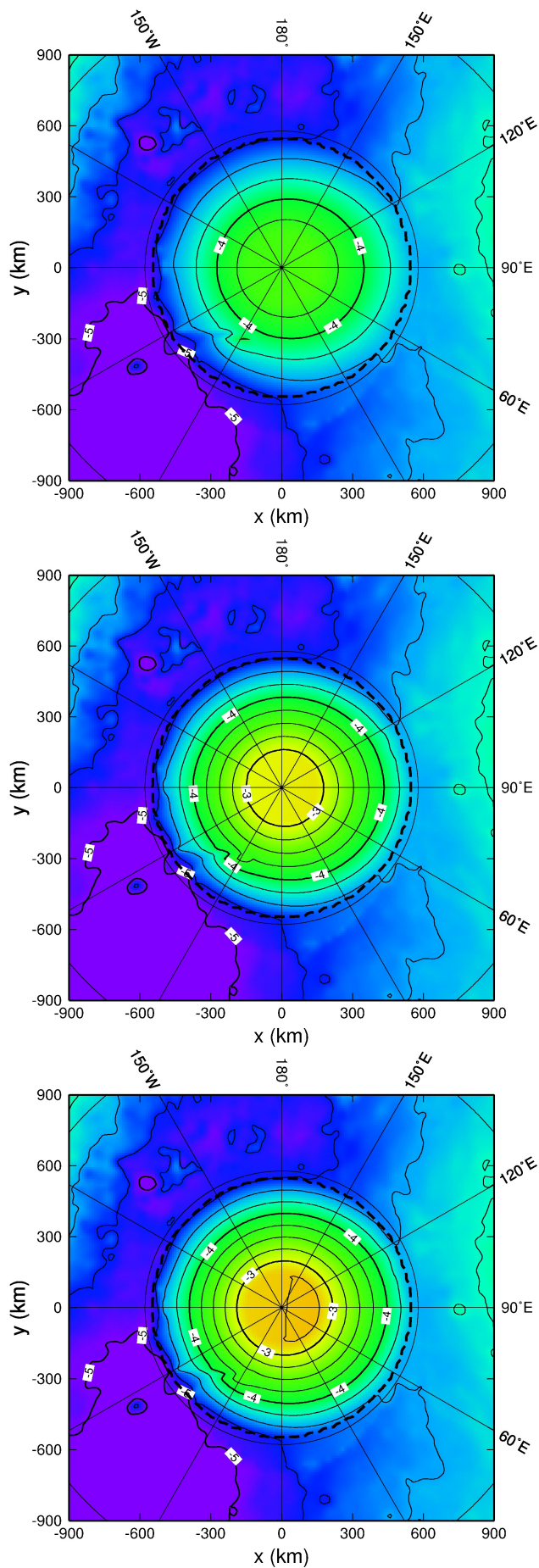
Figure 6.14: Surface topography for the time $t = -4, -3, -2$ Ma for the simulations started with ice free initial condition. Surface topography is with respect to reference geoid. Figure is continued on the next page.

61
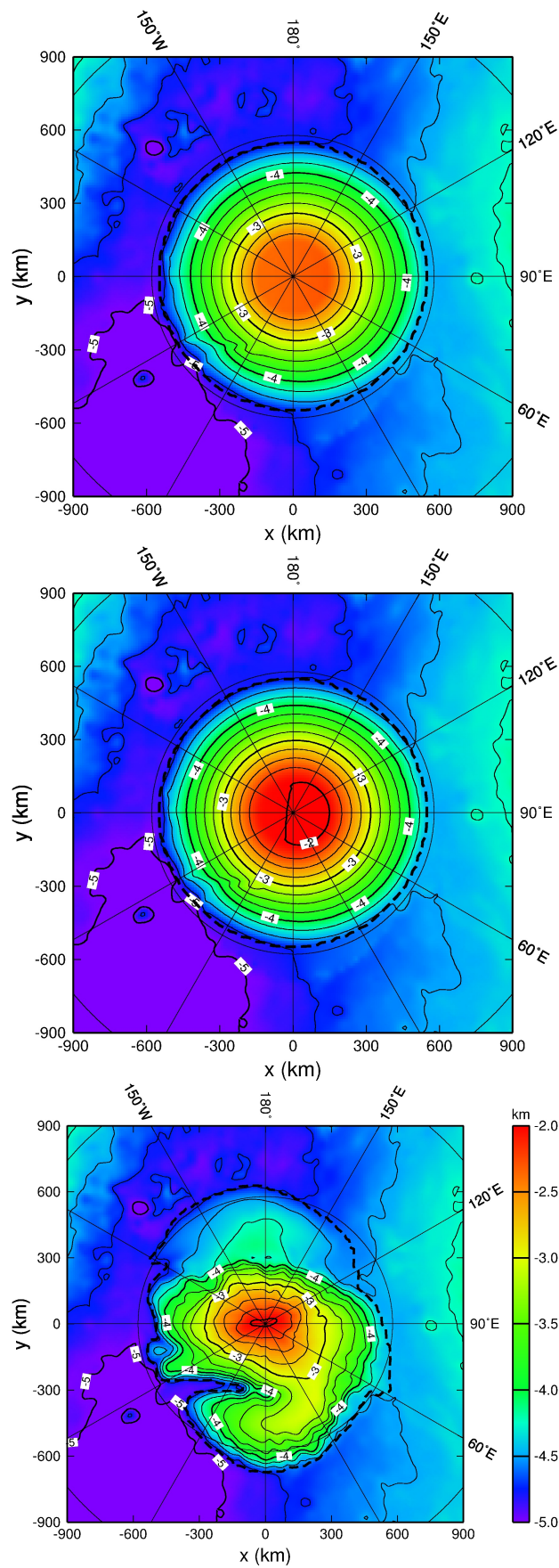
**Figure 6.14:** Continued Fig 6.14. Surface topography for the time $t = -1, 0$ Ma for the simulations started with ice free initial condition. Bottom panel shows MOLA surface topography. Surface topography is with respect to reference geoid.

#### 6.4.1.2   Effect of different flow laws and dust content

The simulation set-up for this is discussed in the section 5.3.1. The influence of the applied flow law and the average dust content is studied. Two series of simulations have been carried out. In the first series different flow laws are tested. Glen's flow law is replaced by Durham's flow law ($n = 4$). Goldsby and Kohlstedt flow law ($n = 1.8, p = 1.4$) is tested for two different grain sizes $d = 1$ mm and $d = 10$ mm (Eq. 2.1). In the second series zero dust content is increased to $10\%, 20\%, 30\%, 40\%$ and $50\%$.

Fig. 6.15 shows variation of accumulation rate $a_{\mathrm{sat}}^{+}$, the maximum surface velocity $v_{\mathrm{s,max}}$ and the maximum basal temperature relative to pressure melting $T'_{\mathrm{b,max}}$ for the simulation series with different flow laws. It is arranged by increasing accumulation rates. In total the accumulation rates are increased only by 1% for different flow laws. This small change in the accumulation rate is correlated with the surface velocity increase by almost two orders of magnitude. This is explained as following, larger flow velocities results in more ice transport from the interior of the cap towards its margin. So more ice is required to build the cap to reach present MOLA maximum surface elevation in given time span. The flow velocities are very small, about few millimeter per year, hence the dynamic influence on the accumulation rate is not significant.

The sequence of simulations with increasing flow velocities is Durham's flow law < Goldsby and Kohlstedt flow law (10 mm grain size) < Glen's flow law < Goldsby and Kohlstedt flow law (1 mm grain size). This is the same behaviour in terms of shear rates as in the case of the simple-shear experiment (see Fig. 2.1). It becomes clear that the relative contribution of the different flow laws vary strongly. For low stresses grain size dependent flow with low stress exponent dominates. It means here Glodsby and Kohlstedt flow law ($n = 1.8$) is influential. For higher stresses dislocation creep with higher stress exponent becomes more important. In this case Glen's flow law ($n = 3$) and Durham's flow law ($n = 4$) dominates. While flow velocities show an increasing trend, the basal temperatures decrease. The reason for this is as the flow velocity increases, the cold ice at the surface starts flowing towards the interior and margins of the cap. In other words, ice flows downward and outward cooling the lower part of the north polar cap. The absolute values of the surface velocity are small so the basal temperatures too vary on small scale. The difference between the basal temperatures for the extreme flow laws, Durham's flow law and Goldsby and Kohlstedt flow law (1 mm grain size) is just more than $1°C$. The flow rate factor exponentially depends on the homologous temperature (Eq. 2.3). So this cooling or the decrease in the basal temperature produces a slight negative feedback for the increasing ice flow. Due to this negative feedback the values for the ice flow vary by 'two' orders of magnitude. On the other hand in the simple shear experiment (Sec. 2.1.2) the shear rates show a variation of almost 'three' orders of magnitude.

Since increasing flow velocities make the ice move downward and outward, it takes longer to reach the targeted thickness. (MOLA value, $h_{\mathrm{max}}$ = -1.95 km). Fig. 6.17 shows the time needed to build the ice cap with present MOLA thickness as a function of different flow laws applied. The build-up time increases in the sequence of Durham's flow law < Goldsby and Kohlstedt flow law (10 mm grain size) < Glen's flow law < Goldsby and Kohlstedt flow law (1 mm grain size).

Fig. 6.16 shows variation of accumulation rate $a_{\mathrm{sat}}^{+}$, the maximum surface velocity $v_{\mathrm{s,max}}$ and the maximum basal temperature relative to pressure melting $T'_{\mathrm{b,max}}$ for the sim-

ulation series with different dust content. The effect of dust content on accumulation rate is much more pronounced than on flow velocities. Accumulation rates vary almost by 30% between the reference simulation and that with 50% dust content. The flow velocities are still very small so ice the dynamics is unaffected. The accumulation rates need to be increased with increasing dust content. This happens because increase in the dust content $\varphi$ increases the density of the composite material (Eq. 3.21). With higher density there is more isostatic displacement of the underlying lithosphere implying more ice is needed to build the cap with the target surface elevation of -1.95 km. Denser the material is due to more dust content, more is the bedrock lithosphere depression in to the underlying asthenosphere. This downward displacement of the lithosphere means higher elevations are needed to reach the present MOLA elevation.

It is also observed that with increasing dust content the flow velocity increases though Eq. (3.24) suggests the dust content should affect the ice fluidity in the opposite direction. This happens due to two indirect effects which over weigh direct hardening. First is increasing ice thickness which produces larger driving stress and the second is increasing basal temperature makes the ice softer. The basal temperatures vary strongly between 67.2°C for 0% dust content and 52.4°C for 50% dust content. Increasing dust content reduces the heat conductivity so there is strong insulation of the ice body and the atmosphere which is colder. Even then the highest attained basal temperature value is well below melting point. So presence of liquid water at the bottom of the north polar cap is unlikely. The current position of the melting isotherm is expected to lie several kilometers deeper in the ground (Clifford *et al*., 2000).

### 6.4.2 Approach based on simplified two cycle obliquity: North Polar Cap

In the another series of simulations the influence of different flow laws and dust content is studied on the dynamics of the north polar cap. The simulation set-up is discussed in the second paragraph of section 5.3.2. The approach based on simplified two cycle obliquity is used with the scheme MAIC (Sec. 3.2). The simulations are started with ice free conditions and run till the maximum surface elevation $h_{max}$ of the simulated cap reaches its present (MOLA) value -1.95 km. Laskar *et al.*, (2004) have provided "real" obliquity data for 10 Ma BP. So simulations can not be run for longer time scales of 100 Ma with this real obliquity data. The approach based on simplified two cycle obliquity help to study the response of the polar cap on longer times scales. The current accumulation rate is taken as 0.1 mm w.e $a^{-1}$. For studying the influence of flow laws, Glen's flow law is replaced by Durham's flow law ($n = 4$). Goldsby and Kohlstedt flow law ($n = 1.8, p = 1.4$) is tested for two different grain sizes $d = 1$ mm and $d = 10$ mm (Eq. 2.1). For all the flow laws influence of dust content is studied. Dust content is varied from 0% to 10%, 20%, 30%, 40% and 50%. In each case the simulation starts with ice free initial condition until the cap is built with present maximum MOLA surface elevation $h_{max}$.

The results are very similar to previous simulation with "real" obliquity approach discussed earlier in this chapter. The variation of flow velocities for different flow laws for varied dust content is shown in the Fig. 6.18. It is clearly seen that variation of flow velocities for different flow laws vary up to greater extent. Though ice flow is very slow with values only a few microns per year, there is remarkable difference for the different flow laws. The sequence of simulations with increasing flow velocities is the same as in the previous simulation Durham's flow law $<$ Goldsby and Kohlstedt flow law (10 mm grain size) $<$ Glen's flow law $<$ Goldsby and Kohlstedt flow law (1 mm grain size). This trend is consistent for all the values of the dust content.

For all the flow laws time taken to build the ice cap ($t_{build}$) with present maximum surface elevation MOLA value (-1.95 km) increases as the dust content increases (see Fig. 6.18). The reason for this is necessarily the same as in the previous case. This happens because an increase in the dust content $\varphi$ increases the density of the composite material (Eq. 3.21). With higher density there is more isostatic displacement of the underlying lithosphere implying more ice is needed to build the cap with present surface elevation. The lowest value for $t_{build}$ is 13.77 Ma with Glen's flow law and 0% dust content and the highest value for $t_{build}$ is 20.18 Ma with Goldsby and Kohlstedt flow law (1 mm grain size) and 50% dust content. It can be clearly seen that there is not much difference in the build-up time $t_{build}$ for different flow laws for one particular dust content value. In case of Goldsby and Kohlstedt flow law ($n = 3$) where grain size of 1 mm is used the behaviour is different than all other three laws. This is so because ice dynamics is unaffected due to vary small surface velocities.

With increasing dust content flow velocity increases though Eq. (3.24) suggests the dust content should affect the ice fluidity in the opposite direction. This happens due to two indirect effects which over weigh direct hardening discussed in the previous section 6.4.1.2. In the case of Glen's flow law and Durham's flow law ice deforms primarily by dislocation glide in the basal plane. At the lower stresses like in Goldsby and Kohlstedt flow law ice deforms by grain boundary sliding. The flow rates depend on the grain size.

65

This influences the magnitude of the velocities through strong influence on the flow rate factor. The effect is more prominent Goldsby and Kohlstedt law with 1 mm grain size (dashed line with asterisk in Fig. 6.18) The velocities are seen higher than other flow laws and the build-up time as well. The reason for the higher build-up time is that with higher flow velocities the ice is transported downward and outward towards the perimeter of the cap. This results in a higher build-up time. Since the ice is moved faster, the time taken to build the cap of required thickness, e.g. the present MOLA value is long. The sequence follows as Durham's flow law < Goldsby and Kohlstedt flow law (10 mm grain size) < Glen's flow law < Goldsby and Kohlstedt flow law (1 mm grain size). With increasing dust content flow velocity increases for all the flow laws. For the discussion about influence of increasing dust content on flow velocities please read the previous section where simulations with "real" obliquity cycles are discussed. In both the cases the results are necessarily the same.
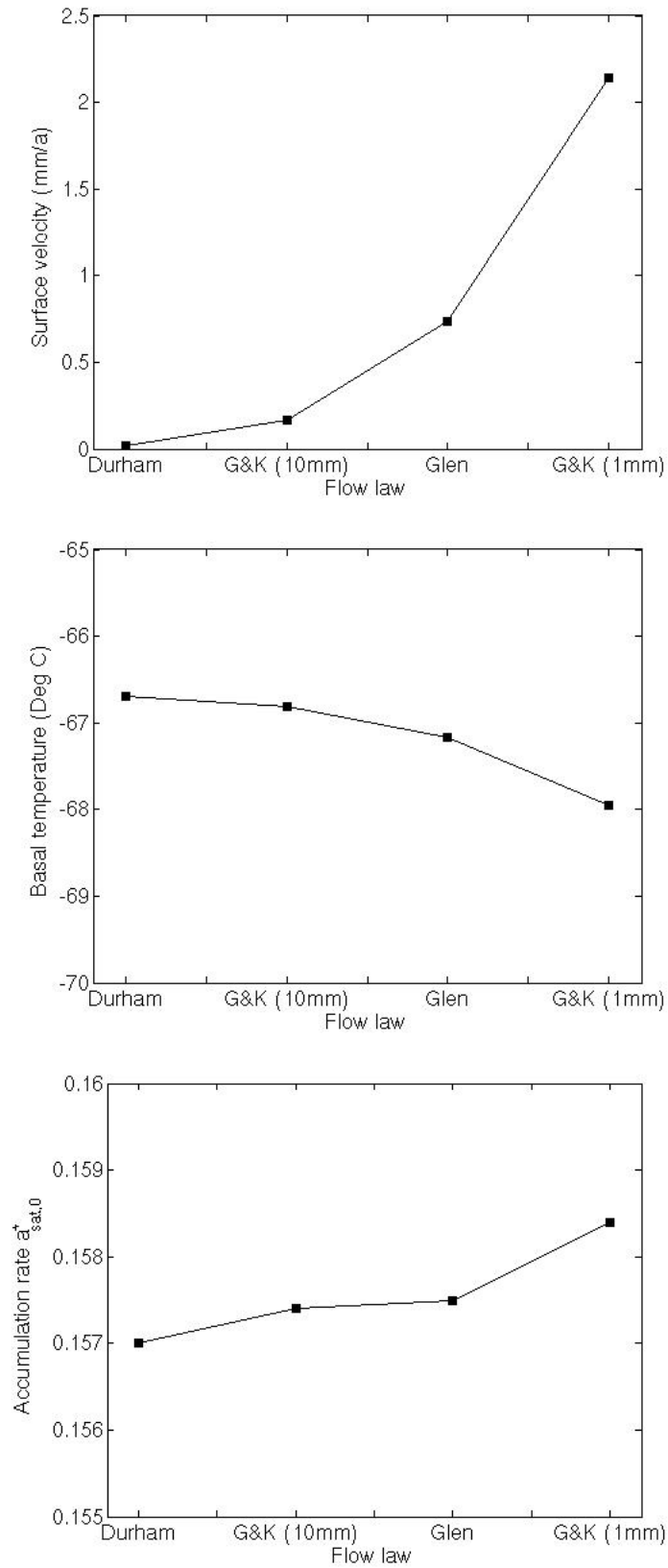
Figure 6.15: Variation of the maximum surface velocity $v_{s,max}$, the maximum basal temperature relative to pressure melting $T'_{b,max}$ and the accumulation rate $a^+_{sat,0}$ for Glen's flow law ($n = 3$), Durham's flow law ($n = 4$) and Goldsby and Kohlstedt's flow law ($n = 1.8$, 1 mm and 10 mm grain size)
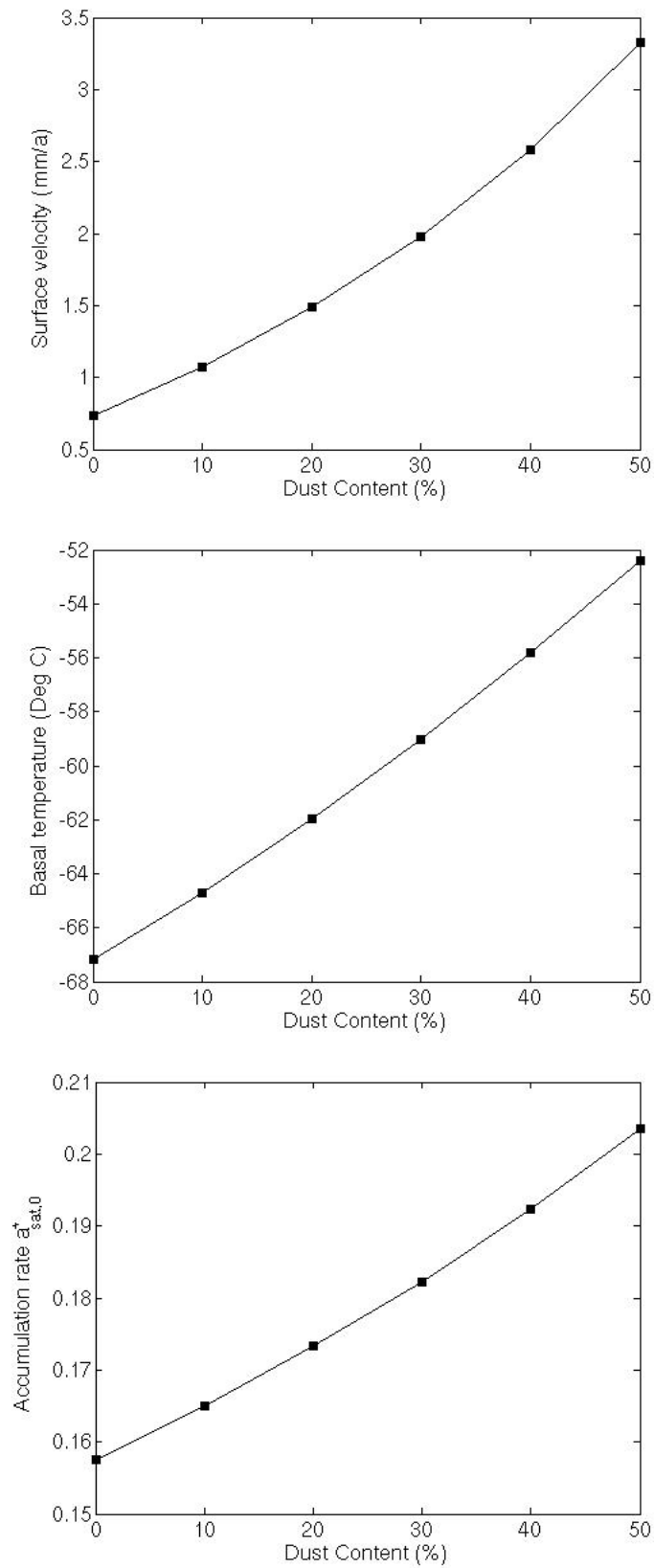
Figure 6.16: Variation of the maximum surface velocity $v_{s,max}$, the maximum basal temperature relative to pressure melting $T'_{b,max}$ and the accumulation rate $a^+_{sat,0}$ for varying average dust content.
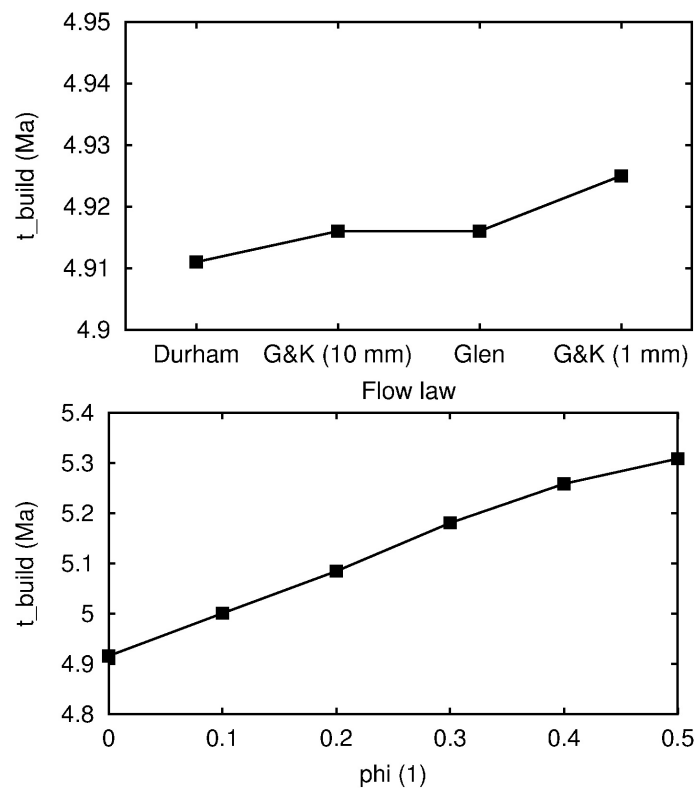
Figure 6.17: Time (Ma) needed to build the ice cap with present MOLA thickness for Glen's flow law ($n = 3$), Durham's flow law ($n = 4$) and Goldsby and Kohlstedt's flow law (1 mm and 10 mm grain size)($n = 1.8$) and for the average dust content factor.
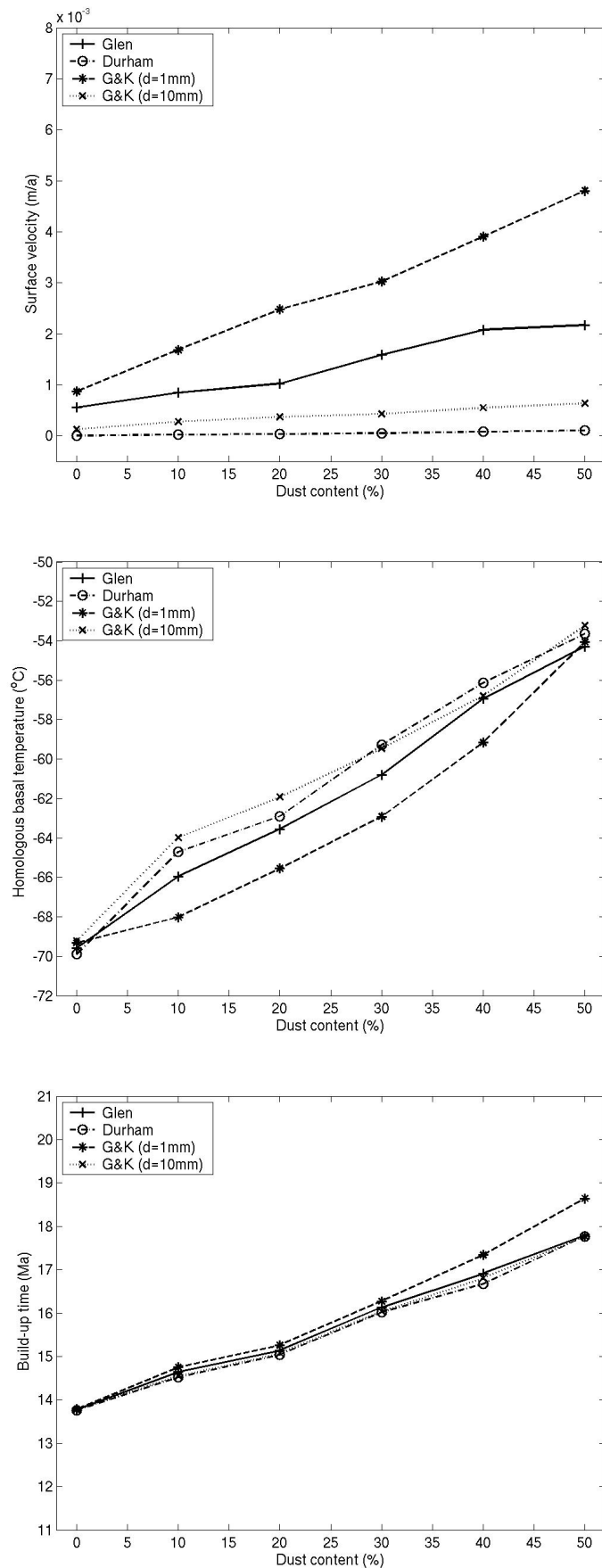
**Figure 6.18:** Variation of the maximum surface velocity $v_{s,max}$, the maximum basal temperature relative to pressure melting $T'_{b,max}$ and the build-up time $t_{build}$ for different flow laws and varying average dust content.

### 6.4.3   Approach based on local daily mean insolation: North Polar Cap

For the north polar cap the simulations are carried out with transient conditions so the climate cycles are involved. Approach based on local daily mean insolation is used for temperature parameterisation (Sec. 3.3) The approach used for temperature parameterisation will be able to produce annual temperatures based on local daily mean insolation and seasonal $CO_2$ cycle.

The simulations are started with ice free initial conditions and are run till the ice reaches the maximum surface elevation $h_{max}$ = -1.95 km which is MOLA present surface elevation. The simulations are run for Glen's flow law and 20% (Hvidberg  2003) dust content. Glen's flow law is the generalised and tested flow law for the terrestrial ice sheets. The present accumulation rate was taken as 0.1 mm w.e.a$^{-1}$. Fig. 6.19 shows the simulated surface topography, surface velocity and homologous basal temperature. Also the present MOLA surface topography is given for comparison. The results are in good agreement with that of simulations carried out using MAIC. In both these cases simplified two cycle obliquity were used. It takes 35.6 Ma to build the cap with surface elevation $h_{max}$. The time taken to build the cap is more than two and half times as that of using the same simulation set-up but the temperature parameterisation MAIC (see Sec. 3.2). With MAIC the time taken to build the cap is 13.78 Ma.

In both the schemes the radiation balance is used. The nonlinear relation between insolation and temperature gives the temperature if insolation is known. In case of MAIC, the annual mean insolation is considered to find out the annual mean temperature needed for accumulation parameterisation. For the approach based on local daily mean insolationa, every day local mean insolation is considered to calculate daily mean temprature. This daily mean temperature cycle produces annual mean temperature cycle which is used for accumulation. The amplitude of annual mean temperature variation is different for both the schemes. The scheme MAIC is more sensitive to obliquity cycle hence the annual mean temperature by it has higher amplitude. Higher temperature amplitude indicate periods of warmer temperature. The temperatures are related nonlinearly with the accumulation rate (Eq. 3.15) producing high accumulation rate at higher temperatures. This affects the build up time of the polar cap. For the scheme based on local daily mean insolation the amplitude of annual mean temperature variation is not as high as in case of MAIC. This produces lower accumulation rates than in case of MAIC taking more time to build the polar cap.

The large scale shape of the ice cap agrees well with that of the MOLA topography. More detailed features like Chasma Borealis are not produced due to axi-symmetric climate forcing. The flow velocities are a few millimeter per year which is almost 4 to 5 orders of magnitude smaller than the values for terrestrial ice sheets. The flow velocities are higher in the western part of the cap. This is because of lower bedrock elevation in that part. Lower bedrock elevation caused more ice thickness hence higher velocities. The maximum value for the basal temperature with respect to pressure melting is $-71.6°C$ which is far below the melting point.
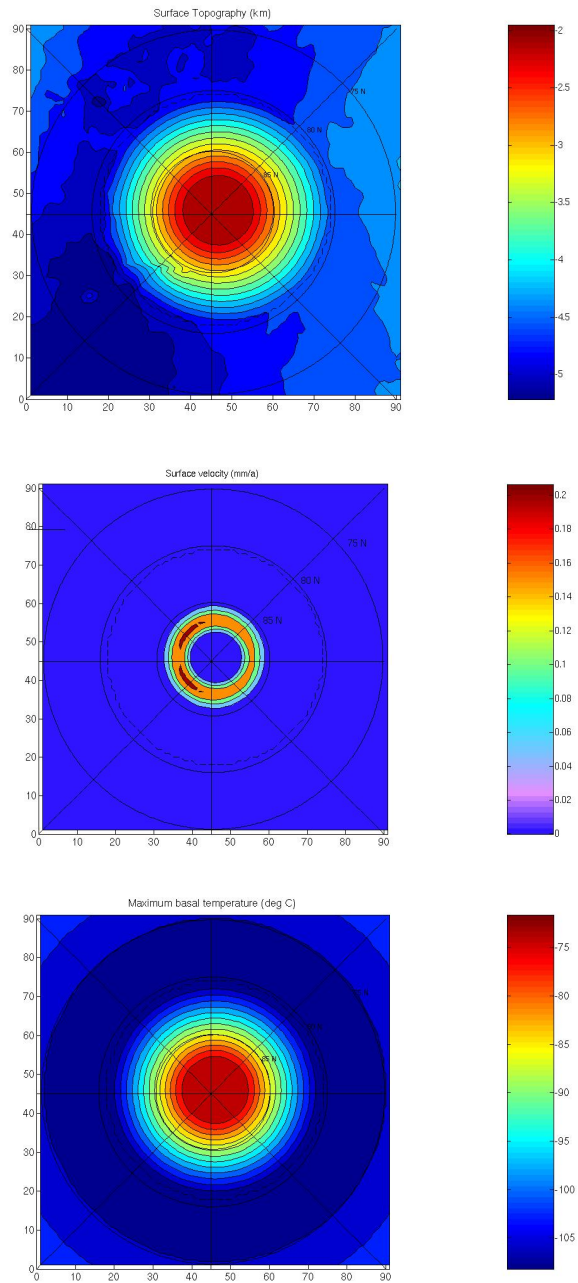
Figure 6.19: North polar cap: Simulated present surface topography (km), simulated surface velocity (mm/a) and simulated homologous basal temperature for the build-up time, 25.65 Ma. Simulations are done with ice free initial condition and local daily mean insolation is used for temperature parameterisation.

# 6.5   Effect of different flow laws and dust content: South Polar Cap

## 6.5.1   Approaches based on MAIC and local daily mean insolation

Simulation for the south polar cap are carried out using the simulation setup discussed in section 5.3.1. The surface of the south polar cap appears rugged indicating it is much older then the north polar cap (Fishbaugh and Head 2002). The simulations are started with MOLA topography as initial condition. Climate cycles are taken into account meaning transient simulations. The approach based on the "real" obliquity cycle is used.

Two series of simulations are carried out one with the temperatures derived by the scheme MAIC and the other with temperatures derived from the local daily mean insolation cycle. Simulations are carried out for last 10 Ma. with Glen's flow law and 20% dust content. Simulations starts with initial time $t_{\text{initial}} = -10$ Ma and ends at final time $t_{\text{final}} = 0$, present time. For both the series the present accumulation rate is kept as 0.1 mm w.e.a$^{-1}$. Different estimations suggest that the present accumulation rate is in the range of 0.01 - 0.1 mm w.e.a$^{-1}$ (Budd *et al.*, 1986, Kieffer 1990). Therefore the value chosen for the simulation is within this range of estimation. This simulation set-up will help to understand impact of climate cycles in the past 10 Ma on the south polar cap. This is an attempt to study the response of the cap to the strong variations in obliquity cycle 5 Ma years ago (Laskar *et al.*, 2002).

The scheme with local daily mean insolation fails to produce the thin $CO_2$ cover found on south polar cap throughout the year. Therefore the temperatures are corrected such that it is just below the $CO_2$ sublimation temperature $-128°C = 145$ K within 85°S. In this scheme the complete $CO_2$ is evaporated in to the atmosphere when polar night enters in to the spring. Hence the insolation in the polar region is received by the water ice cap producing the higher temperatures. Due to the presence of $CO_2$ cover the water ice underneath is insulated producing lower temperature. This effect has not taken care of in the scheme.

Figs. 6.20 and 6.22 shows the present MOLA surface topography which is used as initial condition to start the simulations, and surface topography after 10 Ma of simulation. Topography maps shows the changes occurred in the past 10 Ma BP. Topographic features shows very minor changes (please note the different scales on colourbar). This indicates that the dynamical change in the cap even when obliquity cycle varies strongly is also minor. For the simulations where temperatures are derived from MAIC, here too the response of the south polar cap is not very prominent. The 125 ka obliquity cycle and 1.3 Ma modulation is much more prominent in this case than previous simulations for the basal temperature and flow velocities. Figs. 6.21 and 6.23 shows the basal temperature and ice flow velocity variations for the whole simulation time, 10 Ma BP till the present time. In both the type of simulations it can be clearly seen that temperatures and ice flow velocity follow the obliquity cycle. In the first 2 million years the values of both these quantities rise as the change in the obliquity values. Though the obliquity cycle is reflected in the dynamically and thermodynamically, the values of flow velocities are very very small. The maximum surface velocities in the simulations using the scheme MAIC are of the order of 0.8 mm/a and the basal temperature nowhere exceeds $-80°C$. In case of the simulations where local daily mean insolation cycle is used values are as small as 0.16

mm/a for ice flow and basal temperatures are below $-75°$C everywhere. In both the types of simulations temperatures produced are much below the melting point. Herkenhoff and Plaut (2000) state that south polar cap consists shows 15 craters with diameter larger than 800 m. This indicate that the south polar cap is two orders of magnitude older than the northern cap. This age difference also indicate the stiff and slowly flowing south polar cap as compared to north. The flow velocity obtained by SICOPOLIS which are less than a micron per year supports this. The most of the part of the south polar cap flows with the velocity less than a micrometer per year. Hence the south polar cap can be considered almost stagnant.
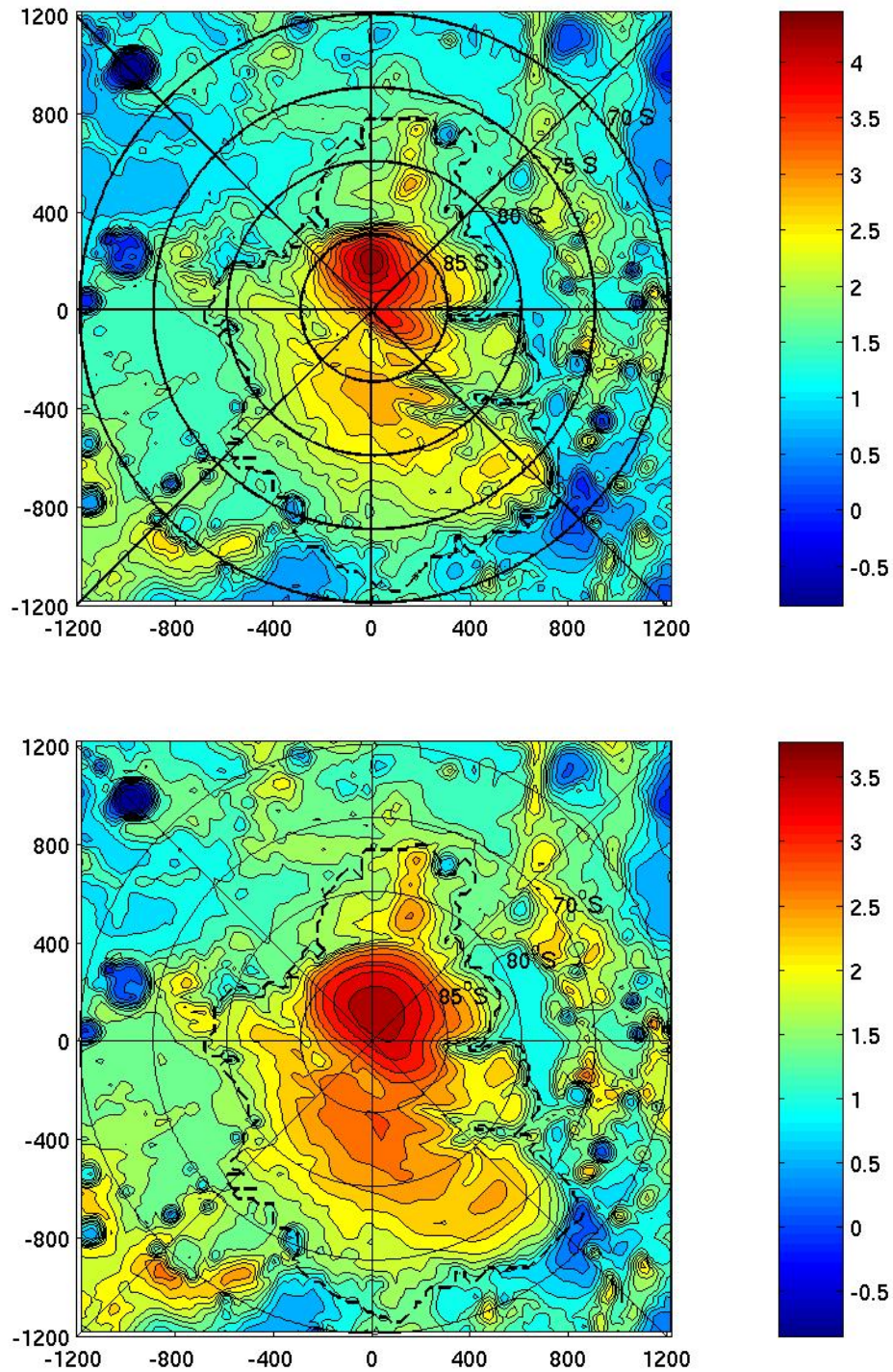
Figure 6.20: South Polar Cap: Present MOLA surface topography used as initial condition (Top) and simulated surface topography (km) after 10 Ma (Bottom). MAIC (Sec. 3.2) is used for temperature parameterisation
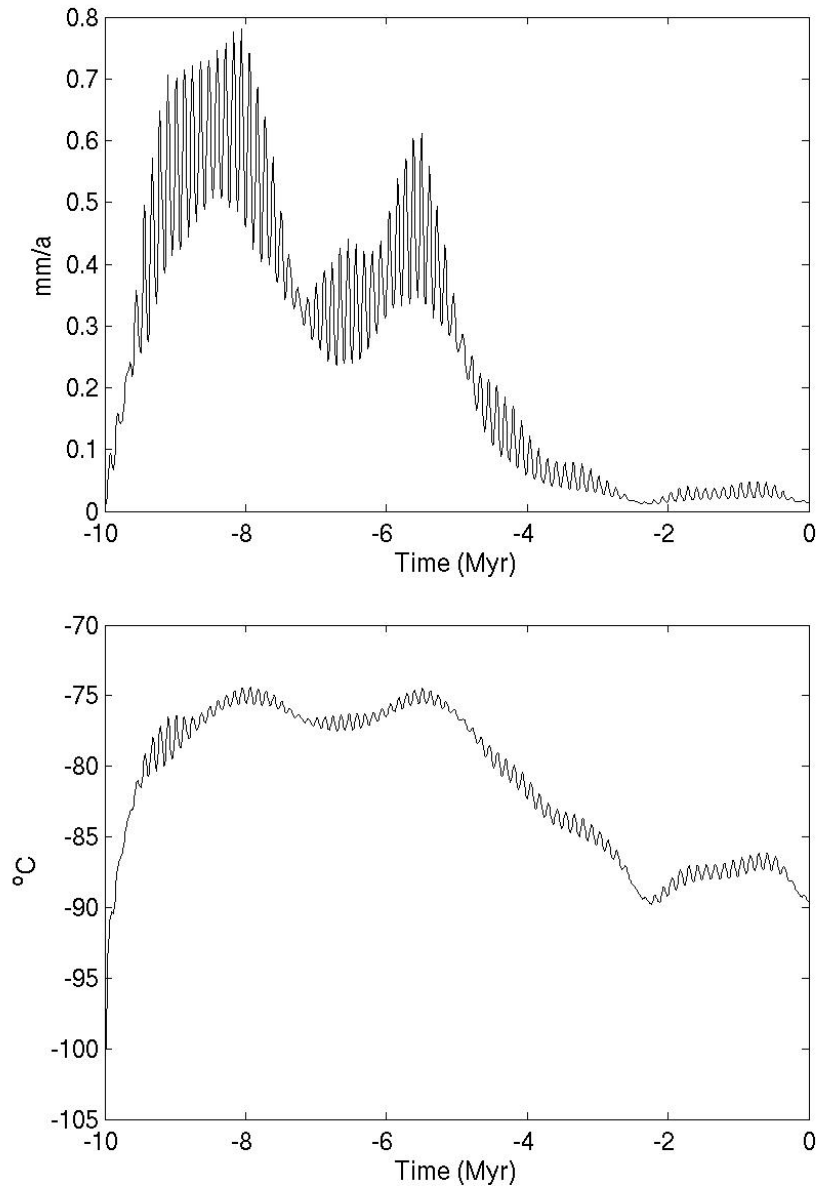
Figure 6.21: South polar cap: The line graph shows the maximum surface velocity (mm/a) variation with time (Top). Maximal basal temperature (°C)variation with time (Bottom). MAIC (Sec. 3.2) is used for temperature parameterisation.
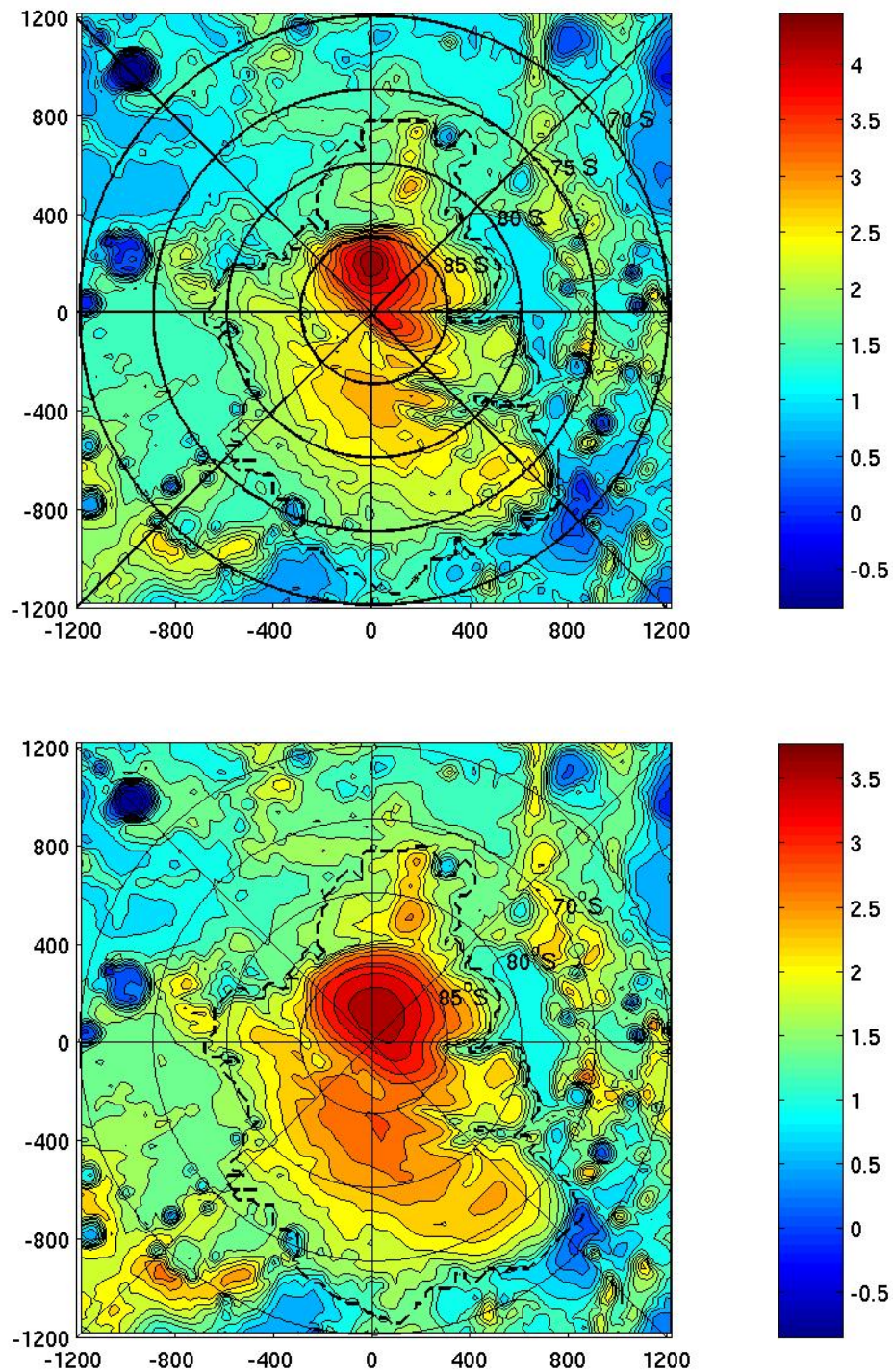
Figure 6.22: South Polar Cap: Present MOLA surface topography )used as initial condition (Top) and simulated surface topography after 10 Ma (km) (Bottom). Local insolation scheme (Sec. 3.3) is used for temperature parameterisation.
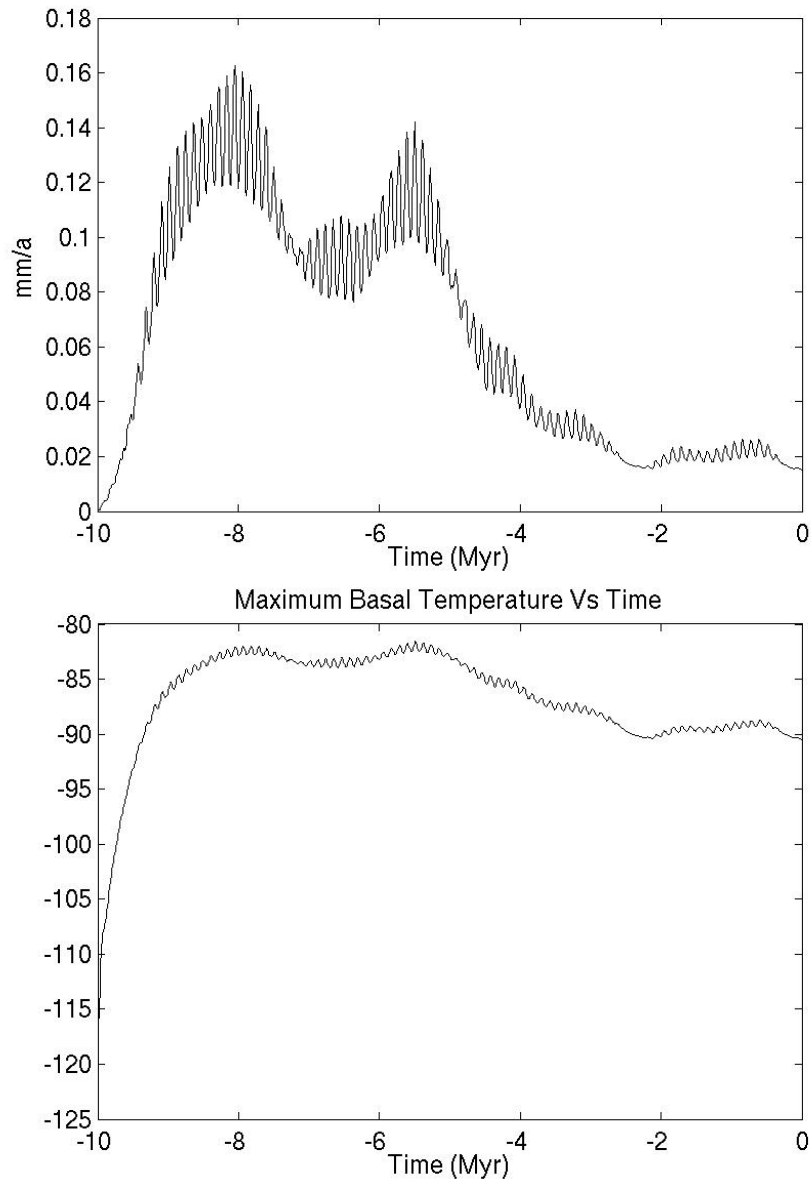
Figure 6.23: South polar cap: The line graph shows the maximum surface velocity (mm/a) variation with time (Top). Maximal basal temperature ( °C)variation with time (Bottom). Local insolation scheme (Sec. 3.3) is used for temperature parameterisation.

# 6.6    Uncertainties in the ice rheology

While experimenting the different flow laws and dust content due to uncertainties in the applicable flow law and dust content, the flow velocities can be predicted within a range of two orders of magnitude. The uncertainties which may occur due to small amount of $CO_2$ ice and $CO_2$ clathrate hydrate are neglected. Nye (2000) has discussed about the stability of the south polar cap if it would have composed of $CO_2$ ice. Solid $CO_2$ is markedly weaker than water ice. The authors suggest that due to its weak strength, the cap will not be able to sustain the present height on longer times scales. This statement is also supports the laboratory experiment done by Durham *et al.*, (1999). So the amount of $CO_2$ ice present in the south polar cap is small and mostly the cap is made up of water ice. This is also applicable to the north polar cap. On the contrary, $CO_2$ clathrate hydrate is thermodynamically stable in the interior of both the polar caps (Jöns 2002). Durham *et al.*, (2003) carried out laboratory experiments on polycrystalline methane hydrate over the temperature range 260-287 K and confining pressure of 50-100 MPa. This experiment shows that methane hydrate is extraordinarily strong as compared to icy compounds. The hexagonal water ice which is used many times for gas hydrates as proxy, methane hydrate is almost 40 times stronger than ice at a given strain rate for the given thermal range when both are solid. Methane and $CO_2$ hydrate have the same structure. Depending upon this experiment it is estimated that $CO_2$ hydrate is at least one order of magnitude harder than pure $H_2O$ ice at fixed stress and temperature (Durham 1998). This will result in a direct hardening effect like it happens in case of dust content. $CO_2$ either in the form of dry ice or clathrate hydrate has a thermal conductivity as low as 0.4-0.6 W m$^{-1}$ K$^{-1}$ (Mellon 1996). Due to low thermal conductivity of clathrate hydrate this direct hardening can be compensated.

# 6.7    Comparison with other studies

Fisher (1993) has studied the evolution of the north polar cap with a model "accublation". The model considers net accumulation in the white areas (0.1 mmw.e. a$^{-1}$) and net sublimation from the dark areas (0.3 mmw.e. a$^{-1}$). The spatially varying mass balance enables the scarps and troughs to be open. Author describes that flow velocities vary from 0 at the surface of the cap to few centimeters at the bottom of the trough. The local ice flow plays a vital part here. It is not possible to take care of the small scale features like troughs and scarps in SICOPOLIS as it does not have the high resolution necessary for these features. So the result stated earlier that ice flow plays only minor role in the evolution of the cap is not applicable for the small scale structures.

Hvidberg (2003) have discussed the relation between the topography and the flow in the north polar cap. The authors assume the polar cap is made of water ice. The ice flow is calculated using finite element ice-flow model. Different accumulations rates are considered for the white and dark layers like in the "accublation" model discussed above. The flow velocities are high up to cm/a in the region of scarps and troughs. But general flow velocities are in the range of 0.1-1.0 mm/a. This agrees well with the results obtained by SICOPOLIS. The finite element model by Hvidberg uses Glen's flow law ($n = 3$) and Goldsby and Kohlstedt flow law ($n = 1.8$) with 1 mm grain size. The flow velocities in

case of Goldsby and Kohlstedt flow law are higher than in case of Glen's flow law but still in the range 0.1-1.0 mm/a. This result agrees well with the flow velocity values found out using SICOPOLIS.

Hvidberg (2005) and Hvidberg and Zwally (2003) suggest that if there is no accumulation and ablation or sublimation then the darker troughs present in the north polar cap would slowly smooth due to ice flow. The estimated time for the closure of deep troughs is of the order of $10^5$ and $10^6$ years. Sublimation rate should be higher than the flow velocities to keep the spiralling troughs open. Still what makes these spiralling originally is not yet clear. This aspect is not taken care of in the SICOPOLIS since it does not support the high resolution required for this study.

Nye (2000) has carried out a study for the polar caps of Mars using a flow model. The caps are considered to be composed of water ice and rock debris. The model used here neglects the accumulation and ablation and calculates what flow would occur in a cap of chosen profile. It is calculated that after certain time the profile will collapse, the central part will fall and outer part of the cap will rise and at the same time perimeter of the cap will move outwards. Here in this approach it is assumed that ice flow governs the changes in the evolution of the cap. The authors have used Goldsby and Kohlstedt flow law with flow law exponent $n = 1.8$ and grain size 1-10 mm. The SICOPOLIS model considers that mass balance governs the evolution of the cap. Hence the approached used by Nye's model and that in SICOPOLIS can not be comparable for the evolution of the cap but only for the ice rheology. The creep rates found by Nye (2000) and those in this study are well in agreement.

Head *et al.*, (2003) suggests that there was recent ice age on Mars that occurred about 2.1 to 0.4 Ma BP. Their study indicates the dusty water-ice-rich mantling deposits found recently on Mars are formed during the recent ice age. The deposits are latitude dependent occurring in both the hemispheres from mid latitudes to poles. Between about 2.1 to 0.4 Ma BP obliquity exceeded 30° causing water ice removal from the polar region and transported it to mid-latitudes. This ice was deposited as a mantle in the mid-latitude region. Periods of low obliquity during this time were very short to allow complete erosion of these deposits. This period of net deposition is considered as glaciation period on Mars.

This glacial period is not observed in the results obtained for the last 5 Ma BP by SICOPOLIS. The model SICOPOLIS is not coupled with atmospheric model. At higher obliquities, when temperatures are warmer, the evaporation rates are also higher in the polar region. The parameterisation in SICOPOLIS for mass balance lacks to take care of this issue. Thus the phenomenon of polar deposits transported to mid-latitudes at high obliquity can not be seen. Also in SICOPOLIS the model domain is restricted only for the polar region and the mid latitudes are not covered.

In order to obtain the glacial age in models, one needs the model where deposition should be latitude dependent, dust and ice mixture. The deposited layer should be geologically recent and should vary in their character as a function of latitude. Among these aspects current SICOPOLIS do take care of the ice and dust mixture deposition and accumulation as a function of latitude. But the deposited material does not vary in character with latitudes currently in the model. In SICOPOLIS the water vapour loss due to ablation is not taken care of once it enters the atmosphere, there is no mechanism which redeposits these lost water vapour to mid-latitudes as described in Head *et al.*, (2003). SICOPOLIS

need to be coupled with atmospheric circulation model in order to get the polar deposits driven to mid-latitudes. For this model domain should be extended to cover the mid latitudes. This will also enable to get seasonal variation in the deposition rates which plays important role in the polar regions.

# 7  Conclusions

The main aim of this study is to understand the dynamic and thermodynamic evolution of the polar caps. The smaller residual caps polewards of about 80°N and 80°S are underlain by massive topographic structures known as polar layered deposits or polar layered terrain. These complexes are reffered to as north and south polar cap for this study. This study has been done using a polythermal ice sheet model SICOPOLIS (SImulation COde for POLythermal Ice Sheets).

The major contribution is made in the form of experimenting with different schemes and studying the evolution of the caps under different conditions using SICOPOLIS. Two new parameterisation schemes for the climate input are developed. The first scheme developed is MAIC (sec. 3.2) which provides simple parameterisation for the surface temperature and accumulation-ablation rate. This scheme is based on radiative balance and is mainly driven by the Milankovitch parameter obliquity.

A second parameterisation scheme developed is based on the local insolation (sec. 3.3). This scheme also uses a radiative equilibrium approach but with daily mean insolation which enables to calculate daily mean surface temperatures globally. The $CO_2$ seasonal cycle of condensation in the polar night and evaporation after the polar night ends is also incorporated in this scheme. Hence it is possible to have seasonal temperatures with the parameterisation based on local insolation which is not possible in case of MAIC due to usage of annual mean insolation.

The parameterisation scheme based on the local insolation produces similar daily mean temperatures as in the Mars Climate Database (MCD). In both the schemes MCD and that using local insolation the $CO_2$ cover observed on the south polar cap through out the year is not produced. This is presumably because after the polar night the whole $CO_2$ cover is assumed to be evaporated which is not the case in reality.

In the beginning only Glens flow law which is used in most of the terrestrial ice sheet models was used in the SICOPOLIS. Goldsby and Kohlstedt (1997) and Durham (1998) suggest that ice has a different behaviour under different temperature and stress regimes. Hence the simulations are done with different flow laws implemented for the different stresses, strain-rate and the different temperature regimes. First Glen's flow law is tested ($n = 3$). Secondly Glen's flow law is replaced by Durham's flow law ($n = 4$). Goldsby and Kohlstedt flow law ($n = 1.8, p = 1.4$) is tested for two different grain sizes $d = 1$ mm and $d = 10$ mm (Eq. 2.1).

Satellite imagery shows that parts of the polar caps appear dark, which indicates that they consist of ice with some amount of mixed-in dust. However, for the average volume fraction $\varphi$ of dust in the ice no quantitative information is available for modelling studies of the polar caps. The dust content is implemented as a function density and heat conductivity. For simulations dust content is increased from initially zero to $10\%, 20\%, 30\%, 40\%$

and 50%. This makes it possible to study the behaviour of polar caps consisting of water ice and dust. After successful results for the north polar cap the model SICOPOLIS has been adapted to the south polar cap and results are obtained.

The main important findings of this study are summarised below.

• In the steady state simulations assuming constant present climate conditions, the north polar cap essentially needs more than 200 Ma to reach equilibrium state. Due to the influence of orbital parameters 200 Ma is an unrealistically long time span for the Martian climate to be constant to reach steady state. Therefore it is unlikely for the north polar cap to be in a steady state (Greve *et al.*, 2004).

• The present large-scale topography of the north polar cap is mainly controlled by the history of the surface mass balance. Ice flow, with flow velocities of the order of 1 mma$^{-1}$, plays only a minor role. Fisher (1993) and Hvidberg (2003) suggests that local ice flow plays vital part in keeping the small structures like scarps and troughs open. It is not possible to take care of the small scale features like trough and scarps in SICOPOLIS as it does not have the higher resolution necessary for these features. So the result stated earlier that ice flow plays only minor role in the evolution of the cap is not applicable for the small scale structures.

• While the overall shape of the north polar cap can be reproduced well with the large-scale approach of this study, a more detailed investigation of structures like the spiralling scarps and troughs and their impact on the ice dynamics is not possible.

• The main obliquity cycle of 125 ka with a modulation of 1.3 Ma is virtually not reflected in the evolution of the topography of the north polar cap, which responds mainly to the long-term average climate conditions. By contrast, the ice flow shows a strong variation over the obliquity cycles. For detailed discussions please see section 6.3.1.1

• Due to large obliquities in the past (Laskar *et al.*, 2002, Jakosky *et al.*, 1993) there may have been strongly increased sublimation rates between 10 and 5 Ma BP. It is highly likely that the north polar cap did not survive this period. If this is considered to be true then in order to build up the present cap from ice-free conditions at five million years before present (which is a possible scenario due to the very large obliquities prior to this time), a present accumulation rate of $\geq 0.25$ mm w.e.a$^{-1}$ (mm water equivalent per year)is required. The estimation for the present accumulation rates is in the range of 0.01 to 1 mm w.e. a$^{-1}$ (Budd *et al.*, 1986, Kieffer 1990).

• For all types of simulations, basal temperatures are far below pressure melting. This result is very robust and are reported in the studies Greve (2000b), Greve *et al.*, (2003) and Greve *et al.*, (2004). This indicates that there are rare chances for liquid water at the base of the polar caps.

• Since the absolute values of ice flow velocities are small for all investigated cases, the topography evolution is mainly controlled by the surface mass balance, and internal

ice dynamics play only a minor role.

• Studying the influence of ice rheology has given a better picture of the ice dynamics of the polar caps. The absolute flow velocities are 4-5 orders of magnitude smaller than its terrestrial ice sheet values. Owing to the uncertainties of the applicable flow law, the dust content and the grain size, ice flow velocities can only be predicted within a range of two orders of magnitude. They are in the range of $0.1$ mm $a^{-1}$ to $1.5$ mm $a^{-1}$ for the north polar cap (Greve and Mahajan 2005) and $0.01$ mm $a^{-1}$ to $0.16$ mm $a^{-1}$ for the south polar cap. These values are in the range of average velocities obtained by Hvidberg (2003). Ice rheology does not have any strong influence on the large scale topography of the polar cap. All the flow laws will play vital role while modelling the small scale structures like scarps and troughs. This is because flow velocities are found as high as cm/a in the trough region of the north polar cap (Hvidberg 2003) and ice rheology strongly influences the flow velocity.

• Herkenhoff and Plaut (2000) state that south polar cap shows 15 craters with diameter larger than 800 m. This indicate that the south polar cap is two orders of magnitude older than the northern cap. This age difference also indicate the stiff and slowly flowing south polar cap as compared to north. The flow velocity obtained by SICOPOLIS supports this. The largest part of the south polar cap flows at speed slower than a micrometer per year which makes the south polar cap almost stagnant.

Most of the work done during this thesis has been published in Greve *et al.*, (2004) and Greve and Mahajan (2005).

# Outlook

The work done during this thesis mainly focus on the dynamic and thermodynamic behaviour of polar ice caps. It mainly contributes to the better understanding of effect of the climate cycles in the past. This study also gives a thorough picture of Martian ice rheology and its influence on the ice flow. Still it falls short due to lack of better knowledge and realistic climate forcing data.

The coupling of the model SICOPOLIS with the Martian atmospheric model will improve the physical basis of the parameterisation for the surface temperatures and the accumulation-ablation rates.

SICOPOLIS needs to be upgraded to higher resolution to study formation of valley like structures Chasma Boreale north polar cap, Chasma Australe (south polar cap) and small scale structures like spiralling scarps and troughs. This will enable to study the role of ice flow locally. MARSIS (Mars Advanced Radar for Subsurface and Ionosphere Sounding) on board Mars Express will provide information about the internal structure layering of the polar caps as well as basal topography. This will provide the better knowledge about the lithospheric deflection improving the simulated polar cap topography.

The inclusion of spatially varying geothermal heat flux can help in understanding the valley like structures Chasma Boreale. The formation of the dark (high dust content) and

light (low dust content) ice layers in the polar cap reflects a cyclic variation in the relative deposition of a mixture of dust and ice over long period of time. This is attributed to the varying obliquity changes. Parameterising the dust content varying according to obliquity cycle in the model can give a better understanding about these layer formation.

# Bibliography

Abe-Ouchi, A. 1993. Ice sheet response to climatic changes: a modelling aproach. Zürcher Geogr. Schr., 54, 134.

Blatter, H. 1991. Effect of climate on the cryosphere. Zürcher Geogr. Schr., 41, 98.

Byrne, S., Murray, B.C., 2002. North polar stratigraphy and the paleo-erg of Mars. J. Geophys. Res. 107 (E6), 5044.

Budd, W.F., D., Laech, J. H. I., Smith, I. N., Radok, U., 1986. The north polar ice cap of Mars as a steady-state system. Polarforschung 56 (1/2), 43-46.

Budd, W. F. and I. N. Smith 1982. Large-scale numerical modelling of the Antarctic ice sheet. Ann. Glacial., 3, 42-49.

Peter Cattermole., 2001. Mars, The Mystery Unfolds,. Terra Punlishing

Calov, R. 1994. Das thermomechanische Verhalten des grönländischen Eisschildes unter der Wirkung verschiedener Klimaszenarien - Antworten eines theoretischnumerischen Modells. Ph. D. thesis, Institut für Mechanik, Technische Hochschule Darmstadt, Germany, 171.

Calov R. and K. Hutter 1996. The thermomechanical response of the Greenland ice sheet to various climate scenarios. Climate dynamics, 12, 243-260.

Clifford, S.M., Crisp, D., Fisher, D.A., Herkenhoff, K.E., Smrekar, S.E., Thomas, P.C., Wynn-Williams, D.D., Zurek, R.W., Barnes, J.R., Bills, B.G., Blake, E.W., Calvin, W.M., Cameron, J.M., Carr, M.H., Christensen, P.R., Clark, B.C., Clow, G.D., Cutts, J.A., Dahl-Jensen, D., Durham, W.B., Fanale, F.P., Farmer, J.D., Forget, F., Gotto-Azuma, K., Grard, R., Haberle, R.M., Harrison, W., Harvey, R., Howard, A.D., Ingersoll, A.P., James, P.B., Kargel, J.S., Kieffer, H.H., Larson, J., Lepper, K., Malin, M.C., McCleese, D.J., Murray, B., Nye, J.F., Paige, D.A., Platt, S.R., Plaut, J.J., Reeh, N., Rice, J.W., Smith, D.E., Stoker, C.R., Tanaka, K.L., Mosley-Thompson, E., Thorsteinsson, T., Wood, S.E., Zent, A., Zuber, M.T., Zwally, H.J., 2000. The state and future of Mars polar science and exploration. Icarus 144 (2), 210-242.

Cook, J.G., Leaist, D.G., 1983. An exploratory study of the thermal conductivity of methane hydrate. Geophys. Res. Lett. 10 (5), 397-399.

Durham, W.B., 1998. Factors affecting the rheologic properties of martian polar ice. In: First International Conference on Mars Polar Science and Exploration. Lunar and Planetary Institute, Houston, pp. 8 9. LPI Contribution No. 953.

Durham, W.B., Kirby, S.H., Stern, L.A., 1997. Creep of water ices at planetary conditions: a compilation. J. Geophys. Res. 102 (E7), 16293-16302.

Durham, W.B., Kirby, S.H., Stern, L.A., 1999. Steady-state flow of solid $CO_2$: preliminary results. Geophys. Res. Lett. 26 (23), 3493-3496.

Durham, W.B., Stern, L.A., Kirby, S.H., 2003. Ductile flow of methane hydrate. Can. J. Phys. 81 (1 2), 373-380.

Dzurisin, D. and K. R. Blasius. 1975. Topography of the polar layered deposits of Mars. J. Geophys. Res., 80 (23), 3286-3306.

Fabré, A., A. Letréguilly, C. Ritz and A. Mangeney. 1995. Greenland under changing climates: sensitivity experiments with a new three-dimensional ice-sheet model. Ann. Glacial., 21, 1-7.

Fastook, J. l. and J. E. Chapman. 1989. A map-plane finite-element model: three modeling experiments. J. Glacial., 35 (119), 48-52.

Fishbaugh, K.E., Head, J.W., 2002. Chasma Boreale, Mars: topographic characterization from Mars Orbiter Laser Altimeter data and implications for mechanisms of formation. J. Geophys. Res. 107 (E3), 5013.

Fishbaugh, K. E., Head, J.W., 2001, Comparison of the North and South Polar Caps of Mars: New Observations from MOLA Data and Discussion of Some Outstanding Questions. Icarus 154, 145-161.

Fisher, D.A., 1993. If martian ice caps flow: ablation mechanisms and appearance. Icarus 105 (2), 501-511.

Fisher, D.A., Winebrenner, D.P., Stern, H., 2002. Lineations on the "white" accumulation areas of the residual northern ice cap of Mars: their relation to the "accublation" and ice flow hypothesis. Icarus 159 (1), 39-52.

Forget, F. 1998. Mars $CO_2$ polar caps. In: Solar System Ices, ed. B. schmitt et al., Kluwer Academic Publishers, 477-507.

Fowler, A. C. 1984. On the transport of mositure in polythermal glaciers. J. Geophys. Astrophys. Fluid Dyn., 28, 99-140.

Fowler, A. C. and D. A. Larson. 1978. On the flow of polythermal glaciers. I. Model and preliminary analysis. Proc. R. Soc. Lond., A 363, 217-242.

Fraedrich, K., Kirk, E., Luksch, U., Lunkeit, F., 2003. Ein Zirkulationsmodell für Forschung und Lehre. Promet 29 (1 4), 34-48.

Goldsby, D.L., Kohlstedt, D.L., 1997. Grain boundary sliding in fine grained ice. I. Scripta Mater. 37 (9), 1399-1406.

Greve, R. 1997a. A continuum-mechanical formulation for shallow polythermal ice sheets. Phil. Trans. R. Soc. Lond., A 355, 921-974.

Greve, R. 1997b. Application of a polythermal three-dimensional ice sheet model to the Greenland Ice Sheet: response to stady-state and transient climate scenarios. J. Climate, 10 (5), 901-918.

Greve, R. 1997c. Large-scale ice-sheet modellingas a means of datingdeep ice cores in Greenland J. Glaciol., 43 (144), 307-310; Erratum 43 (145), 597-600.

Greve, R., 2000a. Large-scale glaciation on Earth and on Mars. Habilitation thesis, Fachbereich Mechanik, Technische Universität Darmstadt, Germany.

Greve, R., 2000b. Waxing and waning of the perennial north polar $H_2O$ ice cap of Mars over obliquity cycles, Icarus 144(2), 419-431.

Greve, R., 2001. Glacial isostasy: models for the response of the Earth to varying ice loads. In: Straughan, B., Greve, R., Ehrentraut, H., Wang, Y. (Eds.), Continuum Mechanics and Applications in Geophysics and the Environment. Springer, Berlin, pp. 307-325.

Greve, R., and R. A. Mahajan, 2005, Influence of ice rheology and dust content on the dynamics of the north-polar cap of Mars, Icarus 174, 475-485. doi:10.1016/j.icarus.2004.07.031.

Greve, R., Klemann, V., Wolf, D., 2003. Ice flow and isostasy of the north polar cap of Mars. Planetary and Space Science 51(3), 193-204.

Greve, R., R. A. Mahajan, J. Segschneider, B. Grieger, 2004. Evolution of the north-polar cap of the Mars: a modelling study. Planet. Space Sci. 52 (9), 775-787. doi:10.1016/j.pss.2004.03.007.

Halfar, P., 1983. On the dynamics of the ice sheets. 2. J. Geophys. Res. 88 (C10), 6043-6051.

Hammer, C. U., Clausen, H. B., Dansgaard, W., Neftel, A., Kristindottir, P., Johnson, E., 1985. Continuous impurity analysis along Dye 3 deep core. In: Langway, C. C., Oescher, H., Dansgraad, W. (Eds.), Greenland Ice Core:Geophysics, Geochemistry and the Environment. No 33 in Geophysical Monographs. American Geophysical Union, Washington DC, pp 90-94.

J. W. Head., J. F. Mustard., M. A. Kreslavsky., R. E. Millikan., D. R. Marchant, 2003. Recent ice ages on Mars. Nature 426, 797-802.

Herkenhoff, K.E., Plaut, J.J., 2000. Surface ages and resurfacing rates of the polar layered deposits on Mars. Icarus 144 (2), 243-253.

Herterich, K. 1988. A three-dimensional modelof the antarctic ice sheet. Ann. Glaciol., 11, 32-35.

Herterich, K. 1990. Modellierung eiszeitlicher Klimaschwankungen. Habilitation thesis, Fachbereich Geowissenschaften, Universität Hamburg, Germany.

Hutter, K. 1982. A mathematical model of polythermal glaciers and ice sheets. J. Geophys. Astrophys. Fluid Dyn., 21, 201-224.

Hutter, K., 1983. Theoretical Glaciology; Material Science of Ice and the Mechanics of Glaciers and Ice Sheets. Reidel, Dordrecht, The Netherlands.

Hutter, K. 1993. Thermo-mechanically coupled ice sheet response. Cold, polythermal, temperate. J. Glaciol., 39 (131), 65-86.

Huybrechts, P. 1992. The Antarctic ice sheet and environmental change: a three-dimensional modelling study. Ber. Polarforschung, 99, 241.

Huybrechts, P. 1993. Glaciological modelling of the Late Cenozoic East antarctic ice sheet: stability or dynamism? Geografiska Annaler, 75 A (4), 221-238.

Huybrechts, P. 1994. The present evolution of the Greenland ice sheet: an assessment by modelling. Global Planet. Change, 9, 39-51.

Huybrechts, P. and J. Oerlemans. 1988. Evolution of the East Antarctic ice sheet: a numerical study of thermo-mechanically response patterns with changing climate. Ann. Glaciol., 11, 52-59.

Hvidberg, C.S., 2005. Polar Caps. In: Water on Mars and Life, Tetsuya Tokano (Ed.), Adv. Astrobiol. Biogeophysics, pp. 129-152.

Hvidberg, C.S., 2003. Relationship between topography and flow in the north polar cap on Mars. Ann. Glaciol. 37, 363-369.

Hvidberg, C.S., Zwally, H.J., 2003. Sublimation of water from the north polar cap of Mars. In: Workshop "Mars Atmosphere Modelling and Observations", Granada, Spain, 13-15 January 2003. Abstract.

Jakosky, B. M. and R. M. Haberle. 1992. The sesonal behavior of water on Mars. In: Mars, ed. H. H. Kieffer et al., The University of Arizona Press, 969-1016.

Jakosky, B.M., Henderson, B.G., Mellon, M.T., 1993. The Mars water cycle at other epochs: recent history of the polar caps and layered terrain. Icarus 102, 286-297.

Jenssen, D. 1977. A three-dimensional polar ice-sheet model. J. Glaciol., 18 (80), 373-389

Johnson, C.L., Solomon, S.C., Head, J.W., Phillips, R.J., Smith, D.E., Zuber, M.T., 2000. Lithospheric loading by the northern polar cap on Mars. Icarus 144 (2), 313-328.

Jöns, H. P., 2002. Young/recent noneolian exogenic dynamics on Mars: large-scale influence by decomposition of $CO_2$ hydrates? Z. Geol.Wiss. 30 (6), 403-421.

Kargel, J.S., Tanaka, K.L., 2002. The martian south polar cap: glacial ice sheet of multiple interbedded ices. Lunar Planet. Sci. 33. Abstract 1799.

Kieffer, H.H., 1990. $H_2O$ grain size and amount of dust in Mars residual north polar cap, J. Geophys. Res. 95, 1481-1493.

Kieffer, H.H., Zent, A.P., 1992. Quasi-periodic climate change on Mars. In: Kieffer, H.H., Jakosky, B.M., Snyder, C.W., Matthews, M.S. (Eds.), Mars. University ofArizona Press, Tucson, pp. 1180-1218.

Larsen, J., D. Dahl-Jensen., 2000. Interior temperatures on northern polar caps on Mars, Icarus 144, 456-462.

Laskar, J., Levrard, B., Mustard, J. F., 2002. Orbital forcing of the martian polar layered deposits, Nature 419(6905), 375-377.

J. Laskar., A.C.M. Correia, M. Gastineau F. Joutel B. Levrarda, P. Robutel, 2004. Long term evolution and chaotic diffusion of the insolation quantities of Mars, Icarus 170, 343-364.

Le Meur, E., Huybrechts, P., 1996. A comparison of different ways of dealing with isostasy: examples from modelling the Antarctic ice sheet during the last glacial cycle. Ann. Glaciol. 23, 309-317.

Letréguilly, A., P. Huybrechts and N. Reeh. 1991a. Steady-state characteristics of the Greenland ice sheet under different climates. J. Glaciol. 37 (125), 149-157.

Letréguilly, A., N. Reeh and P. Huybrechts. 1991b. The Greenland ice sheet through the last glacial-interglacial cycle. Palaeogeogr., Palaeoclimatol., Palaeoecol. (Global Planet. Change Sect.), 90, 385-394.

Lewis, S. R., M. Collins, P. L. Read, F. Forget, f. Hourdin, R. Fournier, C. Hourdin, O. Talagrand and J.P. Huot, 1999. A climate database of Mars. *J. Geophys. Res* 104 (E10), 24177-24194.

Lliboutry, L. and P. Duval. 1985. Various isotropic and anisotropic ices found in glaciers and the polar ice caps and their corresponding ice rheologies. Ann. Geophys. 3 (2), 207-224.

Mahaffy, M. W. 1976. A three-dimensional numerical model of ice sheets: Test on the Barnes ice cap, Northwest territories. J. Geophys. Res., 81 (6), 1059-1066.

Mellon., M. T. 2004. Limits of the $CO_2$ content of the martian polar deposits, Icarus 124, 268-279.

Morland, L. W. 1993. The flow of ice sheets and ice shelves. Continuum mechanics in environmental sciences and geophysics, K. Hutter (ed.), CISM courses and lectures, 337, Springer Verlag, Wien etc., 403-466.

Morland, L.W., 1984. Thermo-mechanical balances of ice sheet flows. Geophys. Astrophys. Fluid 29, 237-266.

Müller, I. 1985. Thermodynamics. Pitman Advanced Publishing Program, Boston etc., pp 521.

Müller, I., 2001. Grundzüge der Thermodynamik mit historischen Anmerkungen, 3rd Edition. Springer, Berlin.

Nye J.F., 1953. The flow law of ice from measurements in glacier tunnels, laboratory experiments and the Jungfraufirn borehole experiments. Proc. R. Soc. London Ser. A 219, 477-489.

Nye, J.F., 2000. A flow model for the polar caps of Mars. J. Glaciol. 46(154), 438-444.

Nye, J.F., Durham, W.B., Schenk, P.M., Moore, J.M., 2000. The instability of a south polar cap on Mars composed of carbon dioxide. Icarus 144 (2), 449-455.

Oerlemans, J. 1982. Response of the antarctic Ice Sheet to a climatic warming: a model study. J. Climatol., 2, 1-11.

Paterson W. S. B., 1994. The Physics of Glaciers, 3rd Edition. Pergamon Press, Oxford.

Paterson W. S. B., 1991. Why ice-age is sometimes "soft", Cold Region Science and Technology 20, 75-98.

Payne, A.J., Huybrechts, P., Abe-Ouchi, A., Calov, R., Fastook, J.L., Greve, R., Marshall, S.J., Marsiat, I., Ritz, C., Tarasov, L., Thomassen, M.P.A., 2000. Results from the EISMINT model intercomparison: the effects of thermomechanical coupling. J. Glaciol. 46 (153), 227-238.

Read, P.L., and Lewis, S.R., The Martian Climate Revisited, Atmosphere and Environment of a Desert Planet, Praxix publishing, Springer.

Rigsby, G.P., 1958. Effect of hydrostatic pressure on velocity of shear deformation of single ice crystals. J. Glaciol. 3 (24), 273-278.

Schubert, G., Solomon, S. C., Turcotte, D. L., Drake, M.J., Sleep, N.H., 1992. Origin and thermal evolution of Mars. In: Kieffer, H. H., Jakosky, B. M., Snyder, C. W., Matthews, M.S. (Eds), Mars, University of Arizona Press, Tucson, pp. 147-183.

Segschneider J., Grieger, B., Keller, H.U., Lunkeit, F., Kirk, E., Fraedrich, K., Rodin, A., Greve, R., 2005. Response of the intermediate complexity Mars Climate Simulator to different obliquity angles. Planet. Space Sci. 53(6), 659-670.

Smith D.E., Zuber, M.T., Solomon, S.C., Phillips, R.J., Head, J.W., Garvin, J.B., Banerdt,W.B., Muhleman, D.O., Pettengill, G.H., Neumann, G.A., Lemoine, F.G., Abshire, J.B., Aharonson, O., Brown, C.D., Hauck, S.A., Ivanov, A.B., McGovern, P.J., Zwally, H.J., Duxbury, T.C., 1999. The global topography of Mars and implications for surface evolution. Science 284 (5419), 1495-1503.

Stern, L.A., Kirby, S.H., Durham, W.B., 1996. Peculiarities of methane clathrate hydrate formation and solid-state deformation, including possible superheating of water ice. Science 273 (5283), 1843-1848.

Thomas, P., Squyres, S., Herkenhoff, K., Howard, A., Murray, B., 1992. Polar deposits of Mars. In: Kieffer, H.H., Jakosky, B.M., Snyder, C.W., Matthews, M.S. (Eds.), Mars. Univ. of Arizona Press, Tucson, pp. 767-795.

Touma, J., Wisdom, J., 1993. The chaotic obliquity of Mars. Science 259 (5099), 1294-1297.

Thorsteinsson, T., 1996. Textures and fabrics in the GRIP ice core, in relation to climate history and ice deformation. Reports on Polar Research No. 205. Alfred Wegener Institute for Polar and Marine Research, Bremerhaven.

Van der Veen, C.J., 1999. Fundamentals of Glacier Dynamics. Balkema, Rotterdam.

Ward, W.R., 1979. Present obliquity oscillations of Mars: Fourth order accuracy in orbital e and I. J. Geophys. Res. 84, 237-241.

Ward, W.R., 1992. Long-term orbital and spin dynamics of Mars. In: Kieffer, H.H., Jakosky, B.M., Snyder, C.W., Matthews, M.S. (Eds.), Mars. University of Arizona Press, Tucson, pp. 298-320.

Zuber, M.T., Smith, D.E., Solomon, S.C., Abshire, J.B., Afzal, R.S., Aharonson, O., Fishbaugh, K., Ford, P.G., Frey, H.V., Garvin, J.B., Head, J.W., Ivanov, A.B., Johnson, C.L., Muhleman, D.O., Neumann, G.A., Pettengill, G.H., Phillips, R.J., Sun, X., Zwally, H.J., Banerdt, W.B., Duxbury, T.C., 1998. Observations of the north polar region of Mars from the Mars Orbiter Laser Altimeter. Science 282 (5396), 2053-2060.

# Acknowledgements

Uncertainties, difficulties, unknown cultural setups and so on, were some of the issues that occupied my mind prior to my trip to MPS, Germany. But all my apprehensions were laid to rest from day One. Thanks to my professors, friends and colleagues, life in the quite village of Lindau was surprisingly entertaining. Encompassing the army of people that made living here more than just routine, in this "short" section, .... well.. would require advanced field theory to deal with the densities!! Thus, omition of a few names should be counted more as a consequence of memory-breach than that of complete oblivion.

Usually "acknowledgements" is the part of the thesis you are most careful about. Simply because you have phantom-thoughts on inexcusable exclusions, order of importance and a host of other subjective concerns. I maintain an "order of thanking" that is only subject to the surroundings perturbing my brain in unpredictable ways. Basically when I think of all the people that I have to thank I think "chronological". On this route of recalling I obviously thank Dr. habil. H. U. Keller for recognising my interests and skills in the subject and for offering me this Ph.D position. I hope I have done justice to your confidence in me. Thank you for this privileged opportunity.

At the beginning of a Ph.D you stand at the hem of a spectrum of interesting and challenging projects. It takes experienced and dedicated experts to define, discuss and designate a problem that fits your profile in science. I thank both my supervisors Dr. Ralf Greve and Dr. Björn Grieger for there choice of project and continual guidance. I thank Ralf for his efforts in making sure that I understand the model I used and also for clearing a plethora of confusions I had. Even though he worked in Darmstadt or Japan during most of the time of my Ph.D, I was amazed at his speed of work and email responses to all my queries!!

Apart from your supervisors you always find people, at least at MPS, to discuss various scientific aspects of your thesis. In this regard I am extremely thankful to Prof. Ulrich Christensen for his abilities and enthusiasm in explaining hard-to-understand concepts. I thank Ulrich for accepting me as his Ph.D student at the University of Göttingen. Special thanks to Dr.Oliver Stenzel, my officemate and a postdoc at the institute has spent countless hours during the past months explaining to me subtleties in the thesis manuscripts and for very constructive scientific suggestions. Not to forget he was the one who always answered my ever increasing queries on LaTeX.

We were the first batch of the IMPRS in Lindau. But the professionalism and concern of Dr. Dieter Schmitt towards all the students, their comfort and organisation is worth commending. I thank him personally for all the help and guidance throughout the three years of my stay, be it scientific or administrative. All the secretaries I thank sincerely, especially our group secretary Sabine, for their efforts in making sure that I spend all my time on research and not on bureaucratic spirals.

I spent considerable amount of my Ph.D time in Darmstadt (Department of Mechanics, Technical University, Darmstadt). It was an enjoyable experience where I was introduced to the interplay between quality science and pure entertainment. I thank all the people there for their hospitality and support.

Support from my family was a vital ingredient in my successful completion of the PhD. I thank my parents and sister for their good-will and encouragement all along. At a more personal and social level its always your fellow students and friends that make your life meaningful. I thank each and everyone of the students in the institute for all the great times I had during the course of my work. Surviving Lindau's "sparse population effects" would have been impossible without their help.

Special thanks of course to my close friends Marilena and Laura, who also apparently are my housemates. Friction often occurred between us because of the overdose of concern we had for each other which I think underpins the kind of relationship we had. Marilena played a very important role in entangling a lot of mess that often appears at the end of writing a thesis. Thank you girls for all your support. Just across my building were two guys, Durgesh and Rajat, who resembled India only when they cooked!! Just joking fellows.I really owe you people a lot of pasta and rice. Special thanks also to my colleague and long time friend Aveek Sarkar for his many scientific ideas and in fact he did explain to me many concepts that I was reluctant to ask the experts. Thank you very much Aveek for always being there.

Even though this short passage will not do justice to the extent to which I am grateful to each one of you who made my life in Lindau worth the living, I would just like to tell you people that if given an opportunity somewhere down the line to re-live this experience .... I would pounce on it!!

# Publications and Contributions

## 1. Publications

Greve, R., and R. A. Mahajan, 2005, Influence of ice rheology and dust content on the dynamics of the north-polar cap of Mars, Icarus 174, 475-485. doi:10.1016/j.icarus.2004.07.031.

Greve, R., R. A. Mahajan, J. Segschneider, B. Grieger, 2004. Evolution of the north-polar cap of the Mars: a modelling study. Planet. Space Sci. 52 (9), 775-787. doi:10.1016/j.pss.2004.03.007.

## 2. Conferences

R. A. Mahajan, Greve, R., J. Segschneider, B. Grieger, Steady state simulations for North Polar Cap of Mars II, EGS-AGU-EUG Joint Assembly, Nice, France, 6-11 April 2003 (Poster)

R. A. Mahajan, Greve, R., Influence of ice rheology and dust content on the evolution of the North Polar Cap of Mars, 35th COSPAR Scientific Assembly, Paris, France, 18-25 July 2004 (Poster)

## 3. Workshops

First Workshop of the Subgroup "Atmosphere and Surface Processes" of the DFG Priority Programme "Mars and the Terrestrial Planets", Darmstadt, 8-9 March 2005 (Talk)

Second Workshop of the Subgroup "Atmosphere and Surface Processes" of the DFG Priority Programme "Mars and the Terrestrial Planets" , Darmstadt, 9-10 March 2004 (Talk)

Third Workshop of the Subgroup "Atmosphere and Surface Processes" of the DFG Priority Programme "Mars and the Terrestrial Planets", Darmstadt, 10-11 March 2005 (Talk)

# Lebenslauf

**PERSÖNLICHE DATEN**

| | |
|---|---|
| Name | Mahajan |
| Vorname | Rupali Arunkumar |
| Geburtsdatum | 18. Juni 1976 |
| Geburtsort | Beed, Indien |
| Staatsangehörigkeit | Indien |

**SCHULBILDUNG**

| | |
|---|---|
| 1981 - 1985 | Grundschule, Aurangabad, Indien |
| 1985 - 1991 | Allgemeinschule, Aurangabad, Indien |
| 1991 - 1993 | Gymnasium, Aurangabad, Indien |

**STUDIUM**

| | |
|---|---|
| 1994 - 1997 | Bachlor, Universität Pune, Fakultät für Physik, Pune, Indien |
| 1998 - 2000 | Master in Weltraumwissenschaften, an der Fakultät für Physik, Pune Universität, Indien |
| 2000 - 2002 | Master in Atmosphärischer Physik/Meteorologie an der Fakultät für Physik, Pune Universität, Indien |

**PROMOTION**

| | |
|---|---|
| Mai. 2002 - Apr. 2005 | Wissenschaftliche Angestellte am Max-Planck-Institut für Sonnensystemforschung |
| WS 2002 - WS 2004 | Promotion Fakultät für Physik, Georg August Universität, Göttingen |